UAB
Universitat Autònoma de Barcelona

BIOCOMPATIBILITY AND FUNCTIONALITY OF GRAPHENE-BASED FLEXIBLE NEURAL INTERFACES

Bruno Rodríguez Meana

UAB
Universitat Autònoma de Barcelona

BIOCOMPATIBILITY AND FUNCTIONALITY OF GRAPHENE-BASED FLEXIBLE NEURAL INTERFACES

Presented by

Bruno Rodríguez Meana

ACADEMIC DISSERTATION

To obtain the degree of PhD in Neuroscience by the

Universitat Autònoma de Barcelona

July 2023

Thesis supervisors

Dr. Jaume del Valle Macià
Dr. Xavier Navarro Acebes

Group of Neuroplasticity and Regeneration,
Institut de Neurociències

NeuroPlasticity & Regeneration

BCFI Departament de Biologia Cel·lular, Fisiologia i Immunologia Universitat Autònoma de Barcelona

INc Institut de Neurociències UAB

The research described in this thesis was conducted at the Department of Cellular Biology, Physiology and Immunology, Institute of Neuroscience, of the Universitat Autònoma de Barcelona in the Group of Neuroplasticity and Regeneration.

This study was found by:

- The FLAG–ERA project "**GRAphene based Flexible neural Interfaces for the control of Neuroprosthetic devices" (GRAFIN). PCI2018–093029. Funded by FLAG–ERA JTC and Ministerio de Ciencia, Innovación y Universidades**. Granted to Xavier Navarro Acebes.
- The H2020 FET–OPEN project **"Ultrasound peripheral interface and *in vitro* model of human somatosensory system and muscles for motor decoding and restoration of somatic sensations in amputees" (SOMA)**. GA 899822. Funded by Horizon 2020 FET Open, European Commission. Granted to Xavier Navarro Acebes.
- The FLAG–ERA project **"Functional stimulation system for rehabilitation of gait and driving neural plasticity after spinal cord injury using graphene–based nerve electrodes" (RESCUEGRAPH)**. PCI2021–122075–2A. Funded by FLAG–ERA JTC and Agencia Estatal de Investigación. Granted to Xavier Navarro Acebes.

Index

I. Abstract

Neuroprostheses aim to restore the lost functions after limb amputation or severe neural injuries. Within a peripheral neuroprosthesis, the interface between nerve and machine is intended to record neural signals and stimulate populations of nerve fibers, constituting a bidirectional interface with high selectivity and efficiency. However, further improvements in functionality are still needed to reach natural–like capabilities to electrically interact with the nervous tissue.

In this thesis, two main issues that currently challenge the potential use of neuroprostheses are addressed. Firstly, the ability of the interface to interact with the nervous tissue depends on its electrical capabilities. Conductive materials with enhanced properties, including low impedance and high charge injection capacity are required, for increasing selectivity and durability of the interface. Secondly, after the implantation of any foreign device into the body, a series of immune processes known collectively as the foreign body reaction (FBR) are initiated. This process aims to destroy or isolate the implant from the rest of the organism. Consequently, the functionality of a device designed to interact with the tissues in which it has been implanted is compromised.

To improve functionality, a new generation of neural interfaces that replaces metal electrodes with engineered graphene has been tested. This new device is based on modified reduced–graphene oxide, named EGNITE (Engineered Graphene for Neural Interface).

The biocompatibility of EGNITE was validated *in vitro* and *in vivo*. Cellular viability in culture was not affected by the presence of EGNITE. Functional and histological tests of animals implanted with intraneural devices containing EGNITE showed similar outcomes to other intraneural interfaces, without evidence of nerve damage or axonal degeneration. Regarding functionality, electrodes made of EGNITE in the conductive contacts were able to selectively stimulate and record different subsets of axons in the sciatic nerve of rats. The threshold for neuromuscular activation was lower than with larger–sized metal electrodes used in previous studies. Recording of sensory signals with good discrimination was possible due to the low signal–to–noise ratio (SNR) of the EGNITE electrodes.

To increase the chronic stability of neural interfaces, metformin was studied as a novel treatment to modulate the FBR to intraneural implants. Metformin reduced the capsule formation around the interface. Additionally, the combination of

dexamethasone and metformin proved to be the most optimal therapy to reduce both early inflammatory reaction and late fibrotic reaction.

In summary, the graphene–based material (GBM) EGNITE is suitable for integration with a neuroprosthesis, improving functionality compared to metallic electrodes. Furthermore, it has been demonstrated that metformin decreased the FBR. It has also been emphasized that combined therapies targeting different phases of the FBR may be the most optimal strategy for improving the chronic stability and functionality of neural interfaces.

II. Abbreviations

AMPK: Adenosine monophosphate–activated protein kinase

AS: Active site

BBB: Blood–brain barrier

CD90: Cluster of differentiation 90

CIL: Charge injection limit

CMAP: Compound muscle action potential

CNAP: Compound nerve action potential

CNS: Central nervous system

CSFIR: Colony–stimulating factor 1 receptor

CTL: Control

CXCL4: C–X–C chemokine receptor type 4

DAMP: Damage associated molecular pattern

DEXA: Dexamethasone

DRG: Dorsal root ganglia

Ecad: Epithelial cadherin

ECM: Extracellular matrix

EGNITE: Engineered Graphene for Neural Interface

ENG: Electroneurography

FAK: Focal adhesion kinase

FBGC: Foreign body giant cell

FBR: Foreign body reaction

FES: Functional electrical stimulation

FET: Field–effect transistor

FINE: Flat interface nerve electrode

GBM: Graphene–based materials

GM: Gastrocnemius medialis

GM–CSF: Granulocyte–macrophage colony–stimulating factor

IAP: Inhibitor of apoptosis

Iba1: Ionized calcium–binding adapter molecule 1

ICAM: Intercellular adhesion molecule

IPF: Idiopathic pulmonary fibrosis

IFN–γ: Interferon γ

IL: Interleukin

LIFE: Longitudinal intrafascicular electrode

LOX: Lysyl oxidase

LOXL: Lysyl oxidase–like

LPN: Lateral plantar nerve

LPS: Lipopolysaccharide

LTB4: Leukotriene B4

MCP–1: Monocyte chemotactic protein 1

MEA: Multielectrode array

MET: Metformin

MMP: Matrix metalloproteinase

MPN: Medial plantar nerve

NETs: Neutrophil extracellular traps

NLRP3: Nucleotide–binding oligomerization domain–like receptor family pyrin domain containing 3

p.o.: Oral administration

ParC: Parylene C

PB: Phosphate buffer

PCL: Polycaprolactone

PDGF: Platelet–derived growth factor

PDMS: Polydimethylsiloxane

PEDOT:PSS: Poly(3,4–ethylenedioxythiophene):poly(styrene sulfonate)

PEG: Poly(ethylene glycol)

PF4: Platelet Factor 4

PFA: Paraformaldehyde

PGA: Polyglycolide

PI: Polyimide

PL: Planar interossei

PLA: Polylactic acid

PNI: Peripheral nerve interfaces

PNS: Peripheral nervous system

PRR: Pattern recognition receptor

PTFE: Polytetrafluoroethylene

PU: Polyurethane

ROS: Reactive oxygen species

RT97: 200 kDa clone RT97

s.c.: Subcutaneous administration

s.i.d.: Once a day administration

SD: Sprague–Dawley

SFI: Sciatic functional index

SI: Selectivity index

SNR: Signal–to–noise ratio

TA: Tibialis anterior

tf–LIFE: Thin–film LIFEs

TGF–β: Transforming growth factor

Th: Helper T cell

TIME: Transverse intrafascicular multichannel electrode

TLR: Toll–like receptor

TLR4: Bacterial products like toll receptor 4

TNF–α: Tumor necrosis factor α

USEA: Utah slanted electrode array

VEGF–A: Vascular endothelial growth factor A

III. Introduction

1. Peripheral nervous system

The human nervous system is divided into the central nervous system (CNS), whose anatomical structures are the brain, the brainstem and the spinal cord, and the peripheral nervous system (PNS), formed by neurons located in the spinal cord and ganglia and their axons, which are bundled together within peripheral nerves. The function of the PNS is to interconnect the CNS with the limbs and the internal organs ensuring a proper response to extrinsic and intrinsic stimuli. For this purpose, the somatic and autonomic divisions of the PNS carry bidirectional information to and from the CNS through afferent sensory and efferent motor neurons respectively. The somatic system is related to voluntary motor control or sensory awareness whereas the autonomic system is related to the subconscious, involuntary control of visceral organs.

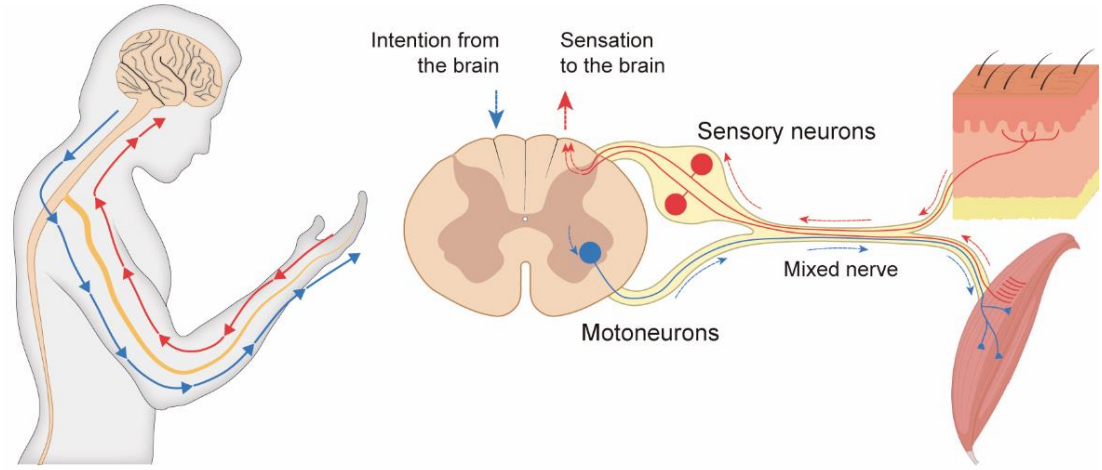

Figure 1. Somatic nervous system. Motor commands (blue arrows) are transduced from primary motoneurons in the motor cortex to secondary motoneurons located in the spinal cord (blue circle) via efferent pathways. Secondary motoneurons connect with skeletal muscle effectors to produce desired movements. Sensory information (red arrows) from receptors located in the skin (touch) or muscles (proprioception) is transduced through sensory neurons whose cell bodies lie in dorsal root ganglia (DRG) (red circles). The sensory afferent pathway extends to the spinal cord and eventually reaches the somatosensory cortex. Motor efferent pathways and sensory afferent pathways usually converge into the same tract (mixed nerves) once outside the spinal cord and the DRG respectively.

In the somatic system, afferent sensory neurons, whose cell bodies lie in the dorsal root and cranial ganglia, transduce stimuli from receptors located in the skin, muscles, and joints to the CNS, providing various classes of sensory inputs, mainly mechanical, thermal, noxious and proprioceptive. Regarding efferent pathways,

upper motoneurons located in the cortex produce motor commands to lower motoneurons in the spinal cord that are connected to specific skeletal muscle effectors. Thus, neural circuitry is set up so that sensory information is integrated into the CNS, which may elicit adequate responses via motor commands (Figure 1).

The conduction velocity of signals transmitted through the axons of neurons depends on the diameter of the axons and whether they are myelinated or not. Each somatic sensory neuron is specified to a sensory modality with a receptive field in the peripheral tissue (Horch *et al.*, 1977). The intensity of the stimulus is coded by the impulse frequency and the number of recruited sensory afferents. Afferent sensory axons can be myelinated or unmyelinated. Efferent somatic motor fibers are myelinated alpha–motor fibers, which innervate skeletal extrafusal muscle fibers, and gamma–motor fibers, which innervate the muscle spindle. The spinal alfa–motor neuron and the muscular fibers it contacts define the motor unit. The increase in both the number of motor units recruited and the frequency of impulses to each motor unit results in a progressive contraction of each muscle. The physiological recruitment of motor units depends on their size. Smaller motor units are fatigue–resistant and are activated first while larger motor units are activated later, are easily fatigued, and only activated if strong force is required (Henneman *et al.*, 1965).

Afferent and efferent axons, belonging to hundreds or thousands of neurons, are bundled together and surrounded by connective tissue to form the peripheral nerves. The epineurium, perineurium, and endoneurium are the three supporting sheaths surrounding peripheral nerves. The epineurium, the outermost layer, contains the blood vessels supplying the nerve and is made of loose connective tissue. The perineurium surrounds each fascicle in the nerve and is composed of perineurial cells and collagen fibers, which are responsible for the tensile strength and flexibility of the nerve. The endoneurium fills the gap between the nerve fibers within the fascicle with fibroblasts, collagen, and other extracellular matrix (ECM) components. Finally, each axon is surrounded by the basal lamina forming the endoneurial tubes, in which axons are accompanied by Schwann cells, that can either myelinate or just surround them (Figure 2).

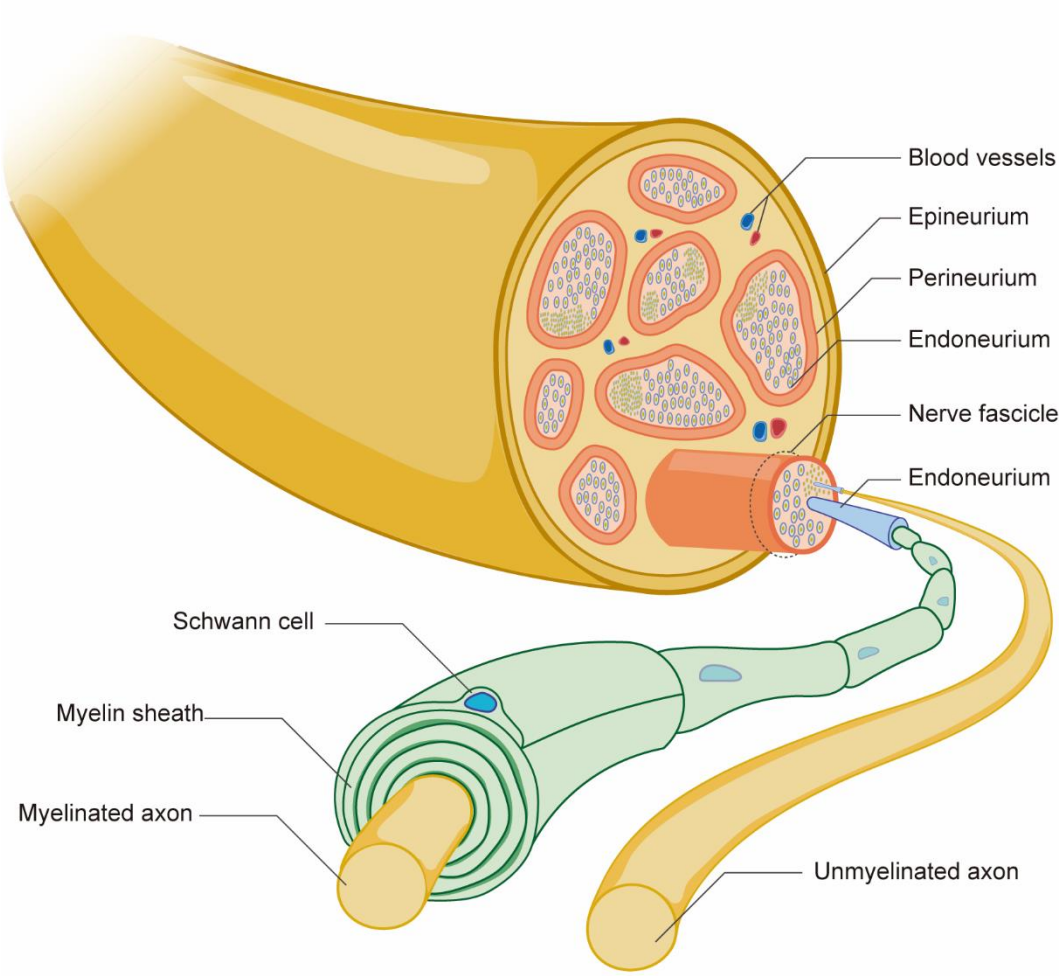

Figure 2. Nerve structure. The nerves are organized into three layers surrounding the axons. The epineurium is the outermost layer, followed by the perineurium that encloses each nerve fascicles. Within each fascicle, axons are surrounded by the endoneurium and accompanied by Schwann cells. Schwann cells can form insulating myelin sheaths around axons (myelinated axons), which increase the speed of action potentials spreading. Although unmyelinated axons do not possess this myelin sheath, they are enveloped by cytoplasmic invaginations of Schwann cells.

Most peripheral nerves are mixed, providing motor, sensory and autonomic innervation to the corresponding projection territory. Nerve fibers are gathered in fascicles, which are somatotopically and functionally arranged (Hallin, 1990). Along the course of a nerve, the fascicular architecture varies, including the eventual formation of branches that innervate different targets (muscular, cutaneous or visceral) (Brushart, 1991; Boretius *et al.*, 2010).

Spinal cord and peripheral nerve injuries, among other neural disorders, produce a partial or total loss of motor, sensory and autonomic function in distal organs. Although the PNS possesses a complex and coordinated mechanism of regeneration, its success depends upon several factors such as the severity of the

lesion. To further expand intrinsic regeneration capabilities, several surgical strategies have been developed to repair the injured nerves (Navarro & Verdú, 2004). However, axons reconnection to previous specific target organs is far from optimal, particularly after a complete nerve transection. Misdirection of regenerating axons, the formation of a neuroma, the chronic denervation and the atrophy of target organs due to the slow rate of axonal regeneration hampers functional restoration (Sulaiman & Gordon, 2013). In the case of limb loss due to amputation or congenital, reinnervation is dismissed.

2. Neuroprostheses

Neuroprostheses are capable of partially restoring or replacing body functions lost after injuries by employing appropriate electrodes implanted in the brain, spinal cord, peripheral nerves, or muscles. These electrodes are also called neural interfaces. Neuroprostheses designed to interface the nervous system follow two main approaches depending on the patient's condition. If the connection between the CNS and the target organ is no longer available, but the muscles responsible for the lost action are still preserved, e.g., spinal cord injuries, brain injuries or neurodegenerative diseases, functional electrical stimulation (FES) systems (Figure 3) have been developed to artificially stimulate the remaining organs or nerves attempting to mimic physiological actions (Marquez–Chin & Popovic, 2020). If the organ is not preserved, i.e., amputation, the missing part of the body is replaced with a bionic prosthesis that is linked to the electrode, bypassing the motor and sensory signals between the CNS and the bionic prosthesis (Figure 3). In peripheral neuroprostheses, the electrode implanted in the nerve records motor inputs from motor efferent axons to control the movement of the bionic prosthesis. The electrode also receives sensory inputs from artificial sensors located in the bionic prosthesis that are codified into electrical pulses exerted by the electrode that travels to the CNS. Proper somatosensory feedback is key to gaining natural and dynamic control of the prosthesis, thus increasing functionality and embodiment. Otherwise, patients must rely on visual cues to track the actions of the prosthesis (D'Anna, *et al.*, 2019). Although the transmission of information between the artificial limb and the patient can relay in the PNS or the CNS, peripheral nerve interfaces (PNI) show a reduced invasivity in comparison with

central implants, due to peripheral nerves being more accessible, and may allow easier topographical discrimination. Moreover, provided that most peripheral nerves contain both motor and sensory fibers, one single device can be useful for both recording motor information and providing somatosensory feedback.

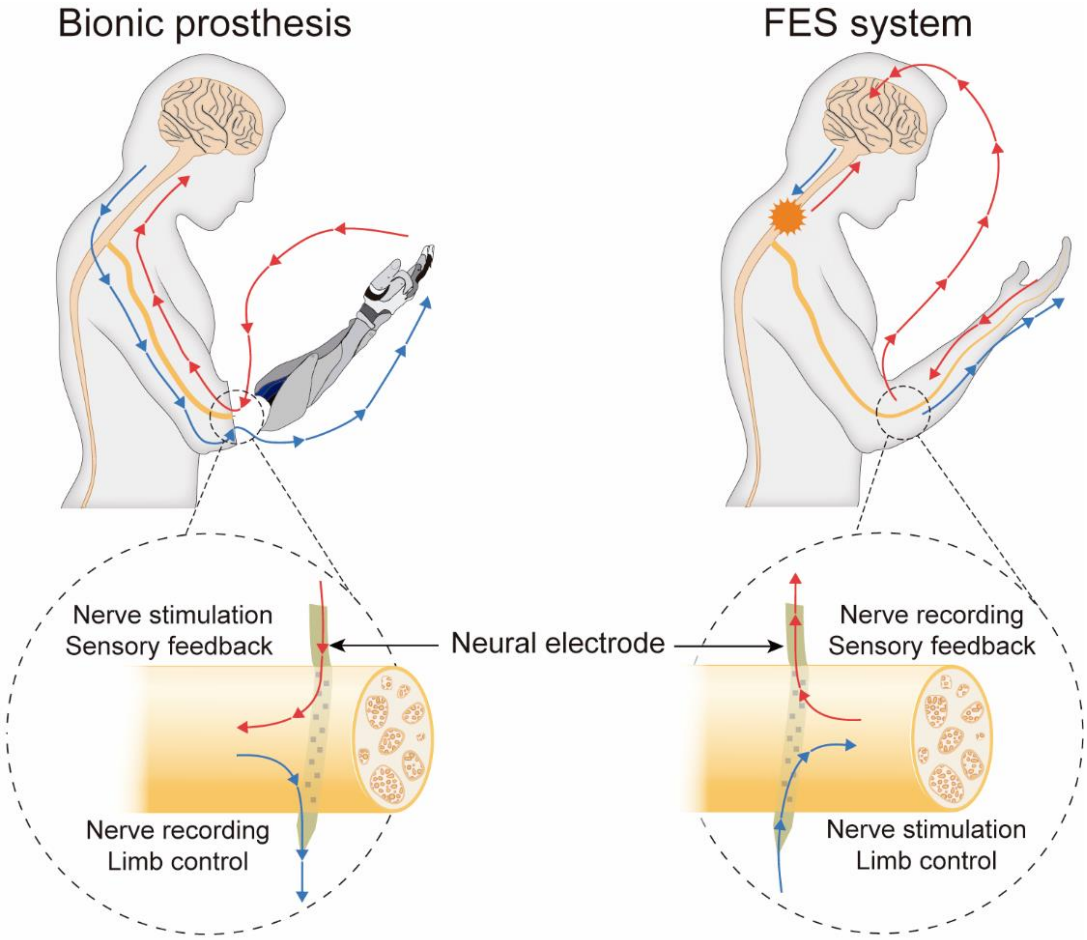

Figure 3. PNS neuroprostheses. Bionic prostheses: A neural electrode located in the nerve becomes the interface to connect the PNS with a robotic limb. The neural electrode records motor information from the patient to control the movements of a bionic limb. Also, the neural electrode provides sensory feedback by stimulating the nerve, based on sensory information (touch, pressure, temperature) collected from artificial sensors in the bionic limb. **FES system:** A neural electrode located in the nerve becomes the interface to bypass an injury in the CNS that has severed communication between the brain and the distal organ. The neural electrode stimulates non–injured motor axons to produce specific movements. Also, the neural electrode records sensory information from the limb coming from sensory axons. This information may be sent to another electrode in the brain to provide conscious sensory feedback or to the same peripheral electrode to readjust stimulation protocols based on the recorded sensations.

3. Peripheral nerve electrodes

Taking into consideration the part of the interface that is implanted, the electrode is formed by three main components: a substrate, the conductive electrical tracks, and the active sites (AS). The substrate gives the electrode its shape and should be electrically inert; it has to resist the implantation procedure and should show high biocompatibility once in contact with the tissue. The most used materials are silicone, polyimide (PI) and parylene (Navarro *et al.*, 2005). The conductive tracks of the electrode are embedded within the substrate and transmit the current between the tissue interface and the machine. The ASs are the uncovered parts of the electrode where the communication between the nervous system and the artificial system takes place (Figure 4). These ASs should be able to deliver enough current to stimulate adjacent axons and to detect extracellular neural signals with respect to the surrounding noise. The most used materials for electrode ASs are gold, platinum and iridium oxide, and they can be coated with different materials, e.g., carbon nanotubes or poly(3,4– ethylenedioxythiophene):poly(styrene sulfonate) (PEDOT:PSS) (Yoshida Kozai *et al.*, 2012), to improve the injected charge available and the impedance.

In a neural electrode that is implanted around or within a peripheral nerve, each AS can stimulate at the same time motor and sensory axons, or different types of sensory axons inducing undesired responses and mixed unpleasant sensations. Indeed, one of the most important features of a peripheral nerve electrode is its ability to selectively interface different axonal populations conveying distinct functions in a common nerve (Tyler & Durand, 2002) and with the best possible long–term performance. The number and distribution of ASs within the electrode surface increase the probability to specifically stimulate and/or record different groups of axons and thus linking different and complementary actions (Badia *et al.*, 2011a) (Figure 4).

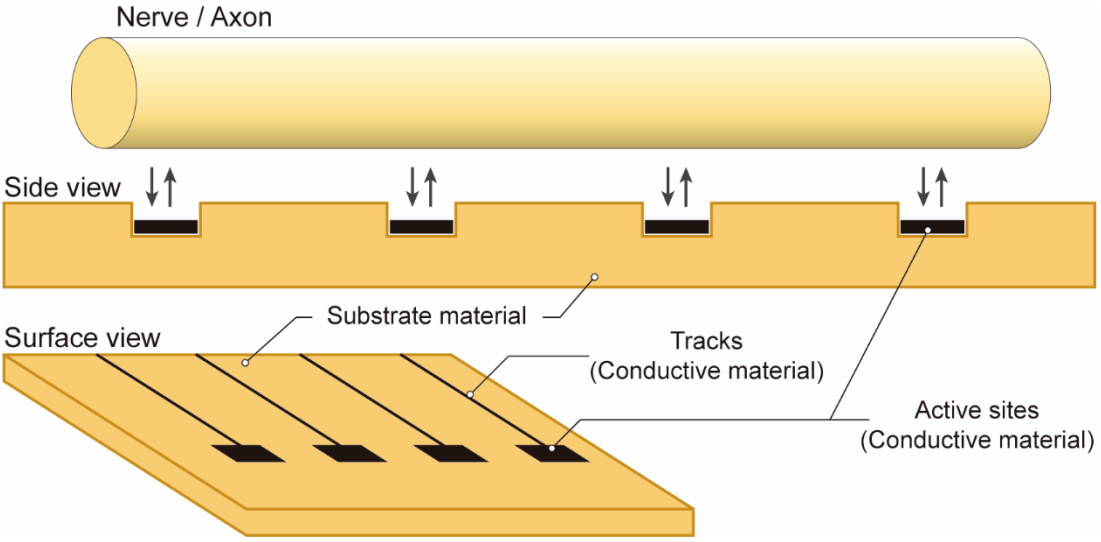

Figure 4. Nerve electrode structure. The conductive material is embedded in the substrate material. The active sites are the exposed portions of the conducting material where stimulation and recording (double arrows) of the nervous tissue occur. The conductive electrical tracks are electrically insulated from the tissue and connect the active sites with the rest of the electrical circuit.

Extracellular stimulation of the nervous tissue

An electrical field is generated when a difference of potential is applied between two electrodes. The voltage–gated sodium and potassium channels of the nearby nerve fibers are opened by this electric field. An action potential is produced and transmitted away from the stimulation site once sufficient channels to surpass the threshold potential have been opened. Action potentials generated in the motor fibers will ultimately cause the neuromuscular junction to release acetylcholine, which will then lead to the innervated skeletal muscle being excited and contracting. In contrast, action potentials produced in sensory axons will translate into sensory inputs and will be conducted along the sensory pathways to upper structures.

The threshold of stimulation is the minimum current required to elicit an action potential and is modulated by a) The separation between the axon and the AS providing the current; the farther the AS is from the axon, the greater the current needed to activate the nerve fiber (Ranck, 1975). b) The resistance of the nerve fiber to the electrical flow; larger axons are the first to be activated, due to the high density of voltage–dependent ion channels, in a phenomenon called inverse recruitment (Blair & Erlanger, 1933). The intensity, duration, and frequency of the applied stimuli are additional significant parameters to establish the stimulation threshold and the resulting input (Gorman & Mortimer, 1983). For example, an inverse relationship

exists between pulse intensity and duration; as the amplitude of the pulse increases, the duration required to stimulate the fiber decreases and *vice versa* (Bostock, 1983).

The ability of an electrode to be selective in stimulation will be given by the ability to stimulate different populations of axons from each of its ASs. Whether this population is activated or not, depends on the threshold of stimulation which ultimately relies on their distance from the AS and on the size of the stimulated fiber. Therefore, to increase selectivity, extensive understanding of the topographical structure of the implanted nerve is essential to guide the placement of the electrode (Badia *et al.*, 2010). When evaluating the selectivity achieved with a particular electrode design, it is usually expressed as the ratio of the specific response obtained after stimulation with respect to other responses relying on the same nerve (Veraart *et al.*, 1993a; Badia *et al.*, 2011a).

Extracellular recording of nerve signals from nerve fibers

At a given point along its path, an action potential shifts membrane potential due to a change in ion concentrations across the neuron membrane. When the action potential continues along the axon, the flow of ions across the membrane stabilizes at that point and the membrane potential remains at rest. Thus, an AS placed nearby an action potential can record the differences in membrane potential between this AS and another which acts as a reference electrode placed sufficiently separated to not be affected by the same action potential.

The magnitude of the potential sensed depends on a) The relative position of the electrode to the axons; voltage amplitude decays with distance from the current source (Gold *et al.*, 2006). b) The impedance of the tissue between the axon and the electrode, and the impedance of the electrode–electrolyte interface; impedance represents the ease with which electric current passes through the tissue and across the electrode–electrolyte interface. For example, the impedance of the epineurium is greater than that of the endoneurium. Thus, an electrode above the epineurium will record a smaller nerve signal than an electrode below the epineurium. Likewise, the smaller the AS area, the higher the electrode–electrolyte interface impedance. Electrode surface modifications such as pores are made to increase electrochemical surface area without increasing geometrical area (Raspopovic *et al.*, 2020). c) The

synchronization of nerve signals; when many axons are activated at the same time by mechanical, chemical, or electrical stimulation the summed current results in a larger signal (compound nerve action potential, CNAP). However, spontaneous signals resulting from natural sensory stimuli typically fire asynchronously. Hence, these signals recorded from the nerve activity (electroneurography, ENG) are characterized by low amplitude and high frequency compare to compound nerve signals (Tyler *et al.*, 2015).

The SNR is the amplitude of the signal of interest concerning the noise and its consideration is fundamental to obtaining high–quality signals. Nerve signals are weak, ranging from 10 to 100 μV within microns of the axon. Therefore, they are easily outweighed by nearby muscle contractions and thermal and shot noise from the recording circuitry. Accordingly, recording requires a very low–noise and high–gain amplifier system. To increase the SNR, ASs should be close to the activated axons and the impedance of the electrode should be minimum (Raspopovic *et al.*, 2020).

To further increase SNR the recording may be processed with the right frequency filters to decrease the input of unwanted signals. For example, low band–pass filters can eliminate EMG signals that typically peak around 300 Hz and high band–pass filters can eliminate thermal or shot noise. Consequently, ENG signals are analogically filtered between 1 and 3 KHz (Raspopovic *et al.*, 2020), which is included in the range of frequencies of neural signals (Haugland *et al.*, 1994).

Types of peripheral nerve electrodes

Different types of electrodes have been designed to interface the PNS. A widely accepted criterion for the classification of the different types of neural electrodes (Figure 5) relies on how they are implanted in the nerve and they interface peripheral axons (Navarro *et al.*, 2005). In this regard, extraneural electrodes are implanted outside the nerve, around the epineurium, showing a reduced selectivity as they will be able to stimulate or record only the most superficial axons. The more invasive intraneural electrodes are implanted transversally or longitudinally within the endoneurium, thus in closer contact with the axons of the nerve, offering an enhanced selectivity. Finally, regenerative electrodes are implanted between the stumps of a

sectioned nerve implying the most significant level of invasivity but with higher potential selectivity than the other interfaces.

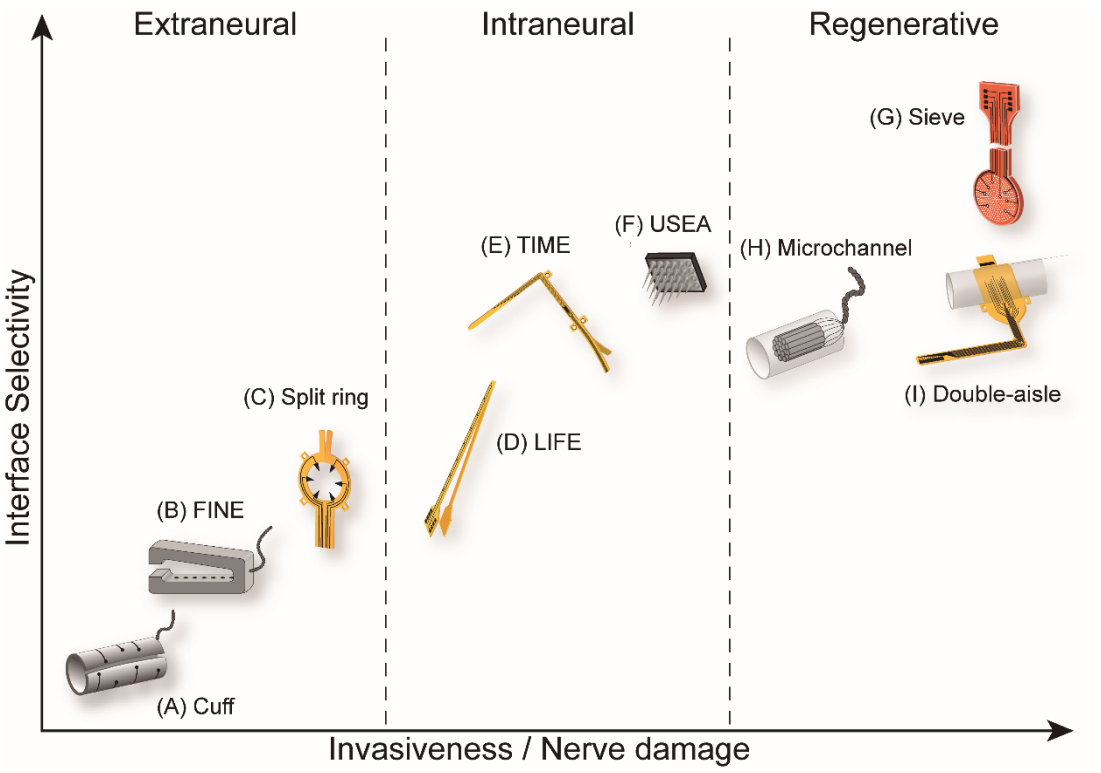

Figure 5. Electrodes to interface the PNS according to their selectivity/invasiveness ratio. Electrodes are classified depending on how they are implanted in a peripheral nerve: extraneural, intraneural and regenerative. **Extraneural**: (A) Cuff, (B) FINE and (C) Split ring electrodes. **Intraneural**: (D) LIFE, (E) TIME and (F) USEA electrodes. **Regenerative**: (G) Sieve, (H) Microchannel and (I) Double aisle electrodes (see text for abbreviations).

Surface electrodes

The easiest solution to interface the nervous system is to place an electrode on the body surface and stimulate the target tissue or record its electrical activity. Indeed, transcutaneous electrical stimulation through surface electrodes is still the most used technique to activate nerves or muscles (Keller & Kuhn, 2008), whereas applications that record electrical activity such as electromyography, electrocardiography and electroencephalography have been used in the clinic for more than a century. These electrodes are easy and cheap to fabricate. However, since the skin presents a high impedance barrier, correct positioning and fixation of the electrodes on the target are essential for the electrode to operate as well as an electroconductive gel to reduce resistance (Guo *et al.*, 2020).

Surface electrodes have been used to activate muscles (either via direct activation of the muscle tissue or through the motor nerve) to induce complex wrist and hand movements similar to functional tasks relevant to daily living in tetraplegic patients (Bouton *et al.*, 2016; Ajiboye *et al.*, 2017), FES systems such as foot drop correction (Wieler *et al.*, 1999) in people suffering hemiplegia, or to stand and walk a few steps (Graupe & Kohn, 1997) in paraplegic patients. On the other hand, surface electrodes have been also applied to activate afferent sensory fibers to induce conscious sensations (Kaczmarek *et al.*, 1991) and to provide sensory feedback in patients wearing myoelectric prostheses (Dosen *et al.*, 2014) and neuroprostheses (D'Anna, 2019). However, a comparison between sensory feedback (electrotactile stimulation) provided through surface or intraneural electrodes in patients wearing a prosthesis has shown that intraneural feedback can deliver more significant information and patients perform better in different motor tasks than when feedback is provided through the skin (Valle et al., 2020)

Extraneural electrodes

For neural interfaces that are implanted in direct contact with the nerve, extraneural electrodes show a low level of invasiveness among the different types of electrodes. The surgical procedure for the implant is less complicated than for other designs, making them easier to handle and safer to position, becoming an ideal option for different biomedical applications (del Valle & Navarro, 2013). On the other hand, as these electrodes are not in contact with fibers situated deep inside the nerve, mostly large myelinated fibers located at the outermost layer can be interfaced (Badia *et al.*, 2011a).

Cuff electrodes: A cuff electrode is based on an open cylinder or a spiral sheath of insulating material that is wrapped around the nerve with ASs exposed in the inner part facing the nerve. These electrodes induce almost no tissue disruption and nerve inflammation is kept to a minimum, although they can induce some compression and reshaping of the implanted nerve. The robustness of these devices in combination with the relatively simple method of fabrication (McCarty, 1965) and the reduced size and thickness of polymer cuffs (Stieglitz *et al.*, 2000) supports that a high number of FES systems and neuroprosthetic applications use cuff electrodes to stimulate or record from peripheral nerves (del Valle & Navarro, 2013). Multichannel cuff

electrodes (Figure 5A), with ASs disposed in tripoles, allow the selective stimulation of different nerve fascicles, each one supplying a different muscle or target (Veraart *et al.*, 1993a; Rodríguez *et al.*, 2000). Provided that the selectivity of these electrodes is lower in comparison with intrafascicular or regenerative interfaces (Badia *et al.*, 2011a), multiple cuff electrodes can be implanted in one or several distal nerves in order to achieve a higher degree of selectivity.

Flat interface nerve electrode (FINE): A variation of the cuff electrode is the FINE electrode (Figure 5B). This device is implanted by applying a small pressure on the nerve, reshaping the nerve into a flattened geometry. The change in shape allows the fascicles to align, approaching the surface, decreasing the distance from the ASs to central fascicles, thus improving selective interfacing (Tyler & Durand, 2002; Leventhal & Durand, 2003). However, it should be taken into account that too much reshaping force applied on the nerve may result in nerve damage (Tyler & Durand, 2003).

Both cuff and FINE electrodes implanted in the median, radial and ulnar nerves of patients showed that these interfaces allowed to deliver the subjects sensory feedback for up to two years, reproducing the natural perception areas and the innervation pattern of the interfaced nerves (Tan *et al.*, 2015). Moreover cuff electrodes have been shown to remain functional for more than ten years after implantation for stimulating motor axon populations without significant changes in the amount of current needed for recruitment (Christie *et al.*, 2017).

On the other hand, it should be taken into account that the epi–/perineurium has a high impedance that decreases the quality of the nerve signals that can be recorded (Raspopovic *et al.*, 2017). Hence, while cuff electrodes have been used for stimulation and also for recording from experimental animal nerves (Haugland *et al.*, 1994; Raspopovic *et al.*, 2010), there are not many studies in humans using cuff electrodes as bidirectional interfaces in neuroprostheses.

Regarding FES systems, while surface electrodes are preferred for their easiness of use and affordability, cuff electrodes offer better long–term outcomes (Popović, 2014). These electrodes can be used for chronic stimulation and/or recording nerve activity (Haugland & Hoffer, 1994; Hoffer *et al.*, 1996) to serve as the link between the nervous system and FES applications. For instance, cuff electrodes

can record somatic or autonomic nerve signals to trigger an external device that will perform a particular action and can also stimulate a nerve that will produce the desired outcome. In this regard, cuff electrodes have been implanted in the peroneal nerve to lift the foot in FES systems for the correction of foot drop (Waters *et al.*, 1975).

Split ring electrode: Other extraneural electrode designs have been reported in the literature. The split ring electrode (Figure 5C) is formed by a PI or parylene–C (ParC) stripe that adopts an open hoop shape with sharp inside projections containing the ASs (Xue *et al.*, 2015; Lee *et al.*, 2017). In the implantation, the split ring is opened and placed embracing the nerve and using the projections to push into the nerve achieving tight contact (Xiang *et al.*, 2016).

Intraneural electrodes

Intrafascicular electrodes are the current standard of intraneural interfaces in neuroprosthetic applications. They are implanted crossing epineurial and perineurial layers to be placed within the endoneurium. As their ASs are in close contact with a restricted subset of axons, they offer better selectivity than extraneural or interfascicular electrodes. Indeed, they need lower intensity for stimulation since they are not affected by the insulating properties of the epi– and perineurium, show lower crosstalk with the adjacent fascicles, and offer an increased SNR ratio for neural recordings (Micera et al., 2010). However, a more intimate contact between the interface and the axons may produce more nerve damage and encapsulation reaction that can interfere with the function of the electrode (Micera et al., 2008; Yoshida, et al, 2010).

Intraneural electrodes have been used to control neuroprostheses and re–create sensory feedback in human amputees, to pilot a wheelchair, or to command virtual robotic devices among other applications (del Valle & Navarro, 2013).

Longitudinal intrafascicular electrode (LIFE): LIFEs (Figure 5D) are inserted longitudinally into individual nerve fascicles, to lay in–between and parallel to the nerve fibers (Lawrence *et al.*, 2004), providing high interfascicular selectivity as they interface a limited group of axons within a given fascicle.

Several versions of LIFEs have been used in cats and rats to stimulate motor fibers and to record nerve signals elicited after stimulation of the skin and joints

(Malagodi *et al.*, 1989; Yoshida & Horch, 1993; Navarro *et al.*, 2007). Thin–film LIFEs (tf–LIFE) were implanted in the median and ulnar nerves of a human amputee to control an advanced robotic hand. The ENG motor signals registered through the electrodes implanted in both nerves were stable during the implant, allowing to perform independent types of hand grip with the prosthesis for one month. The different electrodes could stimulate sensory fibers to evoke discrete tactile sensations and decreased unpleasant phantom limb sensations up to 10 days (Rossini *et al.*, 2010).

Provided LIFE electrodes are implanted in a nerve fascicle, they may obtain high selectivity as they interface only nerve fibers within the implanted fascicle leaving non–implanted fascicles unstimulated. However, targeting multiple fascicles is needed to perform a wide variety of actions and induce sensations related to different body territories.

Transverse intrafascicular multichannel electrode (TIME): The TIME (Figure 5E) is similar to the PI tf–LIFE, but it is designed to be implanted transversally into the nerve in order to access different nerve fascicles with a single device (Boretius *et al.*, 2010). Just like the tf–LIFEs, TIMEs display a symmetrical configuration with ASs facing both sides of the electrode. The TIME was shown to allow good spatial resolution by traversing the entire nerve, and better inter– and intrafascicular selectivity than cuff or LIFE electrodes (Badia *et al.*, 2011a). TIMEs have been used to record nerve signals from different subsets of fibers in various fascicles and to stimulate distinct motor fibers to activate several muscles innervated by distinct branches of the nerve or even by axons within the same fascicle (Boretius *et al.*, 2010; Badia *et al.*, 2011a; Badia *et al.*, 2016). Experiments in rodents demonstrated the biocompatibility of TIME implanted for months, without nerve damage or functional loss, giving room for further human chronic implants (Badia *et al.*, 2011b; Wurth *et al.*, 2017).

An iteration of the TIME is the self–opening intrafascicular neural interface (SELINE). The body of the electrode incorporates four wings that can open transversely after the insertion offering a second dimension of contact between the electrode and the nerve. Therefore, more axons from different fascicles can be interfaced while the wings anchor the device to the nerve, reducing micromotions of the electrode within the endoneurium and decreasing potential fibrotic encapsulation and further electrical insulation (Cutrone *et al.*, 2015).

TIMEs have been used to recreate bidirectional feedback in human amputees (Raspopovic *et al.*, 2014). The main goal was not only to record motor complex information to command an advanced neuroprosthesis (Cipriani *et al.*, 2011), but also to allow the patients to feel what they were holding with the artificial hand without visual clues. After electrical stimulation of afferent fibers with implanted TIMEs in median and ulnar nerves, the patient was able to perceive different sensations referred to appropriate areas of his phantom hand and, after some training, to differentiate between hard and soft objects using a prosthetic hand. In this sense, the sensory feedback provided by TIME from the information gathered by sensors in the prosthesis allowed for a closed–loop control of the neuroprosthesis, improving the accuracy of task performance (Raspopovic et al., 2014; Valle et al., 2018) and even providing proprioceptive sensations with finger position information (D'Anna *et al.*, 2019).

Multielectrode arrays (MEA): The MEA consists of an array of tens of needles transversely inserted into the nervous system (Rutten *et al.*, 1999). The high number of electrical contacts in each device allows interfacing multiple axonal groups with high selectivity. However, MEAs may generate neural damage produced not only by the stiff structure of the electrodes, but also by the injury caused during the insertion of the many electrode tips. An evolution of this design is the Utah slanted electrode array (USEA), in which the needles have varying lengths to reach nerve fascicles at different depths (Figure 5F), thus offering a 3D interface (Branner *et al.*, 2001). Newer versions of these arrays include a higher density of electrodes per area (up to 25 per mm^2) (Wark *et al.*, 2013) and more flexible devices aimed to decrease nerve damage after implantation (Byun *et al.*, 2017; Kang *et al.*, 2019).

MEAs have been mainly used as micro interfaces to record neural signals from the brain cortex, allowing communication of paralyzed patients with computers, robotic assistive devices or even their own limbs (e.g. through FES systems) during years after implantation (Hochberg *et al.*, 2012; Ajiboye *et al.*, 2017). Studies in human amputees have also shown that USEAs implanted in the median and ulnar nerves can record motor nerve signals, which can be used to actuate the movements of a simulated robotic hand, and to stimulate nerve afferents for evoking sensory percepts in the phantom hand, thus enabling the closed–loop control of virtual limbs (Wendelken *et al.*, 2016, 2017). The nerve damage and subsequent inflammation caused

by the electrodes inducing axonal injury, deposition of fibrotic tissue around the implant and release of corrosive substances, which might have damaged the ASs, were the suggested reasons for this decline in electrode functionality (Christensen *et al.*, 2014, 2016).

Regenerative electrodes

Regenerative electrodes are implanted in the gap between stumps created after a peripheral nerve section. As the axons of the PNS retain the ability to regenerate after axotomy, they grow through or along the regenerative electrode, thus making intrinsic new contacts with the ASs placed along the regenerative guidance scaffold.

Sieve electrode: The first report of a regenerative electrode was the sieve electrode, composed of an array of via holes with electrodes built around them and where small populations of axons could grow (Mannard *et al.*, 1974). The sieve electrode design has evolved over the last decades from rigid materials to the highly flexible substrate of PI (Figure 5G), strongly improving its usability. Although no studies in humans have been reported to date, long–term studies in rats and cats have shown that sieve electrodes are able to record neural activity after mechanical stimulation of the skin in the paw (Lago *et al.*, 2006; Panetsos *et al.*, 2008). Long–term studies for a sieve electrode implant showed that axonal regeneration was not complete after 12 months. Moreover, the diameter of the axons and the myelin thickness did not recover to basal values after 12 months (Lago *et al.*, 2005) and some fibers appeared with signs of degeneration (Lago *et al.*, 2006). In this sense, the transparency of a regenerative electrode (i.e., the ratio between the open area that axons can grow through versus the total cross–section area of the electrode) and the diameters of the holes in which the axons need to grow, play an important role. Transparencies that are too low or narrow channels may hamper nerve regeneration and impair the interface (Navarro et al., 1996; Wallman 2001). On the other hand, too large channel size would decrease the selectivity.

Microchannel electrodes: An evolution of sieve electrodes is the microchannel electrodes (Figure 5H) in which the transparency is increased by providing wider channels for the axons to grow (Srinivasan *et al.*, 2015). In this case, the axons grow via thin narrow parallel tubes with embedded electrodes. To improve axonal

regeneration, specific cues can be included within the microchannels, making it possible to specify a certain path for a specific axonal population (del Valle *et al.*, 2018).

Double–aisle regenerative electrode: Other concepts of regenerative electrodes are the regenerative scaffold electrode (Clements *et al.*, 2007) and the double–aisle regenerative electrode (Figure 5I) (Delgado–Martínez *et al.*, 2017). These designs take transparency to its limit as the interface is a planar surface longitudinally placed within a regenerative tube, allowing axons to grow through much wider space, hence diminishing the possible compression of the nerve. With this approach regenerating axons can grow on each compartment of the device, allowing the maximal selective interfacing independent nerve branches (Delgado–Martínez *et al.*, 2017).

4. Foreign body reaction

After the implantation of any medical device, the immune system triggers a healing process. The FBR is a subset of processes within wound healing that occurs specifically when outside elements are within the injury. Restoration of tissue homeostasis is the outcome of both processes; however, this is not always possible. The wound healing as well as the FBR depend on multiple factors. A standard sequence of events following the implantation of a device is characterized by acute inflammation, chronic inflammation, and the tissue remodeling phase. These phases are described in detail in the following sections and summarize in Figure 6.

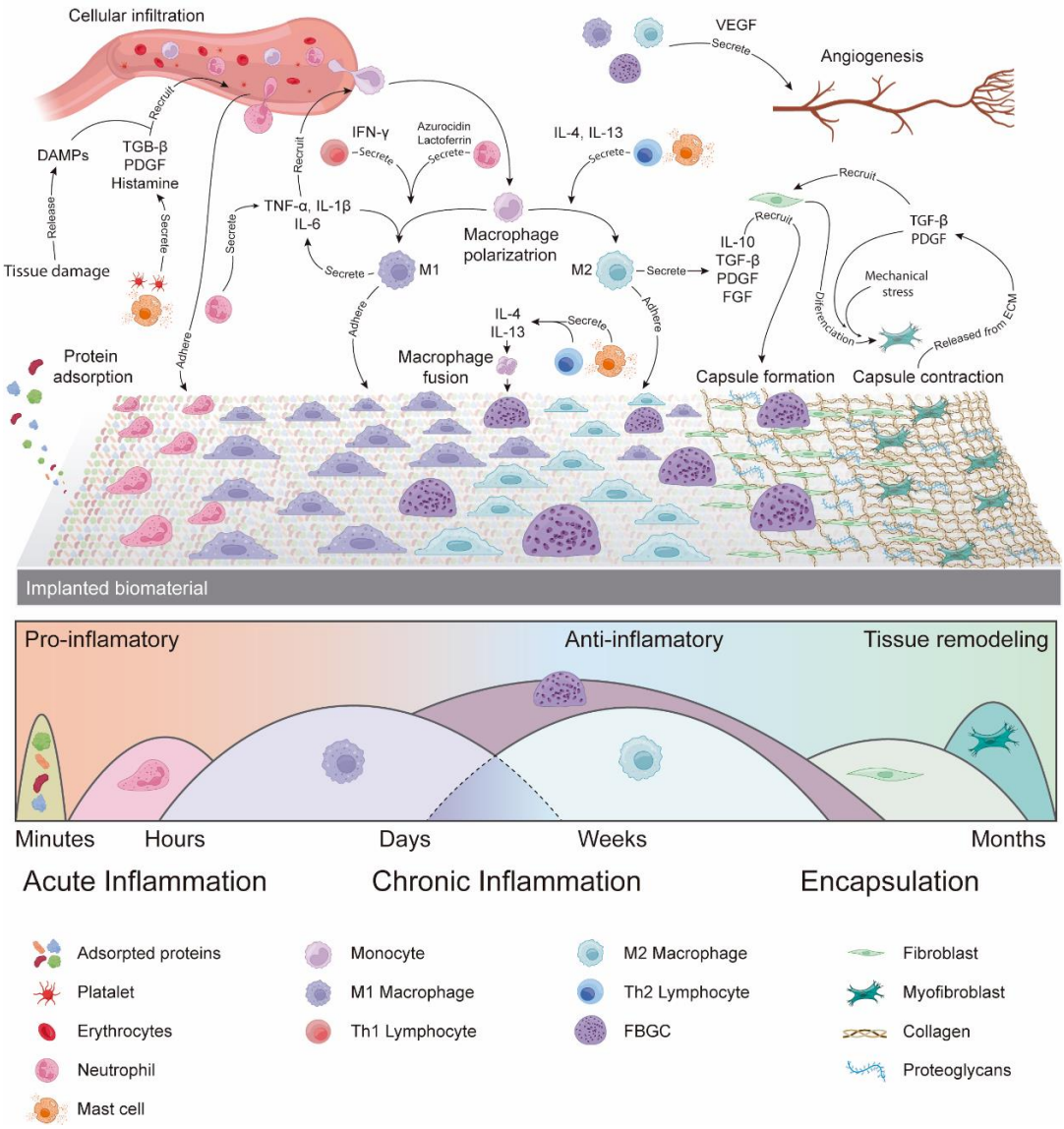

Figure 6. FBR following biomaterial implantation. Proteins from serum adsorb to the material surface crating a provisional matrix to which inflammatory cells attached. Chemoattractant factors released by activated platelets, endothelial cells, injured tissue cells and mast cells recruit circulating inflammatory and infiltrate the tissue by diapedesis eased by the increased capillary permeability. Neutrophils are the first cells involved in the innate immune reaction followed by macrophages. In the acute inflammation, macrophages acquire a proinflammatory (M1) phenotype once in the tissue. Macrophages secrete cytokines to foster macrophage recruitment and to attempt to phagocyte/degrade the foreign body. If the biomaterial remains, the course of inflammation progresses to its chronic stage in which macrophages also play a leading role. During this period, some macrophages fuse to form FBGC, multinucleated cells with superior phagocytic capacity. Over the weeks, macrophages begin to polarize to their anti–inflammatory phenotype (M2) and to recruit fibroblasts capable of generating a new ECM (capsule) that will surround the implanted material. Under the effect of profibrotic factors and mechanical stimuli, fibroblasts mature into myofibroblasts that remodel the existing ECM. Due to remodelling, more profibrotic factors trapped in the ECM are released, which enhance fibrosis. As a result, the capsule becomes more compact, thus isolating the implant from the rest of the body. During the FBR, numerous immune cells secrete angiogenic factors to increase the flow of cells to the site of damage and to support the newly formed tissue. The involvement of the adaptive immune system (Th1, Th2, dendritic cells) in the FBR is not entirely clear, however its production of cytokines seems to be the main polarizing force of macrophages.

Acute inflammation

Provisional matrix

Just after the surgical damage due to implantation, vasodilation of the local blood vessels and increased permeability of the capillaries allows leakage of large quantities of fluid into the interstitial space. Injured cells and resident–tissue immune cells secrete several molecules such as histamine, bradykinin, serotonin or prostaglandins that initiate the inflammation and repair processes, while an increased amount of fibrinogen and other proteins initiate the clotting of the extravasated plasma to stop possible hemorrhage. (Hall & Edward, 2011).

In a few minutes after implantation of a device, plasma components from the blood of damaged vessels, including albumin, fibrinogen, fibronectin, vitronectin, gammaglobulins, lipids, sugars and ions, are rapidly and spontaneously adsorbed on the implant surface (Mariani *et al.*, 2019). This provisional matrix attached to the implant surface conditions the biocompatibility of the implant in future steps resulting in different outcomes in the long term. Subsequently, the composition of this provisional matrix will change depending on the affinity that the different components have for the surface of the implanted device, in a process known as the Vroman effect (Vroman, 1988).

The characteristics of the material can modify the type of matrix that is attached to the material. For example, anti–fouling materials are preferred because they reduce non–specific protein adsorption (DiEgidio *et al.*, 2014). Although both hydrophilic and hydrophobic materials can exert anti–fouling features, more prominence has been given to the former due to its better biocompatibility (He *et al.*, 2021). Hydrophilic materials are covered by a hydration layer which prevents protein adsorption whereas hydrophobic materials prompt hydrophobic interaction with proteins. Therefore, the average unfolding of a protein is larger on hydrophobic surfaces. Notably, hydrophobic portions of biological molecules are universal damage–associated cues that may exacerbate the immune response (Moyano *et al.*, 2012).

Once deposited, the provisional matrix drives the interaction body–material (Hirsh *et al.*, 2013). The ideal material would be that which produces a matrix with the

least immunogenic capacity, reducing the immune response to the biomaterial and therefore increasing its biocompatibility.

Cellular infiltration

Systemic innate immune cells are recruited by chemoattractant factors such as transforming growth factor (TGF–β), platelet–derived growth factor (PDGF), CXCL4 (Platelet Factor, PF4), leukotriene (LTB4), interleukin–1 (IL–1) and histamine released from activated platelets, endothelial cells, injured tissue cells and mast cells. (Anderson, 2008; Mariani *et al.*, 2019). These chemical signals attract circulating cells to the wound site and infiltrate into the tissue by diapedesis helped by the increased capillary permeability.

Neutrophils are the first and predominant cells to reach the damaged area after lesion and bind to adsorbed proteins of the provisional matrix by means of β2 integrins (Anderson, 2008). Toll–like receptor (TLR) and pattern recognition receptor (PRR) also activate neutrophils in presence of bacteria components or dead cell residues (Ode Boni *et al.*, 2019). However, due to the short life expectancy of neutrophils (24–48h) and a shift in chemotactic factor profile orchestrated by neutrophils that secrete chemoattractant IL–8 and pro–inflammatory cytokines IL–1β, tumor necrosis factor α (TNF–α) and IL–6 (Ode Boni *et al.*, 2019), monocytes become the main cellular component in a subsequent phase (Anderson & Jiang, 2016).

Once in the tissue, monocytes differentiate into macrophages in two major phenotypes, M1 and M2, in response to the specific microenvironment. M1 macrophages exhibit a proinflammatory profile to debride the wound along with neutrophils. M2 macrophages become significant towards the resolution of wound healing by secreting anti–inflammatory molecules. Monocytes differentiate under the influence of interferon γ (IFN–γ), TNF–α, granulocyte–macrophage colony–stimulating factor (GM–CSF), bacterial products like toll receptor 4 (TLR4)–binding lipopolysaccharide (LPS), azurocidin, lactoferrin and other TLR ligands (Herrero–Cervera *et al.*, 2022). Of these, IFN–γ is the main cytokine inducing the pro–inflammatory M1 phenotype and the main Th1 cell product (Scatena *et al.*, 2016). Monocytes/macrophages adhesion to the provisional matrix is provided by means of integrins β1, β2 and β3, which bind fibronectin, laminin, intercellular adhesion molecules (ICAMs), complement fragment C3bi, fibrinogen and vitronectin along

with other RGD domain containing extracellular proteins (Anderson, 2008). After biomaterial–cell interaction, neutrophils and macrophages become activated and attempt to destroy/degrade the biomaterial through phagocytosis, proteolytic enzymes, and reactive oxygen species (ROS) released by cytoplasmic granules (Labow *et al.*, 2001). Neutrophils also release neutrophil extracellular traps (NETs), fibrillar nets made of granular proteins, neutrophil elastase, and chromatin (Sperling *et al.*, 2017). Excessive production of NETs favors thrombogenesis, increasing platelets adhesion and activation which reinforce pro–inflammatory cytokines and chemokines production, ultimately amplifying the recruitment of M1 macrophages and causing chronic inflammation. The hostile inflammatory environment created by macrophages and neutrophils may cause biomaterial to breakdown or degrade conveying to the leaching of toxic species into the tissue from underlying layers.

Assuming that the phagocytic cells successfully degrade and phagocytose the biomaterial, the acute inflammatory process would come to an end and the appropriate mechanisms would be activated to return homeostasis to the tissue. Some medical devices are meant to degrade after they have carried out their therapeutic function, thus avoiding chronic inflammation. For example biodegradable scaffolds for tissue regeneration (Bitar & Zakhem, 2014) or some regenerative conduits for guiding peripheral nerve regeneration (Pierucci *et al.*, 2008). Instead, other devices are designed to carry out their therapeutic role for long periods. Generally, these medical devices are too large to be internalized (>5 μm) (Anderson & Jiang, 2016), so cells can not phagocytize them and the FBR transitions into its chronic stage.

Chronic inflammation

Chronic inflammation refers to a prolonged inflammatory response characterized by the simultaneous destruction and repair of the tissue. Monocytes, macrophages, and lymphocytes are most commonly associated with toxicity or infection, whereas in the FBR macrophages and foreign body giant cells (FBGCs) are the main cells implicated. Blood vessel proliferation and the development of connective tissue are common to both inflammation processes and normal wound healing (Anderson & Jiang, 2016). A short duration of this phase is expected with biocompatible materials, however, prolonged periods of inflammation (weeks,

months or even years) may suggest infections, release of toxic products from the biomaterial or implant micromotion within the tissue.

Macrophages play a critical role in the chronic inflammatory phase and in the FBR to implanted biomaterials. Due to their phenotypic diversity and, therefore, their variety in released products, macrophages show pro–inflammatory, anti–inflammatory and tissue remodeling functions. As commented in acute inflammation classical classification of macrophages includes M1 (proinflammatory) and M2 (anti–inflammatory, regulatory, pro–resolutive) macrophages. Even though further characterization of macrophages has led to the description of several subtypes (Scatena *et al.*, 2016; Krzyszczyk *et al.*, 2018), the classical classification helps to explain the different phases of chronic inflammation.

Pro–inflammatory M1 macrophages define the first stage of chronic inflammation characterized by IL–1β, TNFα and IL–6 cytokines release, as well as inflammatory factors, such as various CXCL and CCL chemokine ligands, ROS, NO and matrix metalloproteinase (MMP–2 and MMP– 9) (Krzyszczyk *et al.*, 2018). M1 macrophages also secrete vascular endothelial growth factor A (VEGF–A), which participates in the early and later stages of the FBR inducing the formation of neovessels that maintain cell recruitment (Dondossola *et al.*, 2016). A pro–inflammatory environment enhanced by M1 macrophages along with their phagocytic activity cleans the wound to allow tissue regrowth. M2 macrophages appear towards the end of the inflammatory response and contribute to finishing and resolving inflammation, stimulating healing and restoring tissue homeostasis, characterized by proper vascularization and little or no fibrosis (Scatena *et al.*, 2016). Stimulated by IL–4, IL–10 and IL–13, M2 macrophages express high levels of the mannose receptor (CD206), dectin–1 and secrete IL–10 and TGF–β. A defective transition from the M1 proinflammatory environment to a more M2 anti–inflammatory milieu is believed to contribute to the impairment in tissue repair in chronic wounds (Krzyszczyk *et al.*, 2018).

Although temporal changes in M1/M2 ratio is recognizable in normal wound healing, both macrophage phenotypes are concurrently observed in the tissue–material interface in the FBR (Moore & Kyriakides, 2015; Scatena *et al.*, 2016). Macrophages are sensitive to different materials changing their phenotypic profile

(Jones *et al.*, 2007), which may modify the overall biocompatibility of the implanted device. For example, biomaterials with a persistent M1 pro–inflammatory macrophage response have been associated with scar tissue formation, encapsulation, and seroma formation. On the contrary, biomaterials that elicit an M2 pro–remodeling macrophage phenotype after the M1 response promote stem cell recruitment/proliferation and constructive tissue remodeling with less fibrotic scar (Brown *et al.*, 2012; Scatena *et al.*, 2016). Consequently, several attempts have been made to determine the result of the FBR, shifting the M1/M2 balance, administering drugs or tunning the characteristics of the material itself. However, strategies to promote either the M1 or M2 phenotypes of macrophages will not necessarily be successful because of the complexity of the involvement of both phenotypes in fibrotic reactions (Witherel *et al.*, 2019).

As commented above, implanted biomaterials are usually too large to be internalized by macrophages. In an attempt to increase their phagocytic capability, several macrophages fuse to form FBGCs, large polynucleated cells that are a hallmark of chronic inflammation and specifically of the FBR (Anderson & Jiang, 2016; Mariani *et al.*, 2019). Cell–cell fusion of macrophages depends on the acquisition of fusion competency, cell migration towards each other and cytoskeletal rearrangement. Those processes are conditioned to the presence of the mast cells cytokines, IL–4 and IL–13 but many other factors participate in macrophage fusion. These include monocyte chemotactic protein 1 (MCP–1), matrix metalloprotease 9 (MMP–9), epithelial cadherin (ECad), cell surface receptors and membrane proteins (DAP12, MR, CD44, CD47, DC–STAMP, tetraspanins), signal transducers (Rac1), and the matricellular protein osteopontin (Scatena *et al.*, 2016). FBGCs release similar degradative and chemoattractive factors than macrophages. Besides the superior phagocytosis capabilities of these cells, little is known about other additional functions that they may have compared to macrophages. In addition, even if the FBGCs are capable of engulfing larger particles, generally, the biomaterial will remain impossible to phagocyte due to its size compared to cells. Consequently, FBGCs will adhere to the surface of the biomaterial, forming a barrier between the tissue and the device that eventually may lead to the impairment of implant function.

Tissue remodelling phase

The final stage of wound healing is the formation of new tissue to restore the damaged area. Depending on the localization and severity, wound healing will differ from full tissue restoration to larger areas of fibrosis. In the FBR associated to non–degradable biomaterials, cells cannot completely reconstitute the original architecture. Instead, a scar tissue or fibrotic capsule is formed to isolate the biomaterial from the body (Anderson & Jiang, 2016). Granulation tissue, a hallmark of the healing inflammation, is identified by the presence of macrophages, fibroblasts and vascular endothelial cells and it is the previous step to the formation of scar tissue.

High and constant influx of TGF–β secreted by M2 macrophages foster the recruitment of fibroblasts which synthesize first proteoglycans and collagen to remodel the ECM (Anderson & Jiang, 2016). Mechanical signals of the newly formed ECM, TGF–β and PDGF favor the transition from fibroblast to myofibroblast, cells with both fibroblast and smooth muscle cell phenotypic features which participate in matrix remodeling as well as in capsule contraction in later steps. Besides its superior collagen synthesis, myofibroblasts remodel the ECM, which activates latent profibrotic factors trap in the ECM that enhance fibroblast recruitment (Wipff *et al.*, 2007). Fibroblasts recruited from nearby connective tissue are the main source of myofibroblast (Anderson & Jiang, 2016). Excessive secretion by fibroblast and myofibroblast results in the undesirable fibrotic deposition of ECM. Besides greater ratio of I/III collagen is associated with a greater fibrotic tissue formation (Mariani *et al.*, 2019). Angiogenesis is also promoted through VEGF–A secreted by different immune cells.

The overall result of this process is the formation of a fibrotic capsule around the biomaterial which cannot be eliminated from the body. The thickness of the fibrotic capsule is related to the biocompatibility and the physical properties of the implanted material. For example, circular shapes (Matlaga *et al.*, 1976) and smaller implants (Veiseh *et al.*, 2015) result in a lesser FBR. Even though, a fibrotic capsule may or may not have a positive impact on the implant depending on its function. Thus, de la Oliva, (2018d) suggested a classification regarding the intended function of the implants: 1) implants with an acute or temporal function (e.g., tissue regeneration), in which the material should be degradable and disappears before the encapsulating phases of the FBR are triggered; 2) implants with a chronic supporting function (e.g.,

joint replacement), which should have excellent durability, and 3) chronic implants intended to interact with the tissue (e.g., sensors, neural interfaces, electrodes), in which little or no encapsulation should occur to ensure its chronic functionality (Boddupalli *et al.*, 2016).

The adaptive immune system

The immune system follows two strategies to defend the body, innate and adaptive immunity. Innate immunity concerns non–specific mechanisms to identify and remove foreign substances through the action of monocytes, macrophages, polymorphonuclear cells and some lymphocytes. Adaptive immunity refers to specific mechanisms carried on by lymphocytes (B and T cells) which take more time to develop. Although the innate immune system is the main orchestrator in the progression of the FBR (Rodriguez *et al.*, 2007), the existence of a cross–talk between innate and adaptive immune cells has been pointed out. However, the exact role of the adaptive immune system remains contradictory and unclear.

Cells involved in adaptive immunity have been found in the FBR. Dendritic cells, which are the main antigen–presenting cells to T cells, bridge the gap between the innate and adaptive immune systems. T cells activate other immune cells, kill infected host cells, and regulate the immune response. A subset of T cells expressing CD4 are helper T cells (Th) which under specific signals differentiate into Th1, Th2, Th17 and Treg exerting different functions. B cells are primarily recognized for their ability to produce antibodies and are activated by their own antigen–recognition receptor.

Antigen–dependent (Wang *et al.*, 2022) and independent pathways (Rodriguez *et al.*, 2007) have been proposed to explain role of the adaptative response in the FBR to non–phagocytosable implants. The presence of T cells in the early (Brodbeck *et al.*, 2005; Gretzer *et al.*, 2006) and later stages (Chung *et al.*, 2020) of the FBR has been confirmed. In the early response to pathogens, T cells are recruited in an antigen–independent way due to the expression of appropriate adhesion molecules that drives them to the inflammation site. Hence, this mechanism could also take place in implanted materials (Murphy & Weaver, 2017; Adusei *et al.*, 2021).

Regardless of how the activation of the adaptive pathway occurs, it participates in the FBR. For example, IFN–γ, which is secreted by Th1 cells, participates in the differentiation to M1 macrophages and the fusion of macrophages into FBGCs is supported by cytokines production (Il–4 and Il–13) of mast and Th2 cells. Additionally, surface chemistry, wettability, topography and charge of biomaterials can shift the dendritic cell state towards immunological tolerance or activation (Wang *et al.*, 2022). Nevertheless, although some animal models lacking components of the adaptive immune system have shown an attenuated FBR, in most cases the FBR remains unaltered (Kyriakides *et al.*, 2022).

FBR in nervous tissue

Although FBR is a common set of processes, there are some differences depending on the tissue where it occurs, for instance, CNS is an immune–privileged site with its own immune cells. Thus, the specific features of the host response to implantable devices in the CNS and differences with the PNS will be discussed below.

Central nervous system

After the implantation of a biomaterial in the CNS, microglial cells in the vicinity become activated, sending long projections toward the injury site (Kozai *et al.*, 2012). In the first 24 hours, a great number of microglia cells migrate to surround the implant followed by astrocytes with a response that becomes robust over several days (Szarowski *et al.*, 2003). Blood–brain barrier (BBB) disruption due to implantation also allows systemic monocytes to migrate (Ravikumar *et al.*, 2014). Release of blood and plasma contents such as albumin, globulins, fibrin/fibrinogen, thrombin, plasmin, complement, and hemosiderin from the disrupted BBB foster the recruitment of activated microglia, macrophages, and astrocyte activation. Brain tissue response to injury is also characterized by the release of chemical factors (e.g., TNF–α, IL–1, IL–6, MCP–1, and TGF–β) (Ghirnikar *et al.*, 1998). The continued presence of an implant and the impossibility of cells to destroy it by phagocytosis and other proteolytic molecules causes the chronification of inflammation rather than the initial surgical damage during implantation (Polikov *et al.*, 2005). Micromotion of the electrode, persistent BBB leakage, and mechanical compliance mismatch between electrodes and brain tissue also sustained this persistent response. Chronic inflammation in the CNS

is characterized by the encapsulation of the implanted devices, forming the so–called glial scar, to hamper the progression of tissue damage and isolate the foreign body (McCreery *et al.*, 2016). After one–week microglia and astrocytes can be seen covering an area approximately 3–4 times the size of the injury. At two weeks, the cellular distribution appears to represent distinct, segregated layers with microglia close to the implant and astrocytes wrapping the microglia layer. Finally, from 4 to 12 weeks, both layers become more compact and localized (Szarowski *et al.*, 2003). FBGCs are also present but it is not clear whether macrophages coming from systemic circulation and microglial cells fuse indistinctly to form those multinucleated cells (Moss *et al.*, 2004; Gällentoft *et al.*, 2016).

Peripheral nervous system

Unlike the CNS, the PNS does not have a specific population of immune cells, so the FBR develops similarly to other tissues. As described above, the implantation of biomaterials triggers a process of three main phases: the recruitment of leukocytes in the acute phase, proliferation and chronification of inflammation when the foreign body remains inside the nerve and deposition of a fibrotic capsule around the implant which is part of the tissue remodeling process. Macrophages play a leading role during the entire wound healing process and the FBR. Recent transcriptomic analyses have allowed the discrimination of three populations of macrophages during wound healing: systemic monocytes that differentiate into macrophages in the nerve, nerve resident macrophages of the perineurium and nerve resident macrophages of the endoneurium that are in contact with axons. Although it is not completely clear the exact role of each macrophage population, in a mouse model of sciatic nerve crush injury it was shown that macrophages derived from monocytes were numerically dominant and drove the nerve repair. However, the endoneurium resident macrophages were activated first, increasing their production of monocyte–attracting chemokines. In contrast, epineurium resident macrophages remained quiescent without major changing in their transcriptomic signature. After functional recovery, the remaining macrophages inside the nerve adopt a PNS macrophage profile (Amann & Prinz, 2020; Ydens *et al.*, 2020). It is uncertain, though, whether the same would happen in the FBR, considering that different injuries can lead to different macrophage involvement.

Different studies have described the nerve tissue response to implanted extraneural (Leventhal *et al.*, 2006; Christensen & Tresco, 2018), longitudinal (Lago *et al.*, 2007) and transversal (Badia *et al.*, 2011b; de la Oliva *et al.*, 2019) electrodes and also to multielectrode arrays (Christensen *et al.*, 2014, 2016). An extensive characterization of the FBR to intraneural implants can be found in the reports made by Navarro's group (de la Oliva *et al.*, 2018b; de la Oliva 2018c) and Wurth and colleagues (Wurth *et al.*, 2017). After implantation in rat sciatic nerve, macrophage infiltration increases gradually between day one to one–two weeks, followed by a progressive decline in the next weeks or months. Similarly, FBGCs population increases at 2 weeks but is maintained until 8 weeks. Inflammatory cells were still present in the chronic stage compared to intact nerves even after 8 months. The capsule appears soon around the devices, acquiring maximal thickness at 2 weeks. At that time, the capsule is mainly composed of inflammatory cells. From 2 weeks onward, the capsule undergoes remodeling, transitioning to a more acellular composition. This transition corresponds to the clearance of immune cells, marking the end of the inflammatory phase. By week 8, fibroblasts and collagen are already visible around the implant. The capsule may be stabilized or increased at different stages depending on the material implanted. Lastly, cellular infiltration and capsule development timings are not only determined by the tissue but also by the material implanted. In this regard, specific characterization of FBR to each material and implant should be done to apply the best strategy to reduce FBR. Otherwise, physical isolation, increased impedance and neural loss due to FBR and encapsulation will reduce long–term functionality by a progressive decay in signal recording and stimulation capabilities (He & Bellamkonda, 2007; Grand *et al.*, 2010).

5. Biocompatibility of neural electrodes

Although a significant breakthrough has been seen in the technology of neural implants (Kostarelos *et al.*, 2017; Cutrone & Micera, 2019), the body's response against these devices reduces their potential. Accordingly, strategies to weaken the FBR based on immunosuppression or non–immunogenic materials were developed. However, the FBR cannot be fully ablated since it is part of an innate set of basic reactions to fight against pathogens and recover from wounds. To complement these

strategies, new approaches are aimed at creating materials that interact with the components of the innate immune system to modulate the immune response and to further reduce implant complications derived from FBR (Mariani *et al.*, 2019).

Although biocompatibility is usually thought of as a property linked to the intensity of the body response to the biomaterial, we have also to consider the implant function. In this sense, biocompatibility is related to the ability of an implant to carry out the task for which it has been designed, causing an appropriate reaction in the body (Anderson, 2008). The biocompatibility of a device is determined by numerous factors, from the physicochemical properties of the implanted material (shape, size, surface molecules, Young's modulus), the organ where it is engrafted, the function it has to carry out and the way it is implanted (speed, surgical approach) (He & Bellamkonda, 2007). Implant materials must also be resistant to delamination, corrosion, breakage, and failure of interconnections. Moreover, none of the implanted materials should generate or leach any form of chemical products, such as oxidative species or solvents (Patrick *et al.*, 2011; Szostak *et al.*, 2017).

Biomaterials

Based on their origin, biomaterials can be classified as naturally or artificially– derived. Naturally–derived materials from endogenous origin or that keep similar structure to endogenous compounds, are biocompatible and degradable. Besides, they can integrate with the surrounding tissue, through cellular activities such as cell attachment and cell–cell communication. Nonetheless, special caution must be taken to xenogenic materials which can elicit adverse immune responses. Some naturally–derived materials, used for neural implants, are collagen, gelatin, chitosan, hyaluronan, heparin, alginate, silk, agarose and fibrin (Brovold *et al.*, 2018). A more recent approach makes a profit from decellularized tissue matrices which through a set of physical and chemical steps reduce antigen load and preserve ECM native architecture whose proteins are highly conserved across species (Badylak *et al.*, 2009). These natural scaffolds are mainly used to contribute as a mechanical support that favors infiltrating cells to support regenerative processes (Contreras *et al.*, 2022).

The properties of artificially–derived materials frequently stand in opposition to naturally–derived materials. They may elicit immune response and offer a lower

ability for cell interaction, but their physicochemical and mechanical characteristics can be more easily adjusted. Besides, the increased stability of artificially–derived materials, makes them suitable for long–term application. Polymeric materials such as polyglycolide (PGA), polylactic acid (PLA), polycaprolactone (PCL), polyurethane (PU) or polytetrafluoroethylene (PTFE) are the most widespread in the field of neural applications. Metal (stainless steel, cobalt alloys, titanium) and ceramic (glass, aluminum oxide, zirconium oxide, calcium phosphate) materials are mostly used in orthopedics and dentistry and as part of composite materials, consisting of two or more types of materials (Hassler *et al.*, 2011), as well as enclosing cover for electronic devices.

A neural interface is generally composed of a non–conductive material which is the substrate for a conductive material, that will transmit the electrical pulses. All the components that make the neural interface must be taken into account when assessing biocompatibility, although, certainly, the surface occupied by each one will also determine the intensity of the body response.

Conductive materials

Metals are commonly used as conductive materials located in recording and stimulation ASs and in the conductive tracks along the device. Gold, platinum, tungsten, and iridium are found overall safe and are regularly used in biomedical applications. Silver, silver/silver–chloride, pure iron, cobalt, palladium, and copper are considered toxic, as they provoke immune response and may release toxic elements (Szostak et al., 2017). Neural prostheses functionality relies on their ability to interface neurons. Thus, the smaller the recording and stimulation AS, the more selective the stimulation of axons or neurons and the recording of electrical activity. However, size and impedance are inversely proportional, so smaller ASs able to record from small fields, are noisier, exhibiting worse recording quality (Viswam et al., 2019), and are also less functional because they release small amounts of stimulating current comparing to large ASs (Negi et al., 2012). To decrease the size of ASs without worsening stimulation/recording quality due to increased impedance, metallic materials performance is enhanced when combined with other materials such as conductive polymers (Green & Abidian, 2015) or when their effective geometrical surface is increased (Brunton et al., 2015). Conductive polymers should show

biocompatibility, fast charge transfer and may be functionalized with nano– or drug–releasing structures. Other nanostructured materials such as platinum black, platinum grass, carbon nanotubes or GBMs are roughened or functionalized to increase electrical performance (Pigeon et al., 2003; Chung et al., 2015). For example, carbon nanotubes have a significantly increased surface area and hence improve charge storage capacity and injection limit to efficiently and safely deliver current to the tissue (Szostak et al., 2017).

Substrate materials

The other critical component of chronically implantable interfaces is the dielectric or insulation layer which is the substrate where conductive material is deposited. Dielectrics prevent electrical shunting or attenuation, ensuring that electrical current travels unimpeded through the conductor. They should have a low dielectric constant and no capacitance, allowing small electrical traces to be packed close together (Wellman *et al.*, 2018). Regarding mechanical properties, the material must be flexible and soft to reduce the mechanical mismatch between the device implanted and the host nervous tissue (Young's modulus ranging between 100 Pa and 10 kPa (Kostarelos *et al.*, 2017)). Insulator materials may also serve as passivators by protecting conductor materials from undesirable physicochemical reactions (Won *et al.*, 2018). Some commonly employed insulating–supporting materials include silicone or polydimethylsiloxane (PDMS), PI, ParC, and SU-8.

PI represents a class of polymer of imide monomers. It is a good candidate for flexible neural implants due to its good chemical and mechanical durability, low water uptake and electrical insulation properties (Rubehn & Stieglitz, 2010). Good biocompatibility (Stieglitz *et al.*, 2000) and stability over long–term studies *in vitro* and *in vivo* has been addressed (Rubehn & Stieglitz, 2010; Wurth *et al.*, 2017). However, it has a high Young's modulus (around 5 GPa for thin PI–based devices (Kostarelos *et al.*, 2017)), which may decrease its biocompatibility and integration in the tissue. Different PI–based designs have been developed for PNS (Rodríguez *et al.*, 2000; Stieglitz, 2001; Lago *et al.*, 2007; Boretius *et al.*, 2010) and CNS applications (Stieglitz *et al.*, 1997; Rousche *et al.*, 2001), being the most used substrate for intraneural electrodes in the last decades. The first systematic *in vitro* evaluation of commercial PI

dates back to 1993 (Richardson et al 1993). Although PI is generally characterized as biocompatible, the formulations and manufacturing processes are not always the same. As a result, PI has variable characteristics that can affect its biocompatibility and stability (Constantin *et al.*, 2019)

Graphene–based materials for neural electrodes

Graphene is a two–dimensional nanomaterial with a single carbon atomic layer (Novoselov *et al.*, 2012). Since its discovery, interest in graphene has grown considerably, leading to the development of GBM with varying chemical compositions (pristine graphene, oxide graphene, reduced oxide graphene) and three–dimensional structures (sheets, nanotubes). Neural electrodes may take advantage of this unique combination of features, including high electrical conductivity, chemical stability, flexibility and biocompatibility (Devi *et al.*, 2021; Wei & Wang, 2021). To understand how GBM could become a breakthrough in neural electrodes for interfacing external prosthetic devices, first, it is worth knowing the technological challenges that must be overcome. There are two main features for a neural electrode to consider, as indicated above: the electrical characteristics of the electrode that determine its ability to stimulate and record from the nervous system; and the biocompatibility that determines its integration and stability within the tissue.

Electrical characteristics

Current clinical technology of neural implants is mostly based on millimeter–scale metallic electrodes. However, the control of prosthetic devices relies on selectiveness, meaning stimulating and recording small populations of neurons without activating or recording neighboring populations. This has led to the miniaturization of neural electrodes. For neurostimulation, a minimum level of charge needs to be injected through the electrode to elicit a functional response. The injection capacity of an electrode depends on the electrolytic double–layer capacitance and on its charge injection limit (CIL). Some GBM such as porous reduced graphene oxide or 3D graphene forms, dramatically improved current injection capacity maintaining stimulation capabilities with electrodes of small size (Apollo *et al.*, 2015; Lu *et al.*, 2016). Likewise, when the dimension of a recording electrode is reduced, its impedance

increases, hampering signal recording due to increased noise. In this case, electrode materials with a high double–layer capacitance, such as graphene, may be used (Kostarelos *et al.*, 2017). Furthermore, as graphene is a semiconductor, recording sensors can be fabricated on a field–effect transistor (FET) configuration, based on the modulation of the transistor current induced by the electrical activity in the vicinity of the transistor gate (Hess *et al.*, 2011). In this configuration, the biological signal is amplified which reduces the sensitivity to external noise. Besides, the number of transistors that fit into an array is higher compared to systems that use electrode configuration, increasing spatial resolution. The exceptional transconductance of graphene, which enhances FET's amplification capabilities and its low impedance, leads to recordings with a high SNR (Kostarelos *et al.*, 2017).

Biocompatibility

Any implantable device triggers the FBR. To minimize this process, implanted materials should be biocompatible. Given that graphene exists in many forms, each variant biocompatibility should be studied individually. Nevertheless, GBM used for neural electrode applications has been tested *in vitro* and *in vivo* proving its biocompatibility (Convertino *et al.*, 2018; Nguyen *et al.*, 2021). Furthermore, graphene can be easily integrated into flexible substrates (Apollo *et al.*, 2015) to balance the mechanical mismatch which plays a significant role in the intensity and duration of inflammatory and healing processes after implantation (Lacour *et al.*, 2016). Electrochemical reactions at the electrode–electrolyte interface can impact biocompatibility, for example, acidifying the medium. These reactions occur when the stimulation is produced by faradic mechanisms that involve redox reactions between the electrode and the tissue (Cogan, 2008). Fortunately, some GBM, e.g., porous reduced graphene oxide, have a high charge injection capacity, which increases the amount of current that can be delivered to tissue without irreversible reactions (Lu *et al.*, 2016; Wei & Wang, 2021).

Besides its electrical characteristics and biocompatibility, other aspects make graphene attractive. The transparency of graphene allows the combination of stimulation/recording capabilities with other techniques such as calcium imaging (Kuzum *et al.*, 2014), fluorescent microscopy and optogenetics (Park *et al.*, 2014). Functional modifications on graphene are performed to expand their application.

Altering graphene composition by adding functional groups such as amino, carboxyl, hydroxyl, alkyl halogen, azide or 3D structuring (John *et al.*, 2015) can enhance electrical properties, increase biocompatibility (Devi *et al.*, 2021) or open the possibility of conjugating therapeutic compounds onto graphene surface to develop local drug delivery systems (Sun *et al.*, 2016). For instance, anti–inflammatory molecules, such as dexamethasone, attenuated inflammatory response on coated neural probes (Zhong & Bellamkonda, 2007). Therefore, graphene and GBM have the potential to enhance neural interfaces applicability. Nevertheless, very few studies have been made on chronic *in vivo* results from graphene–based electrodes (Garcia–Cortadella *et al.*, 2021). Long–term stability and functionality are key for this material to become a real therapeutic strategy.

6. Strategies to reduce the FBR

Material–based

To date, no material has completely avoided the FBR or the formation of the fibrotic capsule surrounding implanted devices. Ideally, these materials should be inert or non–recognizable by the body to avoid host response. The shape, porosity, or size, among other properties of the implants, affect the progression and outcome of the FBR (Figure 7). Thus, by altering the characteristics of the materials, it is possible to enhance the biocompatibility of implantable devices.

Biomaterial surface coatings that mimic the body tissue may inhibit undesirable interactions while allowing favorable binding. Hydrophobic phospholipids, an integral part of the cell membrane have been incorporated with polymers, to elicit a more favorable inflammatory response. For example, *in vitro* protein adsorption of PMB (poly(2–methacryloyloxyethyl phosphorylcho–line(MPC)–co–n–butylmethacrylate(BMA)s) phospholipid polymers showed decreased protein adsorption, decreased macrophage–like HL–60 cell adhesion and less IL–1β expression, a common pro–inflammatory M1 marker (Sawada *et al.*, 2003).

Hydrogels are made of polymers exhibiting non–biofouling properties and can be produced in a wide range of Young's moduli. Softer hydrogels have been proven to reduce macrophages activation *in vitro* and promote a less severe FBR *in vivo* compared

to stiffer ones which highlights the importance to minimize the mechanical mismatch between implanted devices and tissues (Blakney *et al.*, 2012). Poly(ethylene glycol) (PEG) and PEG–based copolymers are the most common for neural interface applications (Rao *et al.*, 2011; Heo *et al.*, 2016). However, PEG has exerted undesired effects *in vivo* including oxidative damage and the generation of anti–PEG antibodies (Barz *et al.*, 2011; Shiraishi & Yokoyama, 2019). Zwitterionic polymers are yet another hydrogel, including poly(carboxybetaines), poly(sulfobetaines), and poly(phosphobetaines). Surfaces decorated with zwitterionic molecules bind water molecules more strongly than PEG due to electrostatically induced hydration (Wu *et al.*, 2012). Thus, the formation of a hydration layer prevents hydrophobic interactions of proteins and lipidic membranes of cells with the polymer surface which explain the ultralow nonspecific protein and cell adhesion of these materials (Liu *et al.*, 2016). Zwitterionic hydrogels induced less collagen deposition and shifted the macrophage population to pro–regeneration M2 phenotype, delaying FBR for 3 months in a subcutaneous implant in mice (Zhang, Cao, *et al.*, 2013). More recently, *in vitro* experiments showed reduced fibroblast and macrophage adhesion on PI substrates used for neural interfaces coated with soft hydrogel zwitterionic (Trel *et al.*, 2018). In addition, silicon–coated zwitterionic brain implants reduced the microglia activation and improved BBB integrity, suppressing the acute inflammatory brain tissue response (Golabchi *et al.*, 2019). Even though zwitterionic coatings seem promising, more *in vivo* studies are required. More importantly, a link between reduced FBR and improved electrode functionality in terms of stimulation and recording must be established.

Protein or peptide coatings have also been used to modulate FBR. For example, ECM–based coatings serve as a biomimetic substitute for native ECM in the brain. Since ECM is a natural hemostatic and immunomodulatory agent, implants coated with ECM from different sources accelerate the coagulation cascade and suppress macrophage activation after CNS implants. Moreover, the astrocyte-based coating reduced the severity of astrogliosis 8 weeks following MEA implantation. Nevertheless, it fails to significantly influence the intensity or spatial distribution of FBR (Oakes *et al.*, 2018). Righi *et al.* (2018) designed a laminin–derived peptide coating for PI thin–film electrodes for PNS application. *In vitro* analysis demonstrated its capability to support adhesion, differentiation and sprouting of neuronal and

peripheral glial cells while reducing fibroblasts contamination, which are the main cells contributing to capsule deposition.

Drug–based

Locally drug delivery systems such as microspheres, nanoparticles, hydrogels, or microspheres–hydrogel composites have also proved an effective reduction of FBR. These systems provide a constant and direct drug influx limited by scaffold degradation. Bioactive molecules such as cytokines or anti–inflammatory drugs can be incorporated within the material or delivered through microfluidic systems.

Locally released dexamethasone to attenuate inflammation, FBR and to improve functionality has been addressed by several researchers in CNS (Spataro *et al.*, 2005; Kim & Martin, 2006; Zhong & Bellamkonda, 2007; Mercanzini *et al.*, 2010). However, the improvements produced by dexamethasone were not maintained over time, probably due to the drug source exhaustion (Zhong & Bellamkonda, 2007). Focally release of anti–inflammatory drugs in peripheral nerves has been exploited for nerve regeneration and for cuff and regenerative peripheral interfaces (Park *et al.*, 2015; Fitzgerald, 2016; Heo *et al.*, 2016; Elyahoodayan *et al.*, 2020). However, little is published for intraneural electrodes in peripheral nerves. The small nerve size of most common animal models shrinks its applicability. Nevertheless, size mismatch may be attenuated in larger animal models or humans. Regarding systemic administration, dexamethasone reduced the number of glial cells forming the glial scar around penetrating cortical implants (Spataro *et al.*, 2005). In the PNS, capsule thickness reduction was seen in intraneural implants after 2 weeks of systemic administration. This reduction was maintained for 6 weeks more without any drug administration (de la Oliva 2018c). Besides, long–term improved functionality of transversal intraneural electrodes was demonstrated after 12 weeks of daily dexamethasone administration (de la Oliva *et al.*, 2019).

Minocycline, a second–generation antibiotic belonging to the tetracycline family, has been shown to have a neuroprotective and anti–inflammatory effect (Yrjänheikki *et al.*, 1999). One week of oral administration of minocycline improves the functionality of multi–channel microwire neural implants after 1 month (Rennaker *et*

al., 2007). Likewise, local administration reduced microglial and astrocyte activation in neural *in vivo* implants (Liu *et al.*, 2017; Holmkvist *et al.*, 2020).

More recently, local delivery of the nucleotide–binding oligomerization domain–like receptor family pyrin domain containing 3 (NLRP3) inflammasome inhibitor MCC950, through its incorporation into silicone coating, reduced the inflammation and fibrosis associated with both sciatic nerve implants and subcutaneous implantable devices (Barone *et al.*, 2022).

Finally, note that choosing the type of drug release system is not a trivial issue. Local administration elicits a more specific and less toxic response in the area surrounding the interface although the long–term release of drugs is still challenging. Besides, technical issues arise in PNI, which are limited by nerve size. In contrast, systemic administration has a higher chance of pleiotropic effects which may be detrimental. Moreover, to reach a good concentration at the implant site, a higher concentration of drugs may be administered, expanding toxicological issues. Yet, systemic administration is easier to apply as does not require implant modification and allows for better control of dosage, timing, and the combination of different FBR modulatory drugs.

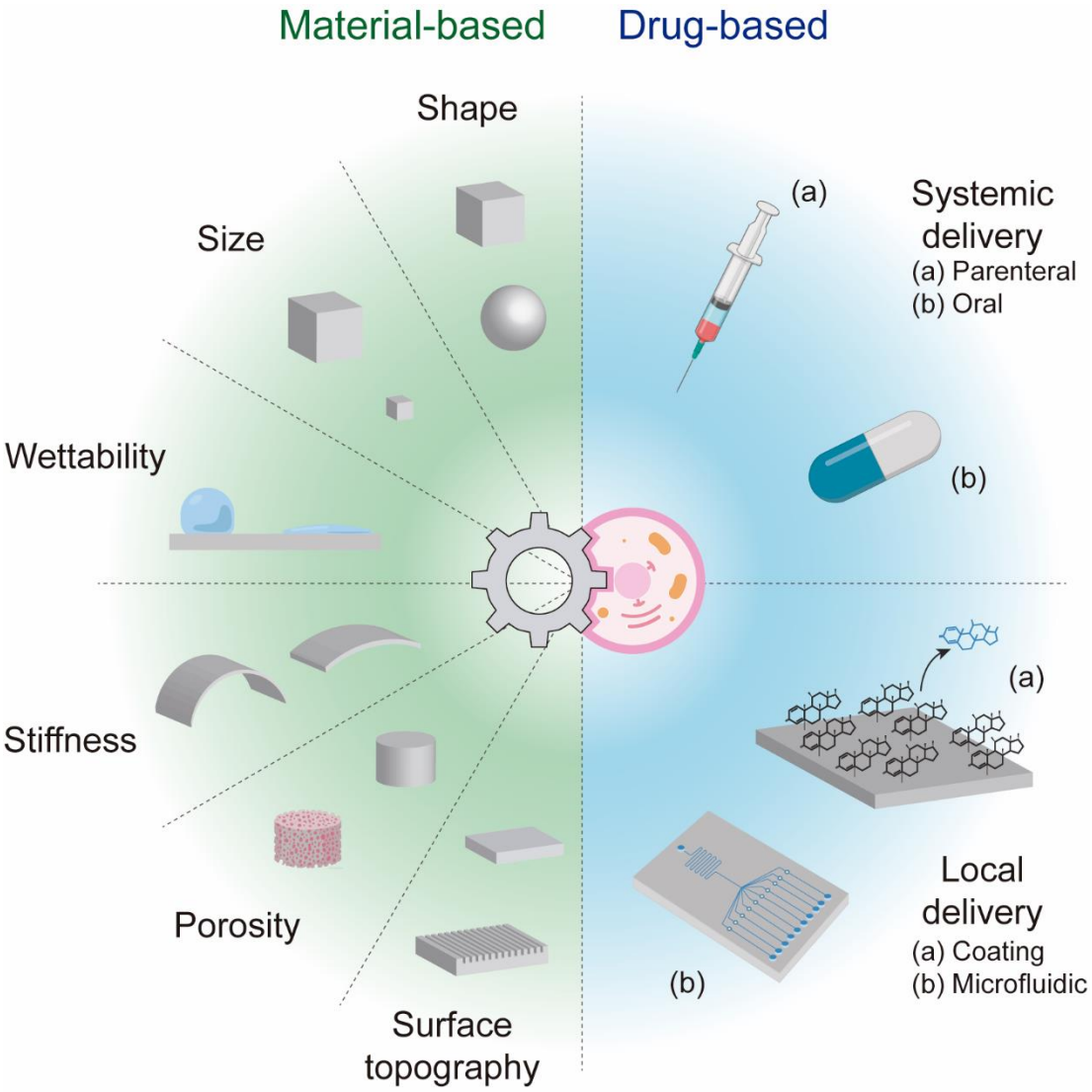

Figure 7. Strategies to reduce the FBR. Material–based strategies tune the physicochemical properties of materials to increase biocompatibility and reduce the FBR. Drug–based approaches relay on the systemic or local released of therapeutic compounds to modulate FBR.

Other strategies

Beyond the realm of neural implants, new approaches to hamper the progression of pathological fibrosis are being investigated. Although wound healing in biomaterial implantation and subsequent scar formation differs from fibrotic diseases such as idiopathic pulmonary fibrosis (IPF), systemic sclerosis and liver fibrosis among others, the identification of therapeutic targets could be exploited for decreasing fibrosis to neural implants.

Macrophages balance

Classically activated macrophages (M1) encourage inflammation and are crucial in the first steps of wound healing clearing dead cells and debris. However, persistent, or dysregulated M1 presence can lead to chronic inflammation, fibrous capsule deposition, and implant rejection resulting in unsuccessful biomaterial integration. In contrast, alternatively activated macrophages (M2) lead to inflammation resolution, vascularization to encourage tissue repair and the integration of the biomaterial.

M1 macrophages are considered mainly detrimental for the development of fibrosis (Lis–López *et al.*, 2021). Thus, shifting macrophages' phenotype towards a pro–resolutive have positive effects in reducing scar tissue (Gower *et al.*, 2014; Jain *et al.*, 2015; Minardi *et al.*, 2016; Yao *et al.*, 2020).

Conversely, other studies addressed fibrosis amelioration after polarization of M1 macrophages. Pulmonary delivery of pro–inflammatory TNF–α to mice, triggered lung fibrosis resolution by reprogramming M2 macrophages to M1 (Redente *et al.*, 2014). Similarly, inhibition of human recombinant colony–stimulating factor 1 receptor (CSF1R) (Hamilton *et al.*, 2014) by Nintedanib decreased M2 polarization *in vitro* (Bellamri *et al.*, 2019). Regardless M1/M2 phenotypes, CSF1R neutralizing antibody prevented radiation–induced lung fibrosis by depletion of interstitial macrophages (Meziani *et al.*, 2018). Another inhibitor of CSF1R, GW2580, was shown to suppress FBR in both rodents and non–human primates for months. GW2580 was locally administered through compact, solvent–free crystals that were coated on top of implantable devices such as a glucose sensor and a muscle stimulator among others. Even more, they reported better functionality of the muscle stimulator after 2 weeks (Farah *et al.*, 2019). In summary, several macrophage phenotypes have been identified to participate differentially in the fibrotic development. However, whether a given phenotype worsens or ameliorates fibrosis is often controversial (Lis–López *et al.*, 2021).

Anti–fibrotic drugs

Delivery of anti–fibrotic drugs may also decrease fibrotic capsule deposited by fibroblast. Unfortunately, quite a few studies have tested satisfactorily this approach on neural implants (de la Oliva *et al.*, 2018c).

Most therapies are intended to decrease TGF–β expression or interfered with its downstream signaling pathway (Rho–associated kinase, mTOR, Wnt, Hedgehog and Notch) as it is an important fibrotic inducer (Rosenbloom *et al.*, 2013; Li *et al.*, 2017; Lotti *et al.*, 2017; Walton *et al.*, 2017). Pirfenidone (Antoniu, 2006), SM305 (Ishida *et al.*, 2006), SIS3 (Jinnin *et al.*, 2006), metformin (Rangarajan *et al.*, 2018) and LDE223 (Horn *et al.*, 2012) are promising options that have reduced fibrosis in several diseases.

PDGF targeting by tyrosine inhibitor kinases (imatinib, sorafenib and sunitinib) also has been used to hamper fibrosis. These strategies attenuate the fibrotic progression in the liver (Westra *et al.*, 2014), lung (Daniels *et al.*, 2004), kidney (Sugimoto *et al.*, 2012) and skin (Distler *et al.*, 2007).

Myofibroblasts

In normal wound healing, myofibroblasts undergo apoptosis upon completion of tissue repair. By contrast, excessive organ fibrosis in pathologic wound healing is sponsored by myofibroblasts resistance to apoptosis (Thannickal & Horowitz, 2006; Fattman, 2008). Actually, apoptosis in myofibroblasts is not inhibited, and neither myofibroblasts are resistant to it. Myofibroblasts are primed for apoptosis, however, they are tightly controlled by pro–survival biochemical (TGF–β1 and PDGF) and biomechanical factors (matrix stiffness), that keep myofibroblasts on the brink of death (Hinz & Lagares, 2020). Consistently, blockage of pro–survival signaling mechanism including protein kinase pathways (PI3K/AKT) (Liang *et al.*, 2014; Saito *et al.*, 2017), focal adhesion kinase (FAK) (Lagares *et al.*, 2012; Kinoshita *et al.*, 2013) and Rho–associate kinase (Bond *et al.*, 2011; Zhou *et al.*, 2013; Hutchings *et al.*, 2017) and inhibitors of apoptosis (IAPs), particularly pro–survival BCL–2 family (Jafarinejad–Farsangi *et al.*, 2015; Moncsek *et al.*, 2017; Pan *et al.*, 2017) have been proved to ameliorate fibrosis in several models.

Another approach to stimulate myofibroblasts clearance upon resolution of wound healing is to induce de–differentiation of persistent myofibroblasts into a more

quiescent fibroblast or proto–myofibroblast. These cells produce less ECM and are more susceptible to apoptosis mechanisms (Penke & Peters–Golden, 2019).

Some regulators of myofibroblasts de–differentiation have been identified (PGE2, MyoD, NRF2) (Yang *et al.*, 2014; Sieber *et al.*, 2018; Penke & Peters–Golden, 2019). Indeed, the reversibility of myofibroblasts has already been demonstrated *in vitro* (Artaud–Macari *et al.*, 2013; Garrison *et al.*, 2013; Sieber *et al.*, 2018; Nagaraju *et al.*, 2019). However, the anti–fibrotic effect on *in vivo* models has not yet been investigated, therefore whether myofibroblast de–differentiation is still a viable therapeutic strategy is under doubt.

Towards the end of wound healing some myofibroblasts acquire an ECM–degradation fibroblast phenotype which is associated with an increased expression of ECM–degrading enzymes such as plasmin, MMP–14 and cathepsin K (Bühling *et al.*, 2004; Zigrino *et al.*, 2016). Although YAP–TAZ inhibition has been implicated in the acquisition of ECM degrading phenotype of fibroblast (Liu *et al.*, 2015), the exact reprogramming process by myofibroblasts turn into fibroblast is not known. Additionally, Wohlfahrt et al. (2019) reprogrammed pro–fibrotic fibroblast into resting fibroblast upon inhibition of the transcription factor PU.1. More importantly, they addressed fibrosis regression in a mouse model of systemic sclerosis.

Inhibition of extracellular matrix cross–linking

ECM cross–linking stabilizes the matrix and promotes resistance to proteolysis (Ricard–Blum *et al.*, 2018). In addition, fibroblast and myofibroblasts activation as well as evasion of apoptosis are increased, possibly due to enhanced matrix stiffness and integrin–mediated signaling (Lagares *et al.*, 2012; Reed *et al.*, 2015; Philp *et al.*, 2018; Schulz *et al.*, 2018). This process is mediated by transglutaminase enzymes and lysyl oxidase (LOX) or its homologs, lysyl oxidase–like (LOXL) enzymes. Inhibitions of these molecules have been strongly related to decreased fibrosis in numerous models (Barry–Hamilton *et al.*, 2010; Olsen *et al.*, 2014; Martínez–Martínez *et al.*, 2016; Harlow *et al.*, 2017; Ikenaga *et al.*, 2017; Bellaye *et al.*, 2018). Nevertheless, an inhibitor of LOXL2, previously tested in a bleomycin–induced IPF mouse model, did not ameliorate fibrosis in patients (Raghu *et al.*, 2017).

IV. Hypothesis and objectives

The applicability and functionality of an electrode designed to interface with the PNS depends on several factors. Among the most important are the design (extraneural, intraneural, or regenerative) and shape, the materials used for manufacturing, and the biocompatibility and safety once implanted. Intraneural designs offer a good trade–off thanks to a reduced invasiveness and a good selectivity in stimulating and recording the PNS compared to extraneural and regenerative electrodes. However, further improvements in functionality are still needed to reach a natural–like capability to electrically interact with the nervous tissue. Equally important is the decrease in functionality due to the FBR, which hampers the chronic usability of the electrodes.

This thesis is based on two hypotheses:

- The *in vivo* functionality of intraneural electrodes can be enhanced by using a novel GBM.
- The chronic stability of intraneural electrodes can be improved by modulating the FBR using anti–inflammatory and antifibrotic drugs.

To address these aims, the thesis has been divided into three chapters with the following specific objectives:

Chapter 1. Biocompatibility evaluation of novel graphene–based intraneural electrodes.

- To evaluate the *in vitro* biocompatibility of graphene–based devices.
- To assess the *in vivo* biocompatibility of novel graphene–based intraneural devices implanted in the sciatic nerve of rats through functional and histological tests.

Chapter 2. Novel graphene–based electrode for interfacing the peripheral nervous system.

- To characterize the ability of intraneural graphene–based electrodes to stimulate and to record the activity of the peripheral nerve.

Chapter 3. Enhancing chronic stability of intraneural implants. Modulation of the foreign body reaction to intraneural implants in the peripheral nerve.

- To assess the effect of metformin on the FBR to intraneural implants by quantifying the number of infiltrated macrophages and the deposited capsule around the implant.
- To develop a combined therapy using the anti–inflammatory drug dexamethasone and the antifibrotic drug metformin for modulating the FBR.

V. Study design and methodologies

This section describes an overview of the study design and the main methodologies performed in each chapter.

Chapter 1. Biocompatibility evaluation of novel graphene–based intraneural electrodes.

In the first chapter, the biocompatibility of a GBM is assessed *in vitro* and *in vivo*.

In vitro

Rat DRG neurons or rat cortical neurons were cultured on top of three different substrates: control culture glass, PI as the substrate of the neural device, and the PI substrate containing the GBM EGNITE. Neuron viability after 4 or 7 days in culture was assessed by the MTT (3–(4,5–dimethylthiazol–2–yl)–2,5–diphenyltetrazolium bromide) cell viability test and after immunohistochemical labeling.

In vivo

Female Sprague–Dawley (SD) rats were implanted with LIFE mock devices containing PI or PI plus EGNITE. Each device has two arms that are bent to face each other. The devices were inserted longitudinally in the tibial fascicle of the sciatic nerve. Functional and histological analyses were performed at 2 and 8 weeks after the implantation.

To evaluate the functional properties of the nerves implanted with longitudinal devices, walking track, algesimetry, and electromyography test were conducted. Walking track assesses locomotion, algesimetry test evaluates hyperalgesia or allodynia and electromyography test assesses neuromuscular function. To study the FBR associated with the implant, histological analyses were performed. Animals were euthanized, and nerves were collected and fixed for cryosectioning. Transversal sections were labeled for ionized calcium–binding adapter molecule 1 (Iba1) to quantify the number of infiltrating macrophages. Capsule thickness around the implant was measured from the implant to the first axons labeled for neurofilament 200 kDa clone RT97 (RT97).

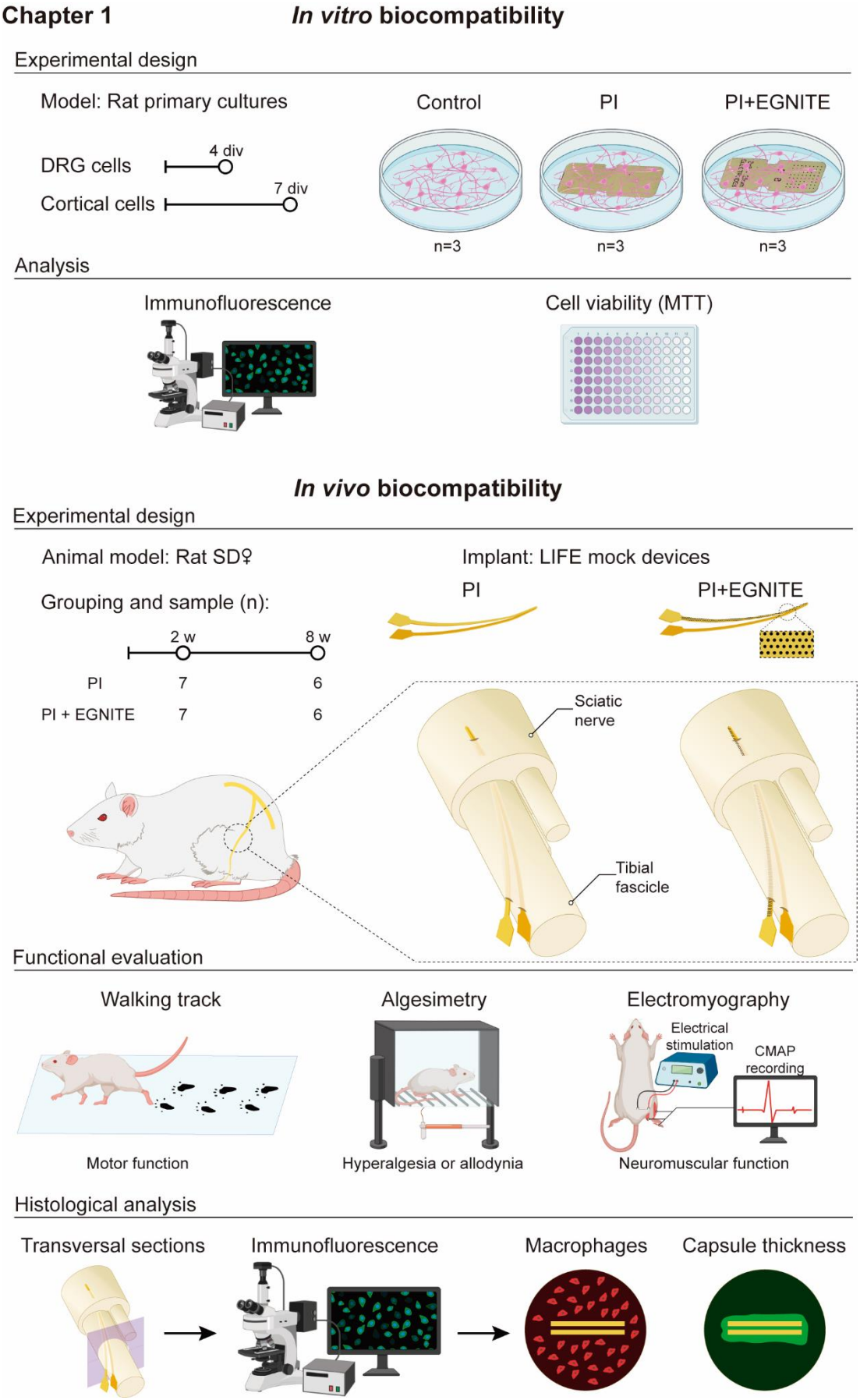
Chapter 1
In vitro biocompatibility
Experimental design
Model: Rat primary cultures
DRG cells
4 div
Cortical cells
7 div
Control
PI
PI+EGNITE
n=3
n=3
n=3
Analysis
Immunofluorescence
Cell viability (MTT)
In vivo biocompatibility
Experimental design
Animal model: Rat SD♀
Implant: LIFE mock devices
PI
PI+EGNITE
Grouping and sample (n):
2 w
8 w
PI 7 6
PI + EGNITE 7 6
Sciatic nerve
Tibial fascicle
Functional evaluation
Walking track
Algesimetry
Electromyography
Electrical stimulation
CMAP recording
Motor function
Hyperalgesia or allodynia
Neuromuscular function
Histological analysis
Transversal sections
Immunofluorescence
Macrophages
Capsule thickness

Chapter 2. Novel graphene–based electrode for interfacing the peripheral nervous system.

In the second chapter, the functionality of graphene–based electrodes are tested.

Working TIME devices were transversally implanted in the sciatic nerve of female SD rats through the tibial and peroneal fascicle. TIME devices have two arms that are bent to face each other. Each arm contains 9 AS of 25 µm of diameter plus 1 larger reference. The stimulation and recording capabilities of graphene–based electrodes were investigated.

Stimulation analysis

Electrical stimulation was delivered through each AS located inside the nerve at 0, 30, or 60 days. The progressive activation of the tibialis anterior (TA), the gastrocnemius medialis (GM), and the plantar interossei (PL) muscles was recorded to create the recruitment curve of each muscle. From the recruitment curve, we calculated the current needed to obtain a response of 5, 30, or 95% relative to the maximum muscle activation. The ability of devices to selectively activate the muscles was also calculated.

Recording analysis

Recording capabilities were tested in acute. The feasibility of the graphene–based electrode to record CNAPs elicited by an electrical stimulus was assessed. Moreover, the selective recording of CNAPs elicited from either the lateral plantar nerve (LPN) or medial plantar nerve (MPN) was explored. The ability of the electrode to record ENG signals elicited by mechanical stimuli and the S/N associated was also evaluated.

Chapter 2

Experimental design

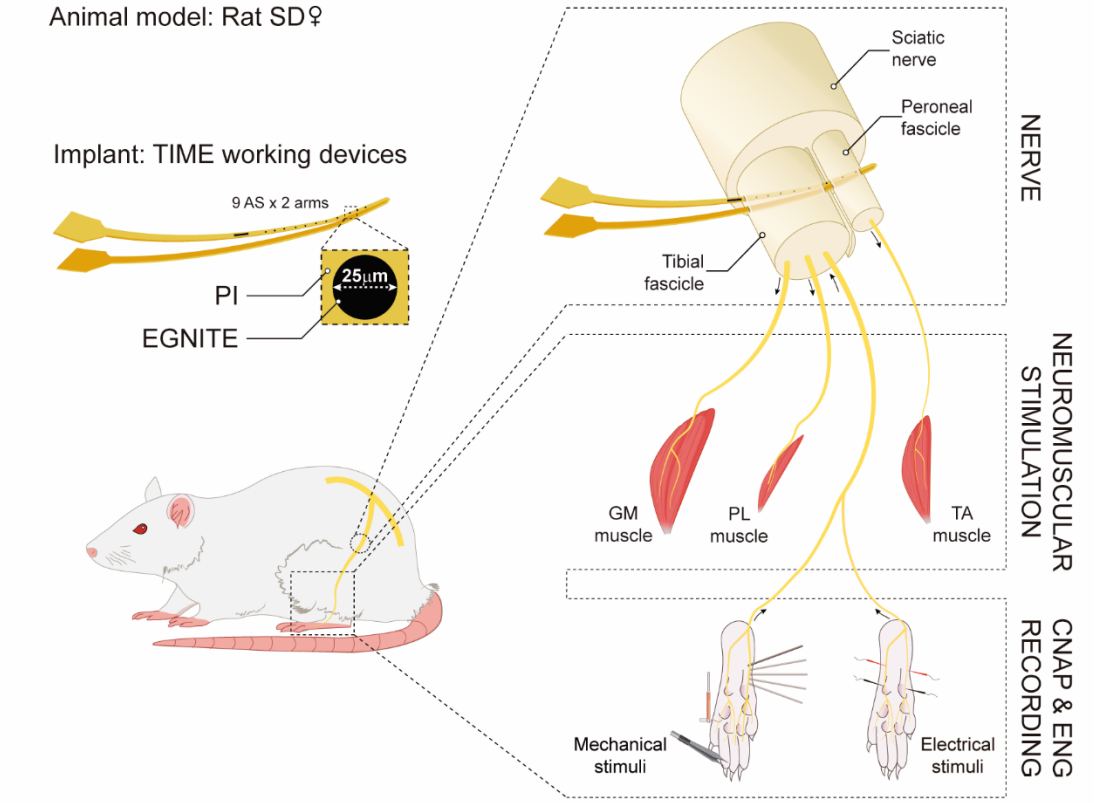

Stimulation analysis

- Recruitment curve of muscle activation:
  - PL muscle
  - GM muscle
  - TA muscle
- Current threshold to activate the muscle at:
  - 5, 30, 95%
- Selectivity to activate specific muscles

Sample (n):

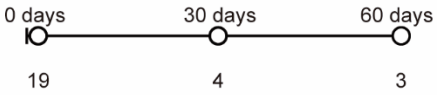

Recording analysis

	Sample (n): Acute
• Capability of recording a CNAP elicit by electrical stimuli	14
• Selectivity to record a CNAP from: MPN LPN	11
• Capability of recording ENG elicit by mechanical stimuli: Light touch Scratch Pain	6
• SNR of mechanical stimuli	6

Chapter 3: Enhancing chronic stability of intraneural implants. Modulation of the foreign body reaction to intraneural implants in the peripheral nerve.

In the third chapter, we investigate the effect of metformin on the FBR of intraneural implants.

Female SD rats were implanted with PI LIFE mock devices. Each device has two arms that are bent to face each other. The devices were inserted longitudinally in the tibial fascicle of the sciatic nerve.

Rats were grouped depending on the administered drug or combination of drugs i.e., control (no drug), metformin, dexamethasone plus metformin, or dexamethasone. Metformin was administered in drinking water throughout the follow–up. Dexamethasone was only administered for a maximum of 2 weeks. Functional and histological analyses were performed at 2, 8, and 12 weeks after the implantation.

To evaluate the functional properties of the nerves implanted with longitudinal devices, walking track, algesimetry, and electromyography test were conducted. Walking track assesses locomotion, algesimetry test evaluates hyperalgesia or allodynia and electromyography test assesses neuromuscular function. To study if metformin modulates the FBR associated with the implant, histological analyses were performed. Animals were euthanized, and nerves were collected and fixed for cryosectioning. Transversal sections were labeled for Iba1 to quantify the number of infiltrating macrophages. Capsule thickness around the implant was measured from the implant to the first axons labeled for RT97.

Chapter 3

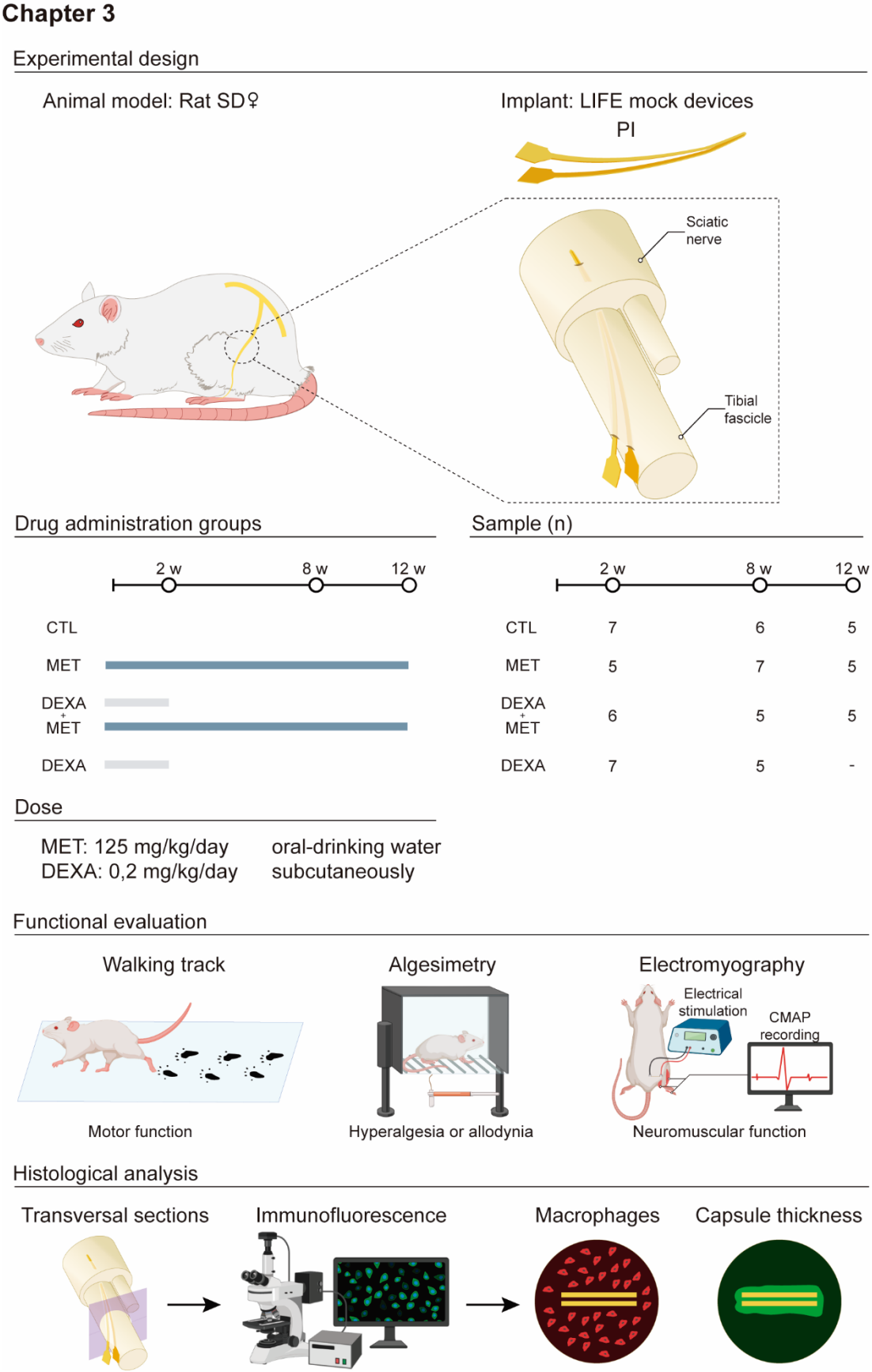
Experimental design
Animal model: Rat SD♀
Implant: LIFE mock devices
PI
Sciatic nerve
Tibial fascicle
Drug administration groups
2 w
8 w
12 w
CTL
MET
DEXA + MET
DEXA
Sample (n)
2 w
8 w
12 w
CTL 7 6 5
MET 5 7 5
DEXA + MET 6 5 5
DEXA 7 5 -
Dose
MET: 125 mg/kg/day
DEXA: 0,2 mg/kg/day
oral-drinking water
subcutaneously
Functional evaluation
Walking track
Motor function
Algesimetry
Hyperalgesia or allodynia
Electromyography
Electrical stimulation
CMAP recording
Neuromuscular function
Histological analysis
Transversal sections
Immunofluorescence
Macrophages
Capsule thickness

VI. Results

Chapter 1

Biocompatibility evaluation of novel graphene–based intraneural electrodes

Overview

Loss of sensory and motor function as a result of nerve injury (e.g., spinal cord injury, brachial plexus injury) or loss of a limb (e.g., amputation) affects several million people worldwide, serving as a powerful motivation for the development of new rehabilitation strategies. Neuroprostheses based on interfacing the PNS are designed to record efferent signals to elicit functional activities and to induce afferent signals to provide sensory feedback, thus constituting a bidirectional interface with the nervous system (Micera *et al.*, 2011). In the last decades, a variety of such PNI have been developed and tested (Navarro *et al.*, 2005; Ferrari *et al.*, 2021). However, translation of these research efforts into clinical applications is rather slow due to technological challenges.

Regarding biomedical applications, it is important that the capability of the device as a bidirectional interface is maintained over extended periods of time. Once implanted, a neural interface must remain within the body of the subject for months or years, so the stability of the materials in the electrode is crucial. Time–dependent loss of neuron–device communication limits the long–term use of such devices. Decreasing functionality is associated with reactive responses that produce an encapsulating cellular reaction around electrodes implanted in the nervous system. Therefore, a major prerequisite for the application of novel nerve electrodes is that the implant must be biocompatible, and also that the organism embodies the interface without creating a thick insulating capsule. After insertion of a device in the peripheral nerve, early and chronic cellular responses occur in a subset of processes known as the FBR (Lago *et al.*, 2007; Christensen *et al.*, 2014; Wark *et al.*, 2014; Wurth *et al.*, 2017; de la Oliva 2018b).

In this work, we assessed whether novel graphene microelectrodes, based on a newly developed reduced graphene oxide, named EGNITE (Viana *et al.*, 2022), are suitable for peripheral nerve implantation when deposited on PI. To this end, *in vitro* and *in vivo* biocompatibility of the EGNITE material was tested. Cortical and ganglionar cells were seeded on top of EGNITE to assess *in vitro* biocompatibility. EGNITE–coated mock devices were implanted in the sciatic nerve of rats for chronic

evaluation, functional and morphological changes in the nerve were studied over two months to evaluate *in vivo* biocompatibility.

Materials and Methods

In vitro biocompatibility study

DRG neurons or cortical neurons from SD rats were cultured on top of three different substrates: control culture glass, PI as the substrate of the neural device, and the PI substrate containing EGNITE (Figure 1A). The pieces containing PI and PI+EGNITE were glued to the culture glass with collagen. Neuron viability after 4 or 7 days in culture was assessed by the MTT (3–(4,5–dimethylthiazol–2–yl)–2,5–diphenyltetrazolium bromide) cell viability test and after immunohistochemical labeling. Both primary cell cultures were performed 3 times with 4 replicates of each substrate condition.

DRG culture

Rats 21 days old were euthanized with pentobarbital. DRG were extracted and kept in cold Gey's balanced solution with 2% glucose. Cleaned ganglia underwent enzymatic digestion with trypsin 1x, collagenase 1x and DNase (1mg/mL) diluted in Hank's Balanced Salt Solution (HBSS, Gibco) for 30 minutes at 37ºC, followed by mechanical digestion. Cells were then filtered with a 70 µm sterile filter to remove myelin fragments and centrifuged at 900 rpm for 7 minutes. Neurons were counted in a Neubauer chamber after homogenization. Four wells per condition were seeded with a concentration of 8000 cells/ml in 24 multiwell plates (500 µL per well) pretreated with poly–D–lysine (0.01 mg/ml) and laminin (1 mg/ml). Cells were maintained in Neurobasal A medium enriched with 2% B27, 2% glucose, 1% glutamine and 1% penicillin and streptomycin. After 24h the medium was changed and replaced every 3 days.

Cortical cells culture

E17 rat embryos were used for the culture of cortical cells. Briefly, female pregnant rats were euthanized with pentobarbital, the embryos were extracted and dissected until the cerebral cortex was obtained. The meninges were removed and cleaned. Cortices were kept in Krebs–Ringer Buffer solution with trypsin and DNase for enzymatic digestion for 10 minutes at 37ºC, followed by mechanical digestion.

Cells were then filtered with a 70 µm sterile filter. Dissociated cortices underwent centrifugation at 1000 rpm for 5 minutes and neurons were counted in a Neubauer chamber after homogenization in DMEM containing 10% FBS. Four wells per condition were seeded with a concentration of 250,000 cells/ml in 24 multiwell plates (500 µL per well) precoated with poly–D–lysine (0.01 mg/ml). Cells were seeded in DMEM medium enriched with 2% B27, 2% glucose, 1% glutamine and 1% penicillin and streptomycin. After 24h the medium was replaced with Neurobasal medium enriched with 2% B27, 2% glucose, 1% glutamine and 1% penicillin and streptomycin, and replaced every 3 days.

Viability evaluation and immunolabeling

At 4 and 7 days *in vitro* for DRG and cortical cells respectively, an MTT assay was performed to determine cell viability. For this purpose, medium was replaced with medium containing 0.15 mg/ml MTT, the culture was maintained for one hour, and cells were lysed with DMSO. Absorbance was read out through a spectrophotometer (Bio–tek) at 560 nm wavelength and data collected using KC Junior software. Readings were normalized against the control group, in which cells only grow on coverslips, to obtain the percentage of cell survival.

For immunofluorescence labeling, coverslips containing cells were fixed for 20 minutes with paraformaldehyde (PFA). After blocking with normal donkey serum, slides were incubated with primary mouse antibody against β3 tubulin (1:500; Biolegend) overnight at 4ºC. Cells were then washed with 0.1% Tween buffer solution and incubated with AlexaFluor 488 donkey anti–mouse secondary antibody (Invitrogen) for 1 h at room temperature. Finally, coverslips with cells were mounted with Fluoromount (Sigma). Images were taken with an epifluorescence microscope (Eclipse Ni, Nikon) and a digital camera (DS–Ri2, Nikon)

In vivo biocompatibility study

To assess the biocompatibility of the developed graphene, PI devices coated or not with EGNITE were longitudinally implanted in the sciatic nerve of rats for 2 or 8 weeks. The intraneural device was designed as a longitudinal strip in which the area of EGNITE in contact with the nerve was increased by a factor of 20, with respect to

conventional active electrodes (Figure 1B, C), aiming to maximize the contact area of the material with the tissue and to investigate immune responses.

All experimental procedures performed were approved by the Ethics Committee of the UAB in accordance with the European Communities Council Directive 2010/63/EU. Adequate measures were taken to minimize pain and animal discomfort during surgery and in the postoperative follow–up.

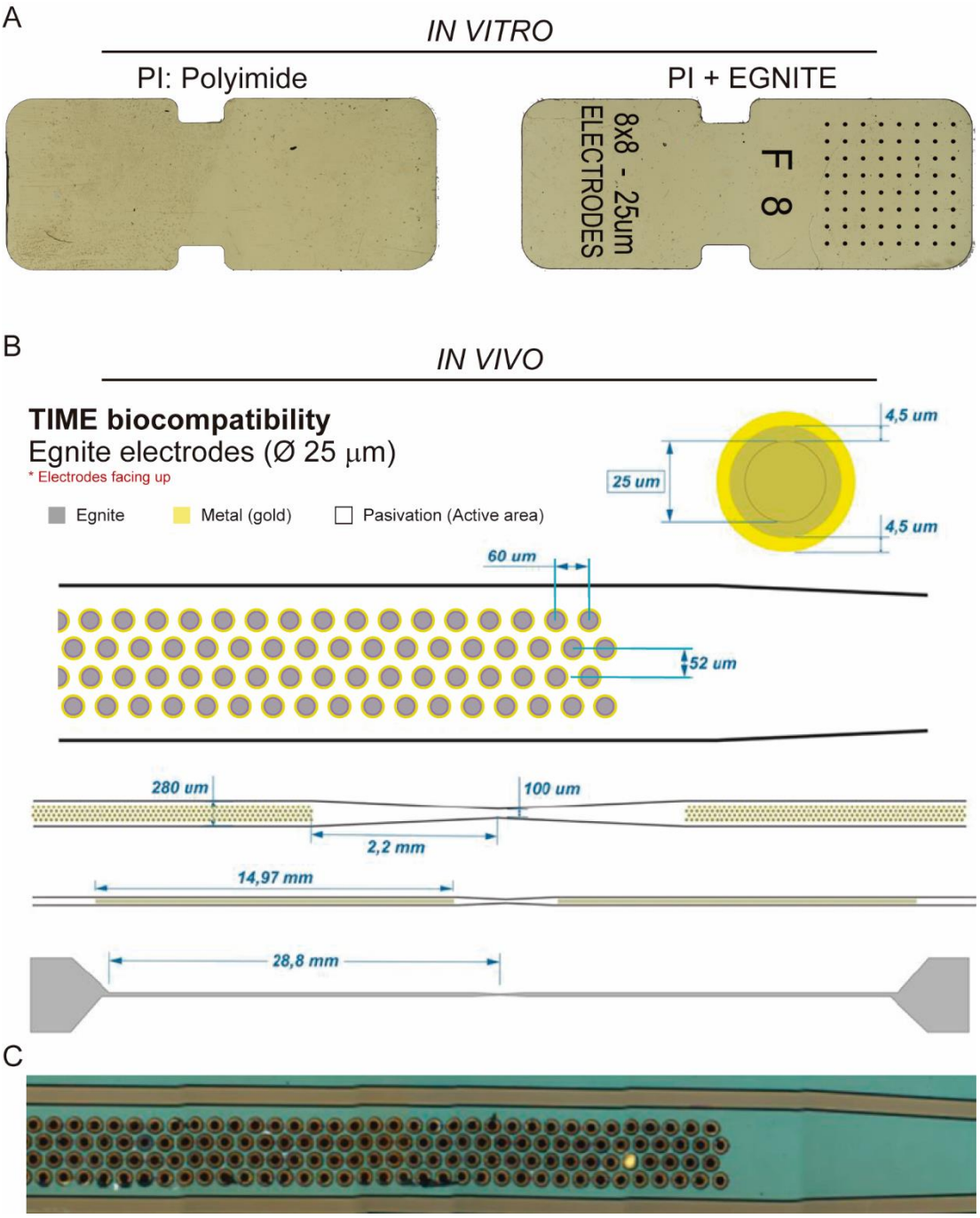

Figure 1. Implants design for *in vitro* and *in vivo* experiments. A) Substrates for *in vitro* biocompatibility tests made of PI or PI+EGNITE. Black dots are made of EGNITE material (64 black dots, ø 25 µm). B) Probe design for *in vivo* biocompatibility tests. C) Image of a section of a fabricated probe with many EGNITE microelectrodes (black dots).

Nerve implantation

Operations were performed under anesthesia with ketamine/xylazine (90/10 mg/kg i.p.) on female SD rats weighing 300–350 g. The sciatic nerve was surgically exposed at the midthigh and carefully freed from adherences to surrounding tissues. PI (PI–2611, HD MicroSystems) devices with no EGNITE (used as controls) and PI devices with EGNITE were inserted longitudinally into the tibial branch of the sciatic nerve with the help of a straight needle attached to a 10–0 loop thread (STC–6, Ethicon), as designed for longitudinal intrafascicular electrodes (LIFE; Lago et al 2007; de la Oliva et al 2018a) (Figure 2). Insertion was monitored under a dissection microscope to ensure the correct placement of the device. The wound was sutured in plane and disinfected with povidone iodine. After surgery, all animals were housed under standard conditions. The incision wounds healed without inflammatory signs and no postoperative complications were observed.

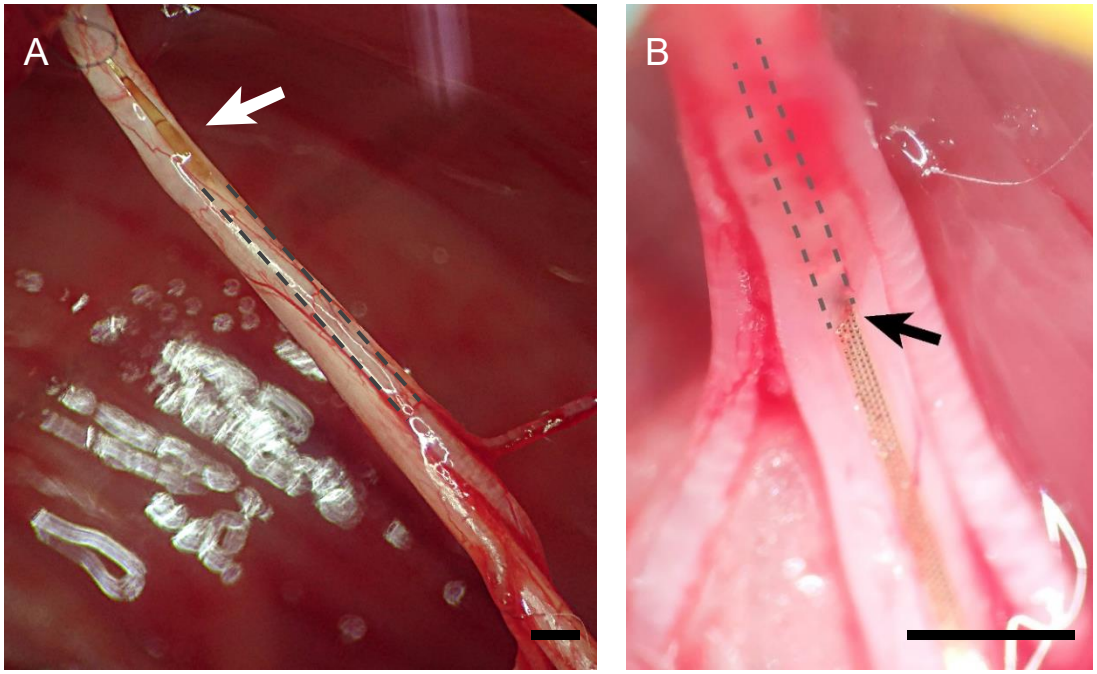

Figure 2. Representative images of implanted devices. A) Microphotograph of a sciatic nerve and a longitudinally implanted PI device already inside the nerve. The arrow indicates the tip of the implant outside the nerve. **B)** Detail of a device with EGNITE inside a sciatic nerve. The arrow indicates the insertion point, and the dashed line indicates the placement of the intraneural device within the tibial fascicle. Scale bar: 1 mm.

Table 1: Experimental set up of the *in vivo* biocompatibility study.

Group	Implant duration	n
PI	2w	7
	8w	6
PI + EGNITE	2w	7
	8w	6

Electrophysiological and functional evaluation

The functional properties of the nerves that had been implanted were evaluated by means of nerve conduction, algesimetry and locomotion tests at 2 and 8 weeks after the implant. The nerve conduction test was performed by stimulating the sciatic nerve proximally with single electrical pulses and recording the compound muscle action potential (CMAP) of the TA, GM, and PL muscles as previously described (de la Oliva *et al.*, 2018a). The nociceptive threshold to mechanical stimuli was evaluated using an electronic Von Frey algesimeter (Bioseb, Chaville, France) following the same protocol described before (del Valle et al, 2018) Rats were placed on a wire net platform in plastic chambers, and a metal tip was applied to the sole of the hind paw until the rat withdrew the paw in response to the stimulus. The walking track test was performed to assess locomotor function after the implant. The plantar surface of the hind paws was painted with blue ink and the rat was left to walk along a corridor. The print length, the distance between the 1st and 5th toes and between the 2nd and 4th toes were measured to calculate the Sciatic Functional Index (SFI) (de Medinacelii et al 1982).

Histological evaluation

After 2 or 8 weeks, animals were deeply anesthetized with an overdose of pentobarbital and transcardially perfused with 4% PFA in phosphate buffer (PB). The sciatic nerve including the implant was harvested, post–fixed in 4% PFA in PBS for an hour and stored in 30% sucrose in PB for cryoprotection.

Analysis of infiltrating macrophages and capsule thickness in the implanted nerves was performed with immunohistochemical labeling. Nerve segments containing the device implanted were sliced (15 µm–thick sections) with a cryostat (Leica CM190). After thawing and blocking with normal donkey serum, slides were

incubated with the primary antibodies rabbit Iba1 (1:500; Wako) for macrophages and RT97 (1:200; Developmental Studies Hybridoma Bank) for axons overnight at 4ºC. Slides were then washed with a 0.1% Tween 20 in PBS solution and incubated with AlexaFluor 488 donkey anti–mouse and AlexaFluor 555 donkey anti–rabbit secondary antibodies (Invitrogen) for 1 h at room temperature. Finally, slides were mounted with Mowiol containing DAPI (Sigma). The number of Iba1 positive macrophages in the whole tibial nerve cross section was semiautomatically quantify using a macro design for Image J software. The capsule thickness was analyzed by dividing the area of the capsule by the length of the implant in the transversal section. The area was quantified as the non–labelled space between the implant and the first axons labelled with RT97. As each implant has two arms, the capsule thickness of an implant is the mean of both arms. Images were taken with an epifluorescence microscope (Eclipse Ni, Nikon) and a digital camera (DS–Ri2, Nikon).

Data analysis

The normality of the data was studied to apply the correct statistical method (parametric or nonparametric) using Shapiro–Wilk test. Statistical comparison between groups for *in vitro* results were made by one–way ANOVA followed by Dunnett`s multiple comparison test. Statistical comparisons between groups and intervals for functional and histological results were made by two–way ANOVA followed by Tukey's multiple comparison test. The GraphPad Prism 8 software was used for all statistical analyses. Differences were considered significant when $p < 0.05$. Results are expressed as mean ± SEM.

Results

In vitro biocompatibility study

The results of the MTT test showed that neuronal survival of both ganglionar (Figure 3A) and cortical neurons (Figure 3B) was similar in the three conditions tested proving that both PI and EGNITE are not toxic *in vitro*. Both DRG and cortical neurons grew well on top of PI with and without EGNITE as shown in Figure 4. In the case of cortical cell culture, EGNITE dots were not even visible, as the device surface was completely covered by a layer of cells.

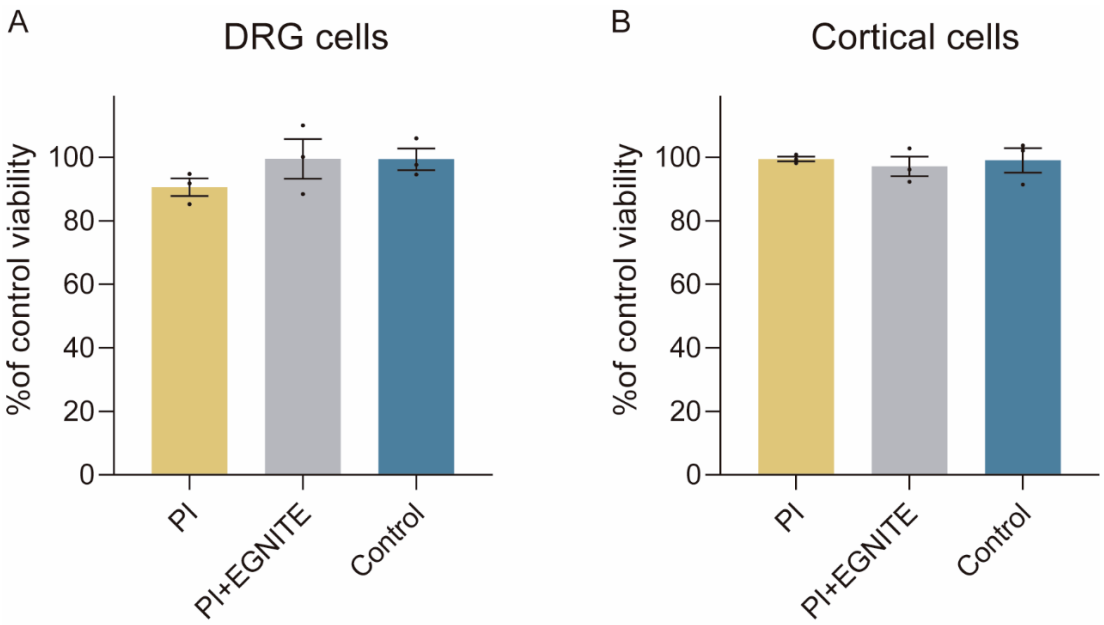

Figure 3. *In vitro* EGNITE biocompatibility assay. Neuronal viability assessed by the MTT test after 4 (DRG, A) and 7 (cortical neurons, B) days *in vitro* for all surfaces. $p>0.05$, one–way ANOVA followed Dunnet' multiple comparison test.

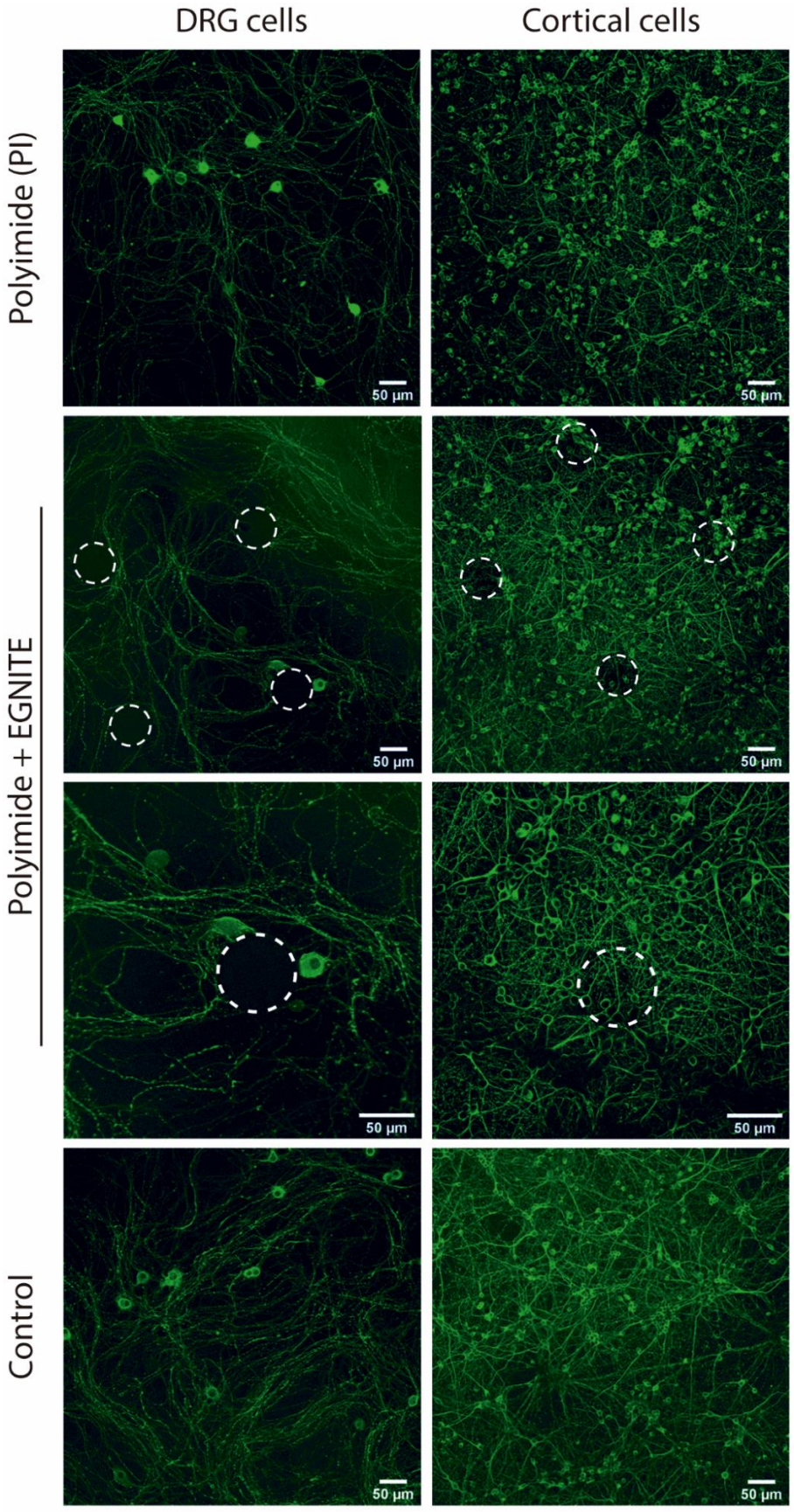

Figure 4. Representative images of cell cultures. Left: DRG neurons (green, b3 Tubulin) cultured on top of different substrates. **Right:** Cortical neurons cultured on the same surfaces. Dashed circles indicate EGNITE material.

In vivo biocompatibility study

Functional evaluation after intraneural implants

The algesimetry tests yielded similar values of pain withdrawal threshold between the implanted and contralateral hindlimbs in the two groups of rats (Figure 5A), without evidence of hyperalgesia that might had been induced by nerve compression or injury. In addition, walking track measurements (Figure 5B) did not show variations between the three groups with the implanted devices at 2 or 8 weeks. The SFI values were close to zero (normal value) at the different time points. In conclusion, there was no evidence of alterations in the motor and sensory functions conveyed by the sciatic nerve after implanting PI devices with or without EGNITE.

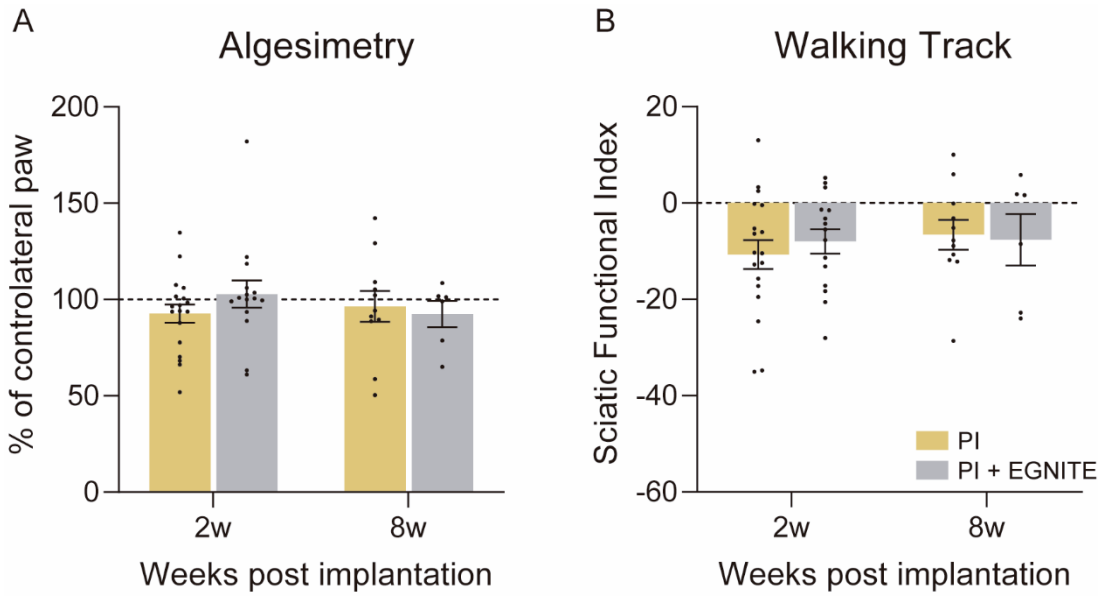

Figure 5. Functional test: Pain and walking assessment. A) Algesimetry test results expressed as percentage of force withdrawal (vs contralateral control paw) of animals implanted with PI and PI with EGNITE. **B)** Plot of the SFI obtained in the walking track test. $p>0.05$, two–way ANOVA followed Tukey's multiple comparison test.

After 8 weeks of follow–up post implantation in the sciatic nerve there were no significant changes in the electrophysiological results of the three groups of rats (control/contralateral, PI and PI with EGNITE). Only a reduction in the amplitude of TA CMAP in the PI group and the GM in the PI + EGNITE group at 2 weeks (Figure 6D, E, F) was found; since the TA muscle is innervated by the peroneal fascicle, where the implants were not placed, and the amplitudes of both muscles recovered at 8 weeks, these decrease can be attributed to the surgery alone and not to the implant.

CMAP latency did not show differences between groups during follow-up (Figure 6D–F), indicating no myelin damage.

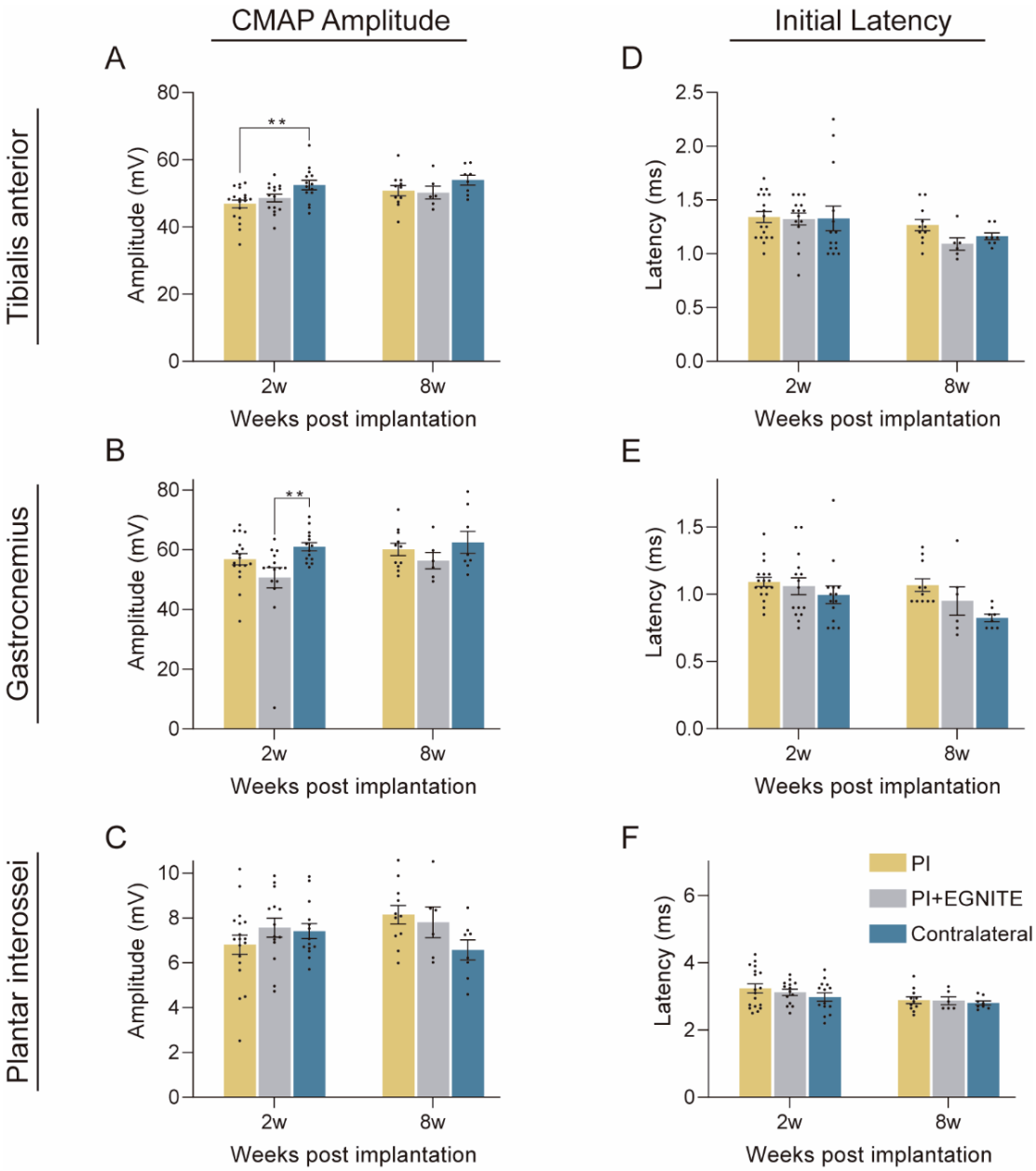

Figure 6. Functional test. Motor nerve conduction. Motor nerve conduction parameters of animals implanted with PI or PI + EGNITE and contralateral paws during 8 weeks follow-up. **A–C)** CMAP amplitude of TA (A), GM (B) and PL (C) muscles. **D–F)** CMAP onset latency of TA (D), GM (E) and PL (F) muscles. **p<0.01 vs contralateral, two-way ANOVA followed Tukey's multiple comparison test.

Inflammatory response

One of the main events during the FBR is the infiltration by hematogenous macrophages into the implanted tissue, as part of the inflammatory phase (Lotti et al.,

2017). Comparison between implants with and without EGNITE revealed no differences in the number of macrophages labeled in the tibial nerve (Figure 7A, C). On the other hand, the last phase of the FBR and one of the main problems for the long–term functionality of intraneural electrodes is the formation of a fibrous capsule around the implant. Figure 7B shows that the capsule thickness was similar for implants with and without EGNITE at both 2 and 8 weeks, indicating that the presence of EGNITE did not induce damage to the nerve and further fibrotic scar formation. Immunohistochemical images (Figure 7D) show numerous axons near the implants (at around 20 µm) at both time points, indicating limited damage and remodeling after the implant, consistent with previous works (de la Oliva et al 2018a). Altogether, the chronic biocompatibility study indicates that EGNITE is suitable for chronic intraneural implantation, inducing no significant nerve damage nor neuroinflammatory response.

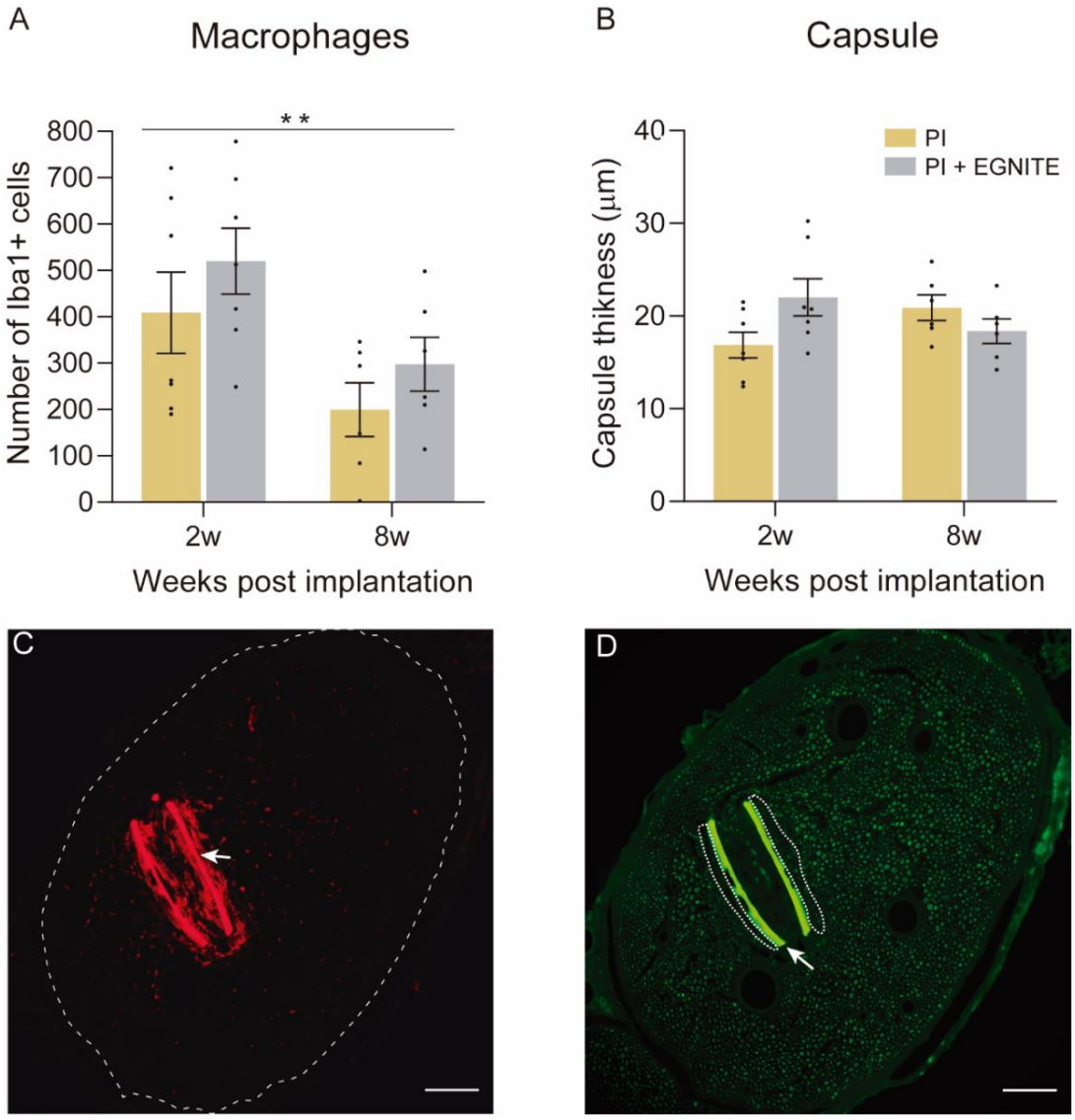

Figure 7. Evaluation of the FBR to intraneural implants. **A)** Number of inflammatory Iba1+ cells in the tibial nerve of animals implanted with PI devices with and without EGNITE. **p<0.01, two–way ANOVA followed Tukey's multiple comparison test. **B)** Tissue capsule thickness around the devices in the tibial nerve of animals implanted with PI devices with and without EGNITE. **C, D)** Representative images of a tibial nerve labelled for inflammatory cells (Iba1, C) or axons (RT97, D) implanted with a device (arrow) at 2 weeks post implantation in the tibial fascicle (dashed line in C) and the tissue capsule (dotted line in D). Scale bar: 100µm.

Conclusions

In conclusion, our results show that both PI and EGNITE are biocompatible materials. None of the implants produced functional alterations other than that caused by the implantation process and the FBR was similar to other implantable neural devices. This is a key first step towards the development and *in vivo* use of neural electrodes using GBM as novel promising conductive material.

Chapter 2

Novel graphene–based electrodes for interfacing the peripheral nervous system

Overview

During the last decades, advances in PNI have provided numerous designs based on their location in relation to the nerve anatomy (del Valle & Navarro, 2013). Overall, the designs are categorized in terms of invasiveness and selectivity. From low to high there are extraneural, intraneural and regenerative PNI. Intraneural PNI implanted within the nerve fascicles and thus in close contact with the axons are presently the preferred option for a bidirectional interface for neuroprostheses used in amputees. They offer a bearable compromise between selectivity and invasiveness (Micera *et al.*, 2008b). The lower intensity for stimulation and the increased SNR of the recordings are favored by their proximity to the axons (Yoshida *et al.*, 2000). Specifically, the TIME type, implanted transversely in the nerve, allows stimulating and recording different subsets of axons in various fascicles over the nerve cross–section with higher selectivity than multichannel cuff and longitudinal intraneural electrodes (Boretius *et al.*, 2010; Badia *et al.*, 2011).

While new PNI designs have been developed, new materials are also being investigated, mainly biocompatible materials with good electrical capacities that allow prolonged use of the prosthesis. Briefly, in a PNI there is a substrate isolating material and the conductive metal lines. Each PNI may have several ASs that are the uncovered parts of the conductive material, from where the electrical charges are transferred. Metallic microelectrodes (i.e. Au, Pt, iridium oxide (IrOx) fabricated on flexible substrates such as PI or ParC are commonly used to fabricate PNI (Navarro *et al.*, 2005). When used at the millimeter scale, these metal interfaces can normally provide robust neural signal transduction. As the electrode size is reduced to the micrometer scale, their performance decreases due to their reduced electrochemical surface area, which increases interfacial impedance and reduces the amount of charge that can be injected into the tissue (Cogan, 2008). The decrease in the size of AS may increase selectivity. The smaller the AS area, the smaller the nerve area that will be interfaced. Consequently, the aim is to work from a device with a few big AS to one with many small AS in order to increase the spatial resolution of stimulation and recording (Khodagholy *et al.*, 2014; Kohler *et al.*, 2017). To address the miniaturization of neural interfaces, electrode modification strategies such as conductive polymer combinations, surface modifications or functionalization have been developed to

increase performance and the electrochemical surface area (Pigeon *et al.*, 2003; Chung *et al.*, 2015) (Szostak *et al.*, 2017). In this work engineered graphene EGNITE has been used in place of metal electrodes to create a new generation of nerve interfaces. High charge carrier mobilities and transconductances are produced by the graphene/electrolyte substantial interfacial capacitance (Dankerl *et al.*, 2010; Hess *et al.*, 2011). Together with a relatively low noise graphene based electrodes are expected to enable recordings with a good SNR (Blaschke *et al.*, 2016).

Materials and Methods

Implant design

The electrode device was designed for intraneural implantation, following the TIME design (Boretius et al., 2010). The device (Figure 1A, B) consisted of two linear arrays of 9 circular microelectrodes (ø 25 µm) and a reference electrode (0.02 mm^2) along a 1.2 mm strip. Each linear array is placed at opposite sides of the stripe. EGNITE microelectrodes are made of a thin film of hydrothermally reduced graphene oxide stacked on top of gold. The arrays of EGNITE microelectrodes were integrated into flexible devices (total thickness of 13 µm) using the biocompatible and flexible polymer, PI, as substrate and insulation, and gold for the tracks. The PI strip has a total length of 57.6 mm and a width of 280 µm. At the center of the strip, it is narrowed down to only 100 µm. For implantation, the strip is folded at the midline to align the left and right sides of the strip and to create an arrow like shape at the tip of the electrode, enabling penetration into the nerve. The PI strip is widened at the ends (pad area) to connect the device with external equipment through a ZIF multiconnector (Viana *et al.*, 2022).

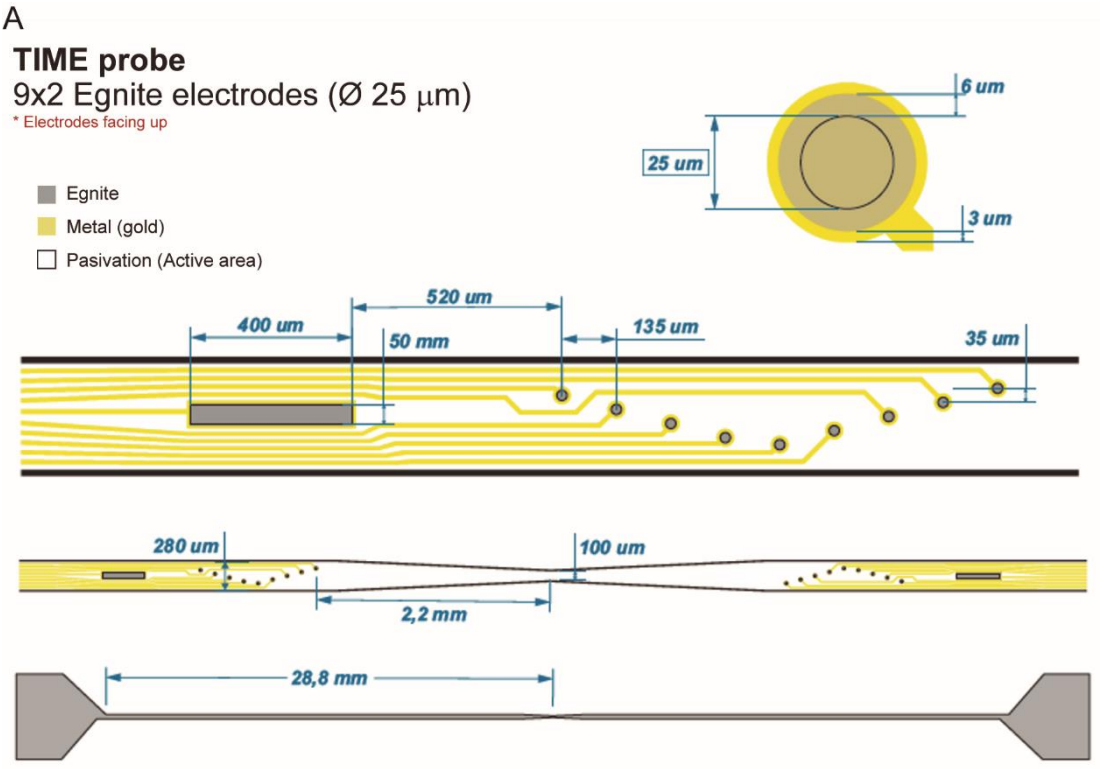

Figure 1. TIME design. A) TIME design for *in vivo* functional tests. (Continued next page)

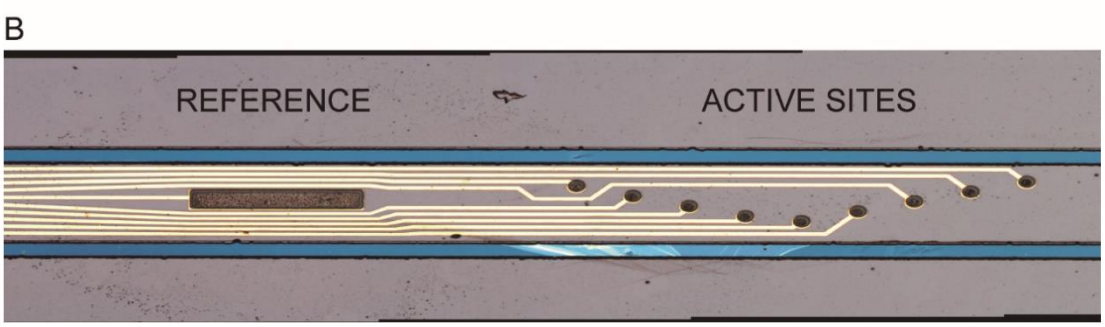

B) Image of a section of a fabricated probe with 9 graphene microelectrodes (black dots) plus a reference (black rectangle). For more details see Viana et al., 2022.

Nerve implantation

To assess the functionality of developed TIME EGNITE devices (Figure 1A, B), they were transversally implanted in the sciatic nerve of rats. After surgery, all animals were housed under standard conditions. Electrophysiological studies of electrical stimulation and recording using the implanted devices were performed acutely and at 30– and 60–days post implantation (dpi).

Operations were performed under anesthesia with ketamine/xylazine (90/10 mg/kg i.p.) on female SD rats weighing 300–350 g. The sciatic nerve was surgically exposed at the mid–thigh and carefully freed from adherences to surrounding tissues. Nerves and EGNITE devices were delicately handled with fine forceps. The devices were inserted transversally across the tibial and peroneal branches of the sciatic nerve (Figure 2A) with the help of a straight needle attached to a 10–0 loop thread (STC–6, Ethicon) (Badia *et al.*, 2011b; de la Oliva 2018b) the thread was passed between the two arms of the device and pulled the arrow–shaped center of the electrode strip. The insertion was monitored under a dissection microscope to ensure correct placement of the device (Figure 2B, C).

After conducting nerve stimulation and recording protocol, the device was attached to adjacent muscle tissue using two suture stitches. In addition, fibrin glue and KwikKast® were used to keep the implanted electrode in place during the time of implantation. To easily access the electrode contacts in chronic experiments, the pads portion of the devices was passed through the muscular incision and placed subcutaneously in the side. The pads were protected with a plastic envelope sealed with Kwik Kast® to prevent the pads not being damaged and covered by fibrotic tissue. The plastic envelope was placed under the skin, the muscle incision was closed with stitches and the skin wound was closed with staples.

All experimental procedures performed were approved by the ethical committee of the Universitat Autònoma de Barcelona in accordance with the European Communities Council Directive 2010/63/EU. Moreover, adequate measures were taken to minimize pain and animal discomfort during surgery and in the postoperative follow–up.

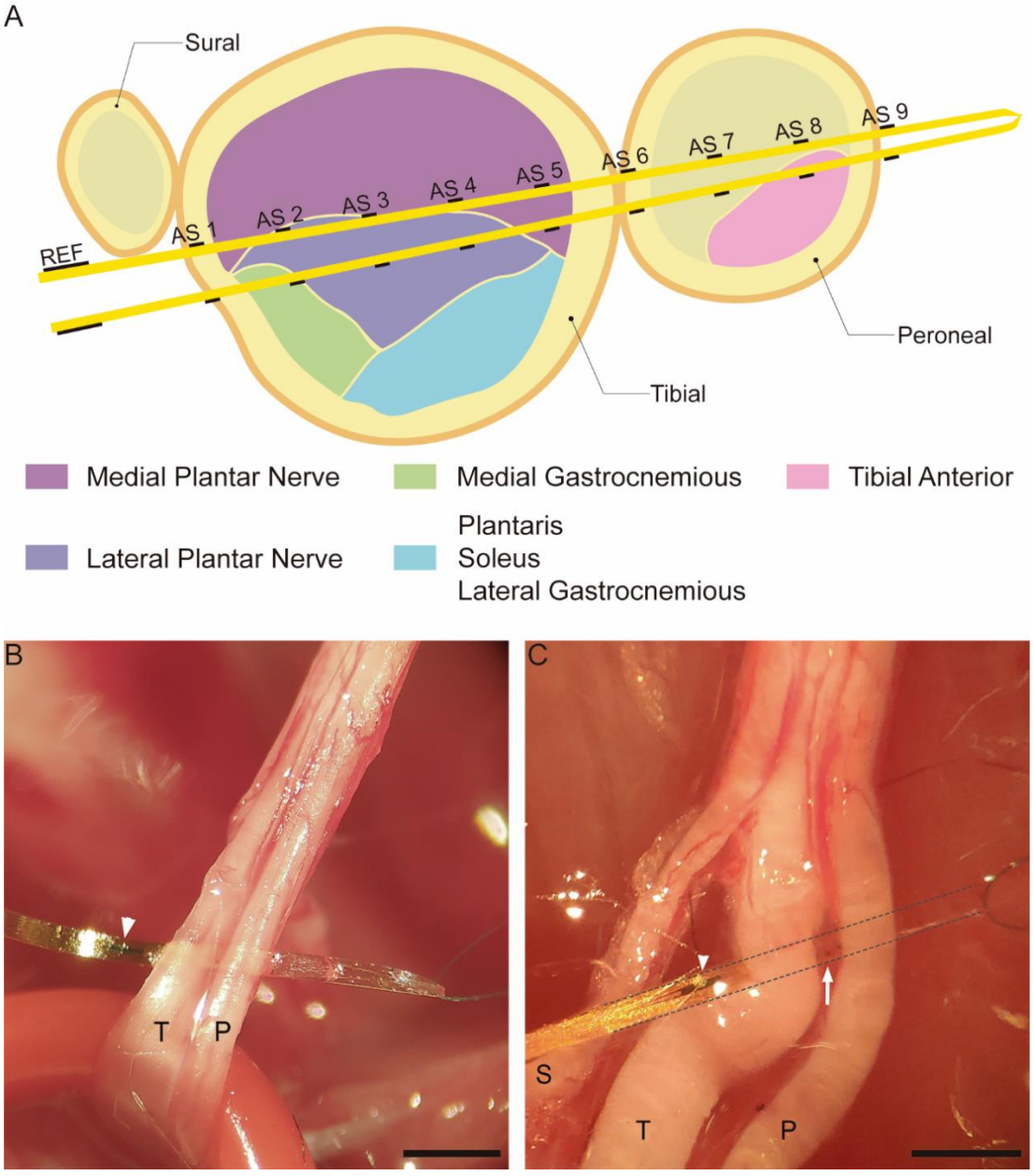

Figure 2. TIME implantation. A) Schematic cross section of an implanted TIME with active sites (AS 1–9) crossing the tibial and peroneal fascicles. Subfascicle topography of the rat sciatic nerve is extracted from Badia et al (2010). **B, C)** Detail of a device within the sciatic nerve. White arrowheads indicate the reference electrode. The white arrow indicates some ASs or microelectrodes between the tibial and peroneal fascicles of the sciatic nerve. S: Sural, T: Tibial, P: Peroneal. Scale bar: 1 mm.

Nerve stimulation protocol

To assess the stimulation performance of the implanted electrodes (n=19), electrical stimulation was applied with the EGNITE devices to the sciatic nerve. At every time point, biphasic current pulses were delivered through each one of the AS against a common reference within the device ribbon part or a needle reference electrode placed near the sciatic nerve. Increasing current pulses with a width of 100 µs and an intensity up to 100 µA, were delivered by a Digitimer DS4 stimulator. Devices used for electrical stimulation have a current limit in the charge they can safely deliver to avoid a decrease in device performance and hazardous chemical reactions. EGNITE devices have a limit of 100 µA with a pulse duration of 100 µs. Above this threshold the electrode may deteriorate as we increase the current applied.

CMAPs were recorded from GM, TA and PL muscles using small needle electrodes placed in each muscle belly (Badia et al., 2011). The CMAPs were amplified (P511AC, Grass), band–pass filtered (3Hz to 3 kHz), and digitized with a Powerlab system (PowerLab16SP, ADInstruments) at 20 kHz using LabChart software. The amplitude of each CMAP was measured peak to peak and normalized to the maximum CMAP amplitude obtained in each experiment by stimulation of the sciatic nerve with two needle electrodes. For each electrode, the threshold current of stimulation which elicited 5, 30, and 95% of the maximum CMAP was determined. The AS with the lowest threshold value in each device was used for analysis.

Finally, the selectivity index (SI) was calculated to quantify the specific activation of a single muscle among the set of three muscles (equation 1) (GM, PL, TA), as previously described (Veraart *et al.*, 1993a; Badia *et al.*, 2011a). The selectivity was considered when any of the recorded muscles CMAP reached 5% and 30% of the maximum CMAP.

$$(1) \qquad SI = \frac{CMAP}{\sum_j CMAP_{nj}} \qquad\qquad (2) \qquad SI = \frac{CNAP}{\sum_j CNAP_{nj}}$$

The stimulation protocol is summarized in Figure 3.

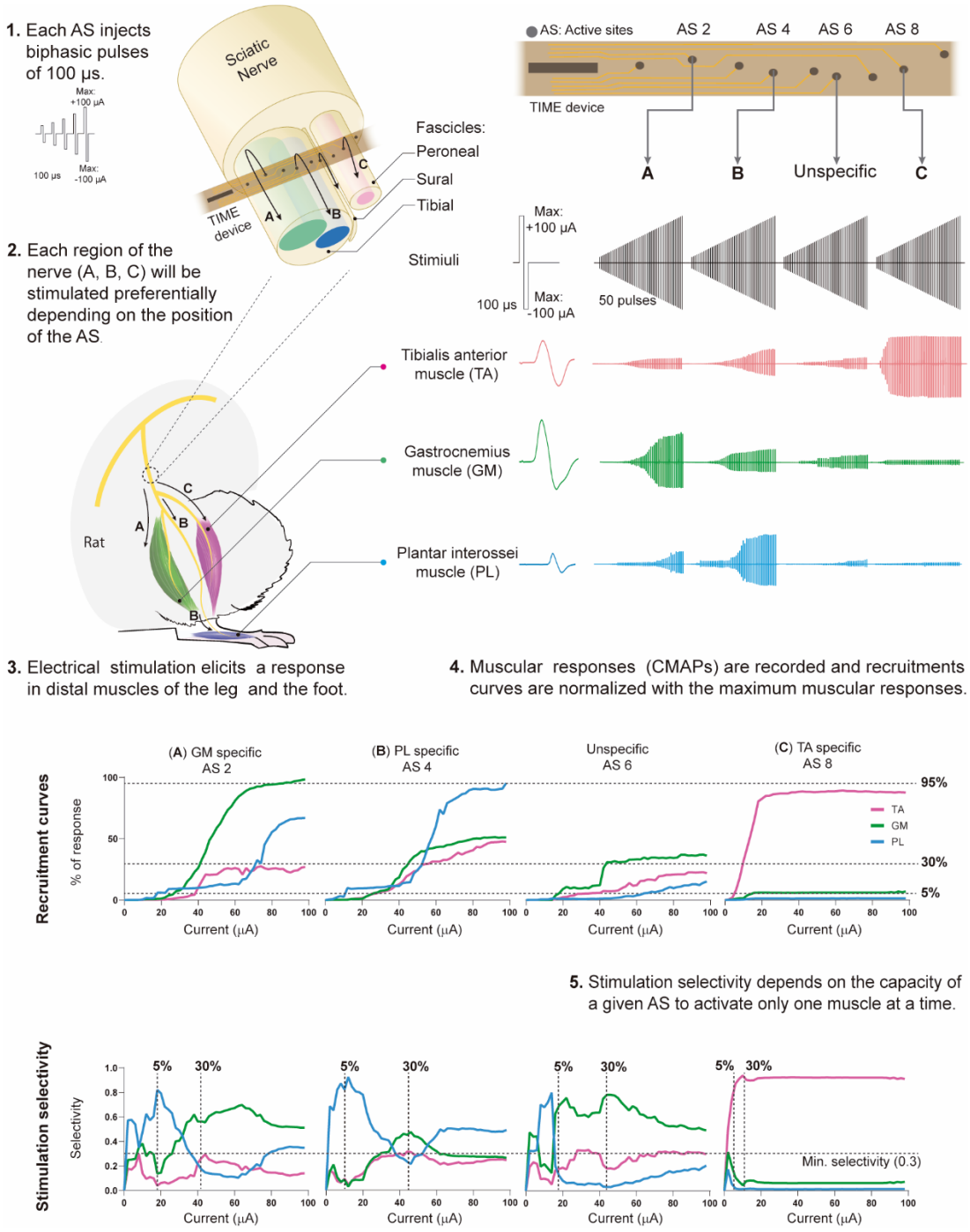

Figure 3. Protocol to analyze stimulation functionality of TIME EGNITE devices. (1) Each AS injects a sequence of 50 biphasic pulses of increasing current (0–100 µA), 100 µs each at 3 Hz. Each set of 50 pulses is repeated twice. **(2)** The TIME is inserted transversally into the tibial and peroneal fascicles of the sciatic nerve. Hence, ASs are interfacing different regions of the nerve (A, B and C) which innervate different muscles (PL, GM and TA). **(3)** Electrical stimulation through each of the ASs elicit a response in distal muscles of the leg and the foot. Muscular responses vary depending on the AS that is being used. **(4)** Monopolar needles are located in the belly of studied muscle to record the CMAPs produced in each step of the stimulation protocol. CMAPs are normalized to the maximum amplitude of each muscle to build the recruitment curve: a representation of the progressive activation of the muscle as the current increases. The threshold currents needed to activate each muscle at 5%, 30% and 95% are used for further analyses.

(Legend continued next page)

(5) Stimulation selectivity measure the capacity of an AS to stimulate one muscle but not the others. Selectivity is calculated at two points: when one of the muscles has reached 5% and when a muscle has reached 30%. Usually, selectivity and current are inversely proportional. Thus, selectivity is often higher at 5% compared to 30%. If the three muscles are activated equally the selectivity is minimum (0.3).

Nerve recording protocol

To assess the recording capabilities of EGNITE electrodes, two different protocols were performed (Figure 4), previously described by Badia et al., 2016.

First, CNAPs were recorded from each one of the AS following electrical stimulation of the distal MPN and LPN at the hind paw (n=14). Ten monophasic rectangular pulses of 10 µs from 1 t0 10 mA (Grass S44 with PSIU6 stimulus isolation unit) were delivered using two small needles inserted on the medial or lateral side of the paw. The amplitude of each CNAP was measured peak to peak and normalized to the maximum CNAP amplitude obtained in each experiment recorded with hook electrodes on the sciatic nerve. The SI was calculated (n=11) to quantify the specific activation of a nerve among the set of two nerves (equation 2). For selectivity calculations, recorded nerve potentials were considered if they were above 5% of the maximum CNAP. Two additional devices (TIME 4 and TIME 5) were tested with a slightly different protocol. To produce a smoother recruitment curve, 50 biphasic rectangular pulses of 100 µs and up to 10 mA (DS4 Stimulator, Digitimer) were delivered.

For the second protocol, evoked sensory activity after pressing the animal hind paw with a thin probe, a Von Frey monofilament and tweezers was also recorded (functional recording) (n=6). The thin probe was used to quickly scratch the sole of the paw. The Von Frey monofilament was used to contact specific areas of the paw (Kennedy *et al.*, 1988). The tweezers were used to pinch toes of the paw to elicit a noxious stimulus. ENG recordings were amplified x1000, band–pass filtered (between 300 Hz and 10 kHz) and fed to a power–line noise eliminator (Hum Bug, Quest Scientific), then digitized at 20 kHz and recorded with LabChart software (PowerLab System, ADInstruments). The total power of the recorded signals and the noise (no stimulus applied) was obtained after applying the short–time Fourier transform with a window of 1 ms, and an overlap of 87.5%. The best recording AS in each TIME was used to calculate the SNR, as the ratio between the mean of the total

power when the stimuli are applied and the mean of the total power when there are no stimuli applied.

The recording protocol is summarized in Figure 4.

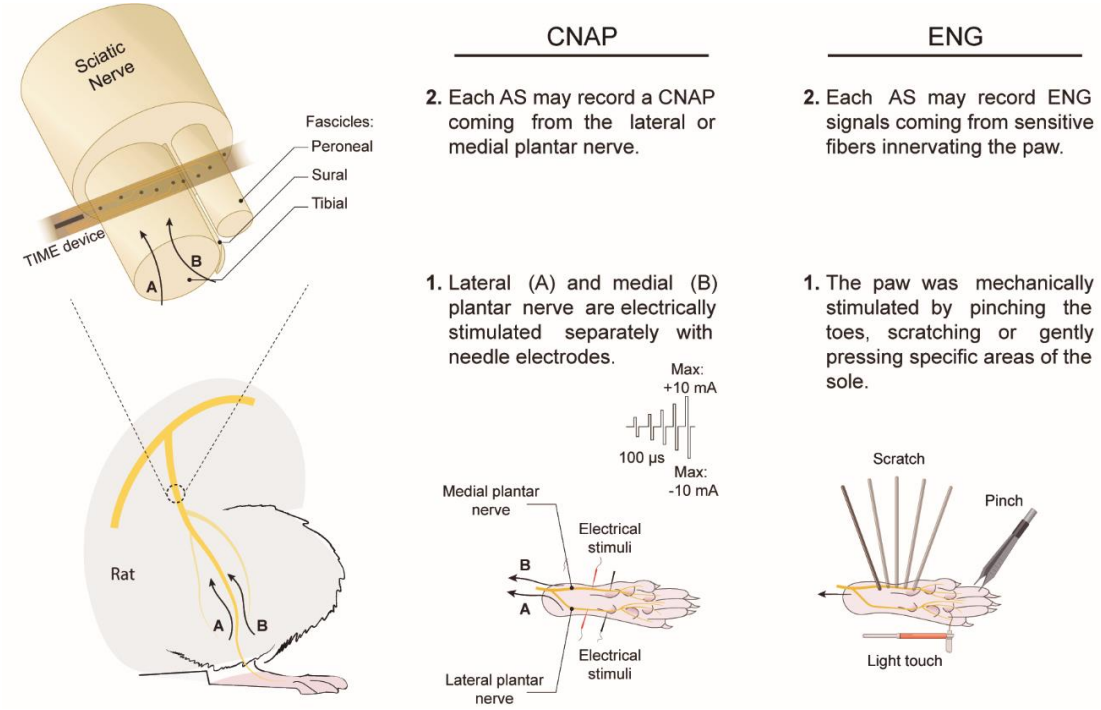

Figure 4. Protocol to analyze recording functionality of TIME EGNITE devices. CNAP. The lateral (A) and medial plantar nerve (B) were electrically stimulated using needle monopolar electrodes with 50 biphasic pulses of increasing current to a maximum of 10 mA at 3 Hz. Elicited CNAPs were recorded though different ASs in the TIME device. CNAPs are normalized to the maximum valued recorded with hook electrodes around the sciatic nerve. **ENG**: The paw was mechanically stimulated by pinching the toes with tweezers, scratching the sole with a probe, and pressing specific areas of the sole with a Von Frey filament. Elicited sensory signals were recorded by each AS in the TIME device.

Data analysis

The normality of the data was studied to apply the correct statistical method (parametric or nonparametric) using Shapiro–Wilk test. Statistical comparisons between two groups or conditions were made by paired T–test and between two or more groups with two variables by means of two–way ANOVA followed by Tukey's or Sidak's multiple comparison test. Differences were considered significant when $p < 0.05$. The GraphPad Prism 8 software was used for statistical analyses. Results are expressed as mean ± SEM.

Results

During the implantation period rats remained in good health. However, two of the animals damaged the ending part of the device which had been placed under the skin the next day of implantation, so they could not be tested at 30 dpi. No further postoperative complications were observed; the incision wounds healed without inflammatory signs, indicating no gross FBR. Plastic envelopes were found covered by a thin fibrotic tissue, and once removed, revealed the devices pad without damage.

Nerve stimulation

The stimulation tests after acute and chronic implantation proved that EGNITE microelectrodes were able to stimulate different axonal subpopulations of the sciatic nerve, depending on the AS used and the intensity of stimulation. For these tests, the EGNITE devices ending pad was connected to a ZIF multiconnector.

Recruitment curves of muscle activity were plotted (Figure 3) for each muscle to calculate the threshold of charge needed to reach 5, 30, and 95% of the maximal CMAP amplitude (Figure 5A). In acute test and chronic test, almost all working devices were able to stimulate minimally the nerve up to 5% of the maximal CMAP amplitude. More than 75% of the devices allowed reaching a response higher than 30%, whereas only slightly more than half of the devices achieved a response higher than 95% (Figure 5B). The constrain in current delivery of 100 µA for EGNITE AS has prevented to produce stronger activation of the muscles in some devices. We exceeded this CIL only if ASs did not produce any response at lower levels, most commonly in chronic experiments.

Of particular interest is the low current needed to activate the motor nerve fibers (Figure 5A). For example, in acute experiments, 30% of the muscle activation (the minimum stipulated to overcome gravity (Boretius *et al.*, 2010)) was elicited by single pulses of less than 50 µA for the three muscles and less than 65 µA were needed to obtain 95% of the muscle activation. Compared to previous studies in which TIME devices with 80 µm diameter electrodes of IrOx were used (de la Oliva *et al.*, 2019), EGNITE electrodes elicited a response with thresholds 2 to 3 times lower (Figure 5C). In chronic tests, the functionality of devices decreased, evidenced by an increased

activation current threshold (Figure 5A), most probably due to fibrotic encapsulation or AS deterioration.

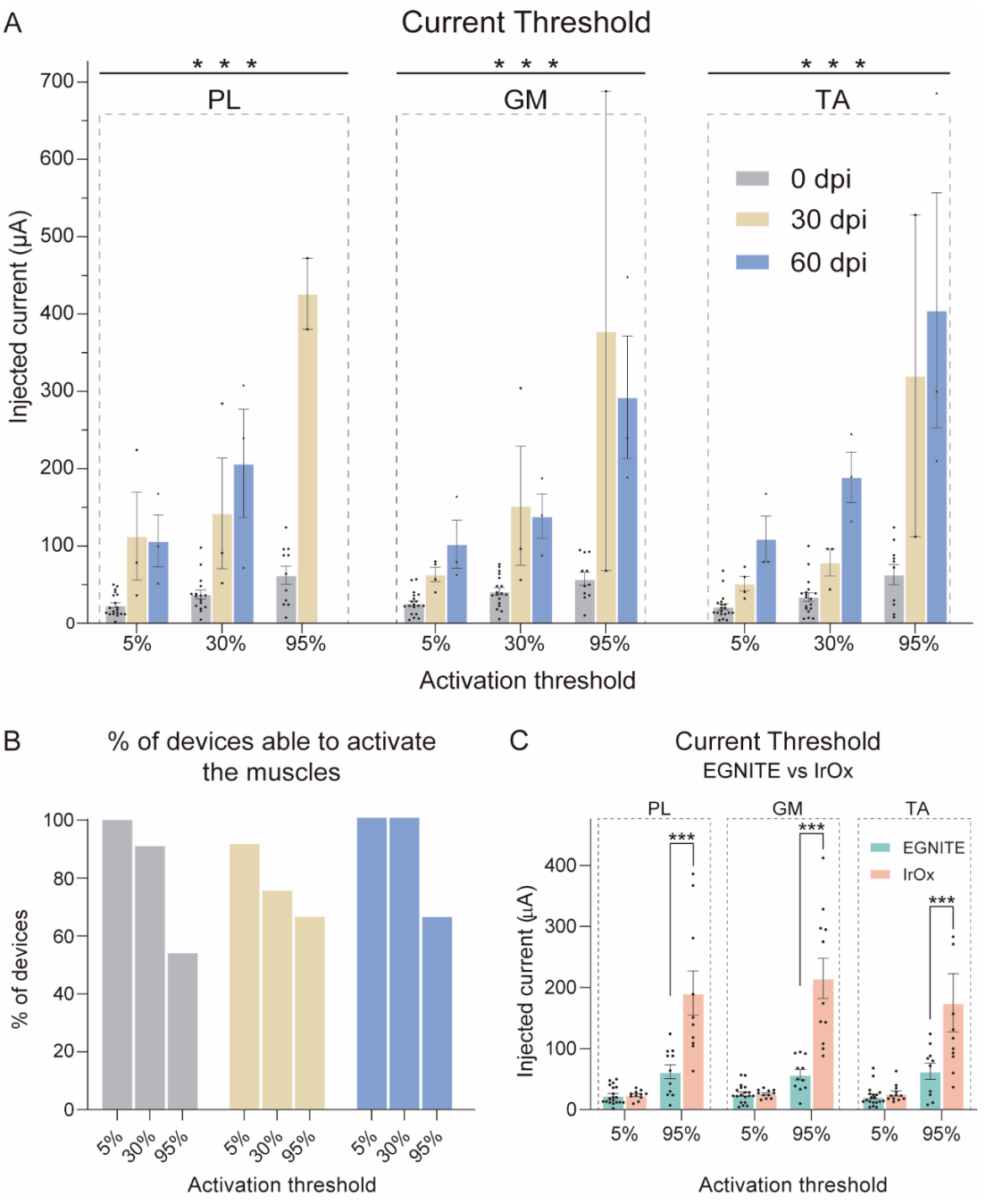

Figure 5. Stimulation capabilities of TIME EGNITE devices. A) Current threshold needed to elicit 5, 30, and 95% of the maximum CMAP amplitude in the PL, GM, and TA muscles over 60 days. ***p<0.001 each muscle vs time, two-way ANOVA followed Tukey's multiple comparison test. **B)** Percentage of working devices able to elicit 5, 30, and 95% of the maximum CMAP amplitude. **C)** Comparative analysis between TIME electrodes made of EGNITE or iridium oxide (IrOx) of the current needed to elicit 5% and 95% of muscle activation at 0 dpi. IrOx data is extracted from (de la Oliva *et al.*, 2019). ***p<0.001, two-way ANOVA followed Tukey's multiple comparison test.

For assessing the selectivity by which the electrodes were able to activate each of the three muscles, SI were calculated (Figure 6A, B). The SI for the three tested muscles ranged between 0.6 and 0.9, similar to that found in other previous studies using TIME design of electrodes (Badia et al., 2011a; de la Oliva et al., 2019). The SI showed changes during the follow–up of chronic implants. For the TA muscle there was a drop in the selectivity at 60 dpi. In the PL muscle the selectivity also decreased at 30 dpi. On the contrary GM selectivity, that was lower at baseline than in the other two muscles, remained stable during the follow–up.

Selectivity differences, among the set of muscles, may be explained due to the different location of axons innervating the muscles inside the sciatic nerve. It is easier to obtain high selectivity of the TA muscle because it is innervated by the peroneal nerve. However, this fascicle is smaller and is close to the tip of the implant. Thus, the selectivity of this TA is more conditioned by the movements of the implanted electrode within the nerve that may displace AS from peroneal nerve. The nerve fibers that innervate the PL and the GM muscles are located in the same branch, the tibial nerve (Badia et al., 2010); thus, obtaining high selectivity between these two muscles is more complicated compared to the TA muscle. Regarding the better stability in GM selectivity, its nerve fibers are well circumscribed and farther from the tip of the implant, so there are more possibilities that the ASs remain within this fascicle during the follow–up. Figure 3 shows an example of an implanted device and how the position of each AS within the sciatic nerve causes the selectivity to shift between the muscles. In this case, AS 8 is placed within the peroneal nerve since it shows high SI for the TA muscle. On the other hand, AS 2 and 4 are located within the tibial nerve, being AS 2 likely the closest to the GM fascicle and AS 4 in the fascicle supplying the plantar muscles. AS 6 is in between the tibial and peroneal nerves and its ability to activate any of the muscles is low.

SI was calculated when one of the muscles reached 5% activation and when it reached 30% activation. The selectivity obtained in the latter is lower than in the former level. When a stimulus pulse is given at low intensity from an AS, the current is limited to a small area around and stimulates few axons. The greater the applied current, the greater the stimulated area and, therefore, selectivity is reduced. Hence, the more current we apply, the greater the activation of a muscle, but the higher

chance to activate other muscles at the same time, decreasing selectivity (see Figure 3 bottom graphs).

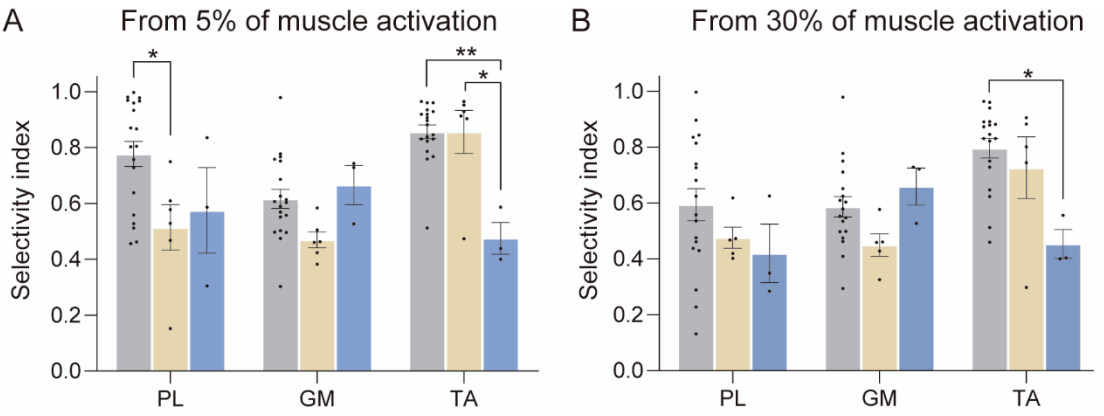

Figure 6 Stimulation selectivity of TIME EGNITE devices. A, B) SI by muscle from 5% and 30% respectively of the maximum CMAP amplitude. *p<0.05 **p<0.01, two-way ANOVA followed Tukey's multiple comparison test.

Nerve recording

CNAP recording

To evaluate the recording capabilities of EGNITE devices, CNAP evoked by electrical stimulation of the MPN or LPN (Figure 7, 8), and ongoing single potentials elicited by mechanical stimuli on different areas of the paw of the animal (Figure 9) were recorded from each AS in the device. First, it is worth noting that not all the AS of the devices tested allowed recording of CNAP or functional signals, either because they were not working, or because the AS was not at the adequate point in the nerve to detect the small neural signal.

The EGNITE devices were able to record small CNAPs, from a few µV in amplitude; we accepted deflections above 5 µV as actual potentials. The electrical stimulus was increased in steps, producing CNAPs of increasing amplitude (Figure 7A). The CNAPs were recorded as triphasic potentials at a latency compatible with a conduction velocity corresponding to Aα and Aβ nerve fibers. These CNAPs were elicited by electrical stimulation of both MPN and LPN separately. All devices successfully recorded CNAPs during the acute test, with a mean maximum amplitude of about 200 µV (Figure 7B), but only a couple were able to do so at 30 dpi. Representative examples of CNAPs are shown in Figure 7A.

Eleven devices were employed to assess the recording selectivity of CNAPs from the MPN and LPN. The mean SI for both nerves was approximately 0.7 (Figure 7C). Six devices achieved 100% selectivity in at least one AS, meaning that a specific AS was able to record CNAPs from one nerve and not the other. Conversely, two devices obtained 0% selectivity for one of the nerves, indicating that they were unable to record the activity of one of the nerves. Finally, three devices showed a selectivity greater than 0.6 for both nerves simultaneously. This suggests that in most cases (8 devices), each TIME implant is selective to one nerve.

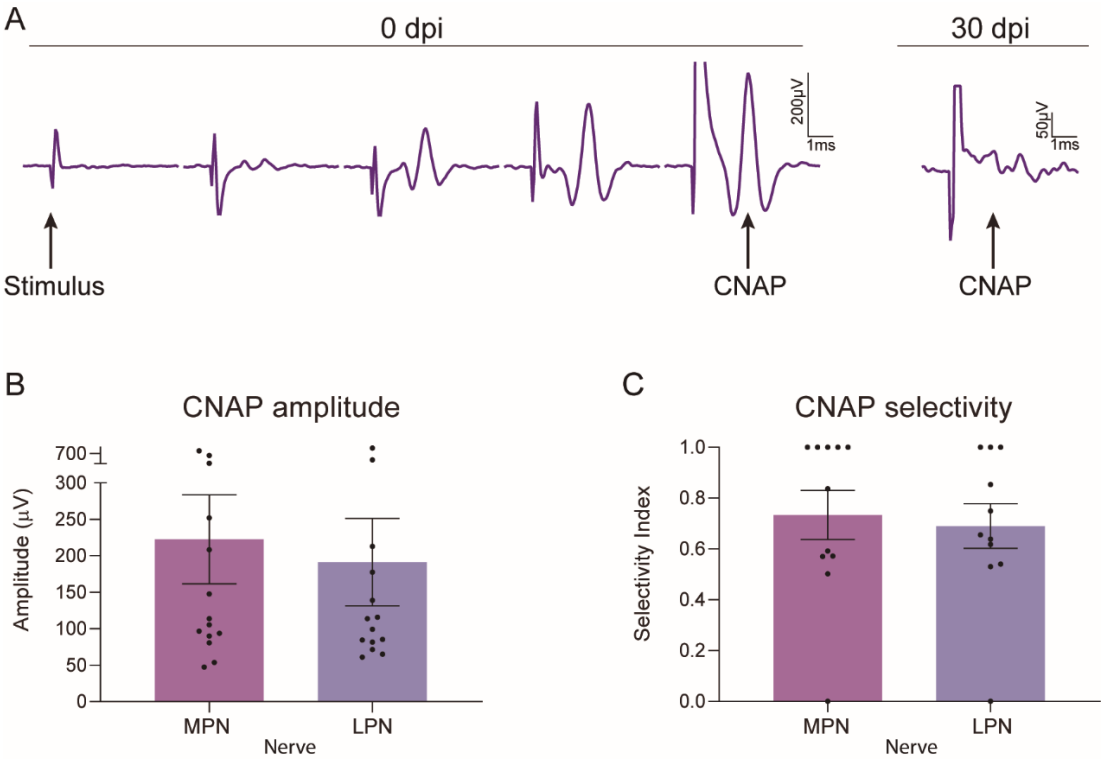

Figure 7. Recording capabilities of TIME EGNITE devices. CNAP. A) Representative CNAPs recordings elicited by electrical stimulation of the distal plantar nerve at 0 and 30 dpi. B) Maximum CNAP amplitudes elicited by electrical stimulation of the MPN or LPN, recorded from implanted devices at 0 dpi. T–Test. C) CNAP selectivity of the MPN and LPN. The maximum selectivity value among all ASs in each device for both nerves was used for the analysis. T–Test.

Two additional devices were analyzed with a stimulation protocol that allowed for a higher resolution recruitment curve (more stimulation steps) (Figure 8A–D). In these two cases, only one arm of the device was analyzed due to time constraints of the *in vivo* procedure. The TIME 4 recorded CNAPs equal to or close to the maximum CNAP of the LPN from AS 2, 3, 4, 5, and 6, while AS 1, 7, 8, and 9 recorded low–amplitude CNAPs (Figure 8B). For MPN CNAPs (Figure 8A), the

amplitude of the recordings was lower, although AS that recorded high–amplitude potentials for the LPN recorded also higher potentials for the MPN compared to the others. Figure 8E, F shows how the recording profile of each AS has an impact on selectivity. In the TIME 4 (Figure 8E) AS 2, 3, 4, and 5 have higher selectivity for the LPN, while AS 1, 2, 7, and 8 do not show selectivity as the values are close to 0.5. In the case of TIME 5, the plot representing the recruitment curves show that AS 4, 5, 6, 7, and 8 recorded higher action potentials for the MPN (Figure 8C) compared to the LPN (Figure 8D). Consequently, these ASs have higher selectivity, as seen in Figure 7F, while AS 2, 3, and 9 show selectivity close to 0.5. AS 1 did not work, and therefore, it does not appear in the plots.

The analysis of the recruitment curves and selectivity indicates that the distribution of ASs within the nerve affects the ability to record signals from one nerve fascicle or the other. In Figure 8G and H, a possible location of ASs within the nerve is presented based on the results previously described. In the case of TIME 4 (Figure 8G), it is assumed that the device passed through a region of the nerve where the fibers from the LPN are located, while the fibers from the MPN are located further, which explains why the amplitudes of the recorded signals from the MPN are lower but still not negligible. In the case of TIME 5 (Figure 8H), ASs recorded higher potentials for the MPN, so the implant will be near the fibers coming from the MPN. Conversely, none of the ASs recorded high amplitudes of the LPN, so these fibers could be on the opposite side from where ASs are located and, therefore, outside of their recording range. Spatial selectivity of CNAPs in TIME implants was also addressed in Badia et al. (2016).

The nerve fibers supplying both MPN and LPN are located in the same tibial branch (Badia et al., 2010). As in the case of motor fibers innervating the GM and PL muscles, it was difficult to obtain high selectivity between axons placed in the same fascicle of the sciatic nerve. In addition, the small amplitude of the neural signals makes it difficult to detect the signals at low level of activation, thus being conducted by a few, well localized, nerve fibers. For these reasons, the selective targeting of specific sensory afferences by one AS is more difficult to achieve compared to motor efferent fibers in the study protocols used (see also Badia et al., 2016).

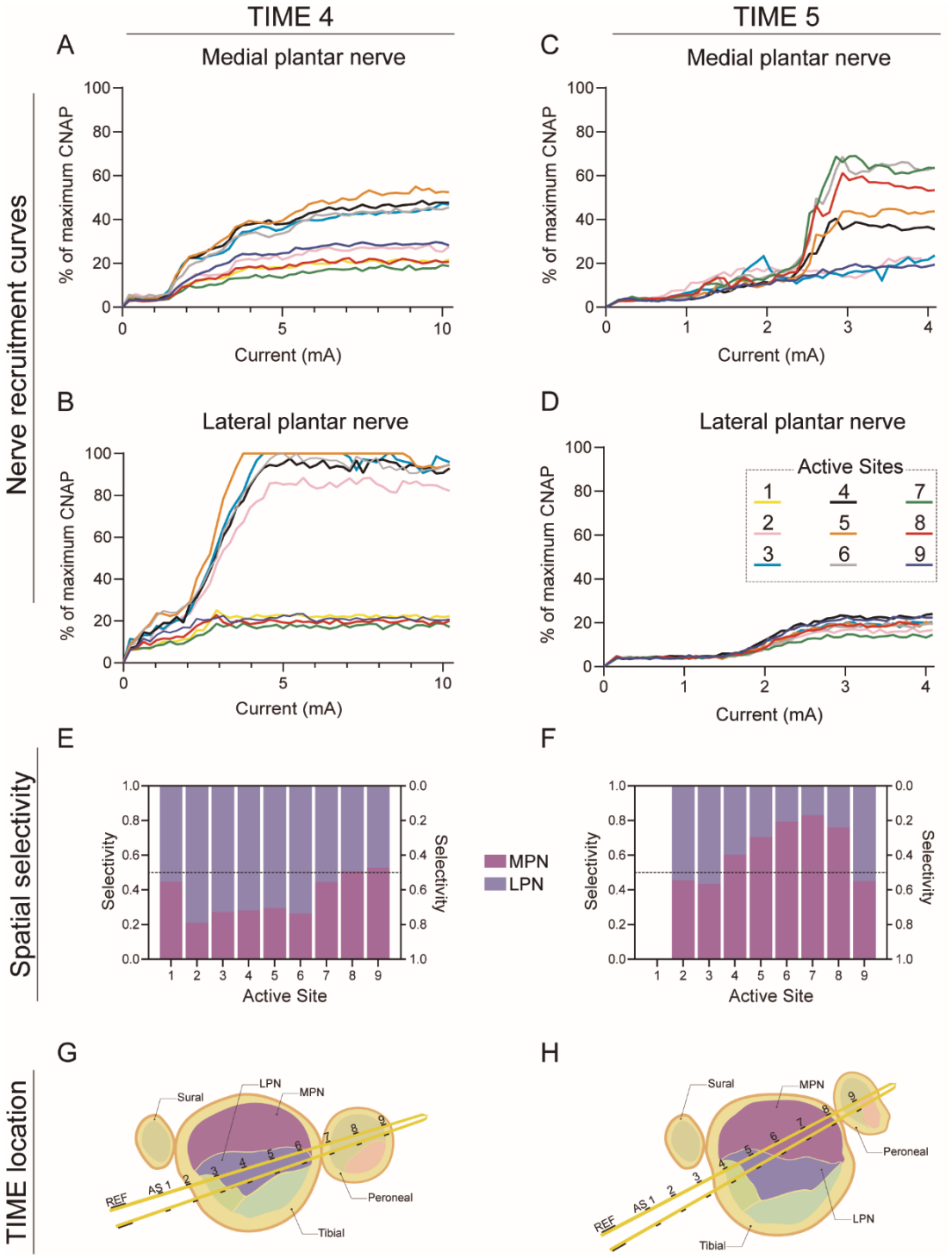

Figure 8. Recording capabilities of TIME EGNITE devices. Spatial selectivity. A–D) Nerve recruitment curves of the CNAPS elicited by stimulation of the MPN (A, C) and LPN (B, D) recorded from each AS of the TIME 4 and 5 devices placed in the sciatic nerve at 0 dpi. E, F) Selectivity from each AS of the TIME 4 (E) and TIME 5 (F) calculated in the same step of the current increasing stimulation protocol. G, H) The hypothetical location within the nerve of TIME 4 (G) and TIME 5 (H) devices, deduced based on selectivity data.

Mechanical stimuli recording

Regarding the recording of nerve signals, the CNAP are the easiest to record due to the spatial summation produced by the simultaneous stimulation of several axons. On the other hand, the mechanical stimuli that produce single action potentials are not so simultaneous, therefore the amplitude is lower, and the recording more difficult. In the functional recording protocol, we performed three different maneuvers while recording from 6 devices implanted (Figure 9):

- Noxious stimuli by pressing the toe (Figure 9A): The noxious stimuli elicited a reflex muscular response. Neural signals were in general masked by motor unit action potentials, that are quite larger in amplitude. All working ASs were able to record these muscular signals.
- Fast and light scratch of the sole of the paw (Figure 9B): Providing that a lot of axons of the sole skin are activated and the dynamic type of stimulus, it was easy to detect the signals form the noise, with an average close to 1.5 in the SNR plot (Figure 9D). The AS that worked well in stimulation tests were in general capable of recording better neural signals.
- Pressure on specific areas (Figure 9C): As fewer axons are being activated and the stimulus is static, it was significantly more difficult to differentiate signals form the noise (Figure 9D), with SNR average that in some cases were below 1 (TIME 6).

The SNR for the studied mechanical stimuli was similar to those obtained by Badia et al. (2016) using TIME devices containing larger IrOx ASs. To improve the recording capabilities of EGNITE devices we compared recording using one AS as active electrode with 5 AS joined, so the recording area was larger. With this configuration recordings were easier to distinguish from the noise (Figure 9D, TIME2). Moreover, it was possible to record signals elicited by pressing specific areas of the paw more often than with single AS.

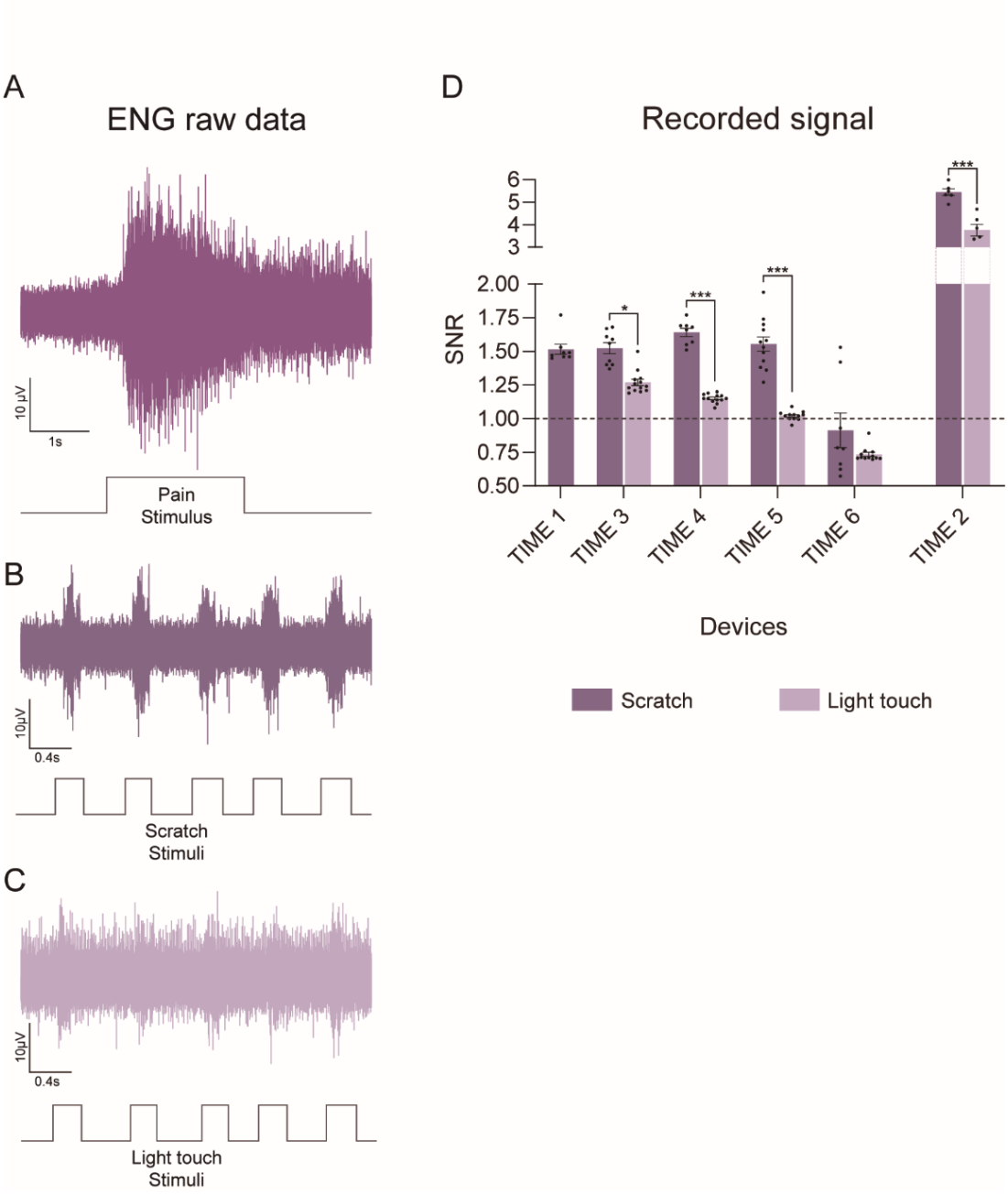

Figure 9: Recording capabilities of TIME EGNITE devices: Mechanical stimuli. A–C) Representative raw ENG recordings elicited by mechanical stimuli on the paw (A: Pain; B: Fast scratch; C: Light touch) recorded in the sciatic nerve with TIME devices. **D)** SNR of the mechanically elicited nerve signals in six TIME devices. In the TIME 2, five AS where shunted. When the values are below the dotted line the neural signal is indistinguishable from the noise. *p<0.05 ***p<0.001, Two–way ANOVA followed Sidak's multiple comparison test.

Conclusions

In this chapter we have studied the functional properties of EGNITE–based intraneural electrodes for stimulation and recording in the PNS. Neural stimulation was proven to activate specific subsets of axons within the fascicles of the sciatic nerve with low current thresholds in acute and sub–chronic conditions. Neural recordings of CNAP and ENG evoked by mechanical stimuli were feasible but were more affected by decreased functionality over time. This knowledge is essential to advance towards new materials that provide neuroprostheses with fine and precise control of stimulation and recording. Our work constitutes further proof that graphene–derived materials, and specifically EGNITE, is an optimum material to form part of a neural electrode for advanced neuroprostheses control.

Chapter 3

Enhancing chronic stability of intraneural implants. Modulation of the foreign body reaction to intraneural implants in the peripheral nerve.

Overview

Neuroprostheses have been an area of interest in the field of neuroscience, as they provide potential to restore the lost neural functions after a nerve injury or loss of a limb. Neural electrodes are used within neuroprostheses to create a bidirectional communication interface between the nervous system and an external device or system, such as a prosthetic limb (del Valle & Navarro, 2013). However, the use of these implants is limited by the FBR, leading to inflammation and fibrosis around the implant site.

The FBR is a complex biological process that occurs when a foreign object is introduced into the body. It is a natural response of the immune system to protect the body from potential harm caused by the presence of foreign substances. This reaction involves a series of events, beginning with the adsorption of proteins onto the surface of the implant and the recruitment and activation of immune cells. Immune cells then release cytokines and chemokines that promote inflammation and recruit fibroblasts, which deposit collagen around the implant site. Over time, this process concludes with the formation of a fibrous capsule around the implant, leading to an increased impedance, an increased threshold to stimulate axons, a decreased sensitivity, signal attenuation, and in some cases, implant failure (Grill & Thomas Mortimer, 1994; Lotti *et al.*, 2017; de la Oliva *et al.*, 2019; Gulino *et al.*, 2019; Carnicer–Lombarte *et al.*, 2021).

To address this issue, several strategies have been proposed to reduce the FBR and improve the biocompatibility of neural implants. These strategies include surface modification of the implant material and the use of anti–inflammatory or anti–fibrotic drugs among others (Carnicer–Lombarte *et al.*, 2021).

Dexamethasone is a corticosteroid that has been investigated as a potential strategy to reduce the FBR to neural implants. Dexamethasone can be administered systemically or locally, such as using coatings or hydrogels, to reduce inflammation and fibrosis around the implant. Systemic administration of dexamethasone has been proven to reduce the capsule around intraneural devices (de la Olive et al, 2018c) and significantly improve chronic functionality (de la Oliva *et al.*, 2019). However, there are concerns about the possible side effects of long–term use of systemic

corticosteroids, including osteoporosis, metabolic, and cardiovascular disease (Desgeorges *et al.*, 2019).

Metformin is a safe and widely used agent for type II diabetes that has been shown to prevent fibrosis in different tissues. This antifibrotic effect is attributed to adenosine monophosphate–activated protein kinase (AMPK) activation, which interferes with TGF–β1 signaling, a key pathway involved in fibrosis (Rangarajan *et al.*, 2018). While the effects of metformin on fibrosis in peripheral nerves have not been directly studied, the results seen in other tissues suggest that it may be a promising candidate for reducing the formation of a capsule around intraneural implants.

In this chapter, we hypothesized that metformin ameliorates the fibrosis associated with an intraneural implant. To test this hypothesis, we used mock LIFE devices implanted in the sciatic nerve of rats and treated them systemically with metformin and with dexamethasone for comparison.

Materials and Methods

Surgical procedure

Operations were performed under anesthesia with ketamine/xylazine (90/10 mg/kg i.p.) on female SD rats weighing 300–350 g. The sciatic nerve was surgically exposed at the midthigh and carefully freed from adherences to surrounding tissues. A piece of PI was longitudinally implanted in the tibial branch of the sciatic nerve with the help of a straight needle attached to a 10–0 loop thread (STC–6, Ethicon), as designed for the longitudinal intrafascicular electrodes (Lago *et al.*, 2007; de la Oliva, 2018b) (Chapter 1 Figure 1B and Figure 2A). The insertion was monitored under a dissection microscope to ensure the correct placement of the device. After surgery, all animals were housed under standard conditions and periodically subjected to functional and electrophysiological evaluations. Then, at predesigned intervals, animals were euthanized, and the sciatic nerve harvested for histological studies.

Drug administration

Treatments to reduce FBR to intraneural PI devices started 2 days before the surgery to ensure appropriate systemic levels. We assayed two individually administrated drugs, metformin to reduce fibrosis, dexamethasone to reduce macrophage activation, and the combined administration of these two. The group distribution of animals in groups, doses, and administration pathways are summarized in Table 1. The control (CTL) group did not receive any treatment. Metformin (MET) (Qualigen) was administered in the drinking water (p.o.) (125 mg/kg/day) up to 12 weeks. Dosage was selected according to human use and considering the amount of water that SD rats drink per day. Dexamethasone (DEXA) (Kern Pharma) was administered subcutaneously (s.c.) once a day (s.i.d.) for 2 weeks (0.2 mg/kg/day). Dosage was selected according to previous reports (de la Oliva *et al.*, 2018c). One group received metformin alone. A second group was treated with both metformin and dexamethasone. A third group was given only dexamethasone. This last group was conceived in a previous work (de la Oliva *et al.*, 2018c) but histological quantifications were performed again.

Table 1. Groups and treatments given in this study.

Drug group	Treatment duration	Implant duration	Dose	Administration	n
CTL	–	2w	–	–	7
		8w			6
		12w			5
MET	2w	2w	125 mg/kg/day	p.o.	5
	8w	8w			7
	12w	12w			5
DEXA + MET	2w (D) + 2w (M)	2w	0.2 mg/kg/s.i.d. (D) 125 mg/kg/day (M)	s.c. (D) p.o. (M)	6
	2w (D) + 8w (M)	8w			5
	2w (D) + 12w (M)	12w			5
DEXA	2w	2w	0.2 mg/kg/s.i.d.	s.c.	7
	2w	8w			5

p.o.: oral; s.c.: subcutaneous; s.i.d.: once a day; D: Dexamethasone; M: Metformin.

Electrophysiological and functional evaluation

The functional properties of the nerves that had been implanted were evaluated by means of nerve conduction, algesimetry, and locomotion tests at 2, 8 and 12 weeks after the implant. The nerve conduction test was performed by stimulating the sciatic nerve proximally with single electrical pulses and recording the CMAP of TA, GM, PL muscles as previously described (de la Oliva *et al.*, 2018a). The nociceptive threshold to mechanical stimuli was evaluated using an electronic Von Frey algesimeter (Bioseb, Chaville, France) following the same protocol described before (del Valle et al, 2018). Rats were placed on a wire net platform in plastic chambers, a metal tip was applied to the sole of the hind paw until the rat withdrew the paw in response to the stimulus and the force applied was registered. The walking track test was performed to assess locomotor function after the implant. The plantar surface of the hind paws was painted with blue ink and the rat was left to walk along a corridor with white paper on the floor. The print length, the distance between the 1st and 5th toes and between the 2nd and 4th toes were measured to calculate the SFI; (de Medinacelii et al 1982).

Histological evaluation

After 2, 8 and 12 weeks, the animals were deeply anesthetized with an overdose of pentobarbital and perfused transcardially with 4% PFA in PB. The sciatic nerve

including the implant was harvested, post–fixed in 4% PFA for an hour and stored in 30% sucrose in PB for cryoprotection.

Analysis of infiltrating macrophages, capsule thickness, and representative images to show capsule evolution in implanted nerves were performed with immunohistochemical labelling. The nerve segments containing the implanted device were sliced (15 µm–thick sections) with a cryostat (Leica CM190). After thawing and blocking with normal donkey serum, slides were incubated with the primary antibodies rabbit Iba1 (1:500; Wako) for macrophages, RT97 (1:200; Developmental Studies Hybridoma Bank) for axons, and CD90 (1:150; BD Pharmingen) for fibroblasts overnight at 4ºC. Slides were washed with 0.1% Tween 20 in PBS solution and incubated with AlexaFluor 488 donkey anti–mouse and AlexaFluor 555 donkey anti–rabbit secondary antibodies (Invitrogen) for 1 h at room temperature. Finally, slides were mounted with Mowiol containing DAPI (Sigma). The number of Iba1 positive macrophages in the whole tibial nerve cross–section was semiautomatically quantified using a custom–made macro for Image J software. The mean capsule thickness was analyzed by dividing the area of the capsule on the implant by the length of the implant in the transversal section. The area was quantified as the non–labeled space between the implant and the first axons labeled with RT97. As each implant has two arms, the capsule thickness of an implant is the mean of both arms. Images were taken with an epifluorescence microscope (Eclipse Ni, Nikon) and a digital camera (DS–Ri2, Nikon).

Data analysis

Results are expressed as mean ± SEM. The normality of the data was tested with the Shapiro–Wilk test. Statistical comparisons between groups were made by two–way ANOVA followed by Tukey's multiple comparison test. Differences were considered significant when $p < 0.05$. GraphPad Prism 8 software was used for all statistical analyses.

Results

The incision wounds healed without inflammatory signs and no postoperative complications were observed in any of the rats with the intraneural implant.

Functional evaluation

The algesimetry tests yielded similar values of pain withdrawal threshold of the preoperative test, implanted and contralateral hindlimbs in all groups (Figure 1A), without evidence of hyperalgesia that might have been induced by nerve injury. In addition, walking track measurements (Figure 1B) did not show variations between the three groups at any time point. The SFI values were close to zero (normal value) at the different time points. In conclusion, there was no evidence of alterations in the motor and sensory functions conveyed by the sciatic nerve after the PI devices were implanted and the administered drugs did not alter this outcome.

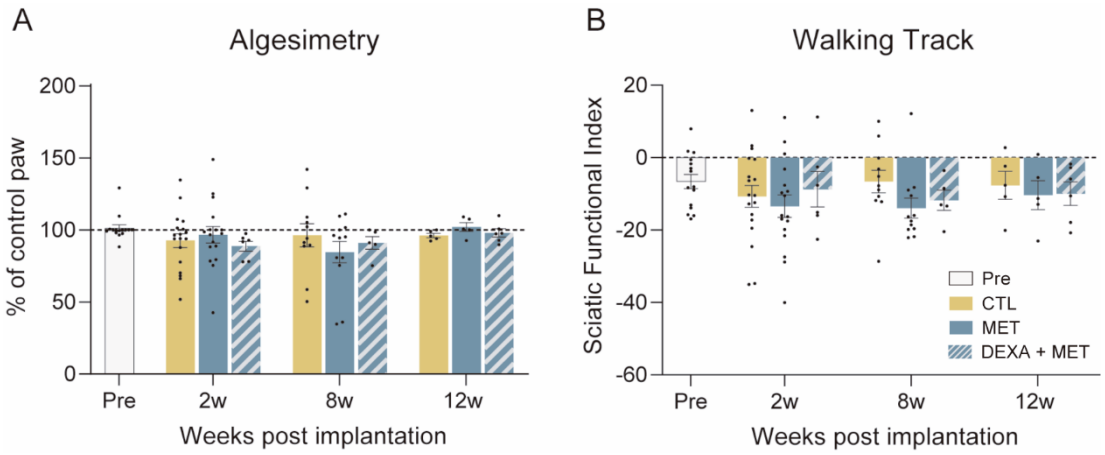

Figure 1. Functional test. Pain and walking assessment. A) Algesimetry test results expressed as percentage of force threshold for withdrawal (vs contralateral control paw) of animals before the implantation and after the implantation and treatments for 12 weeks. **B)** Plot of the SFI obtained in the walking track test. * P<0.05, two–way ANOVA followed by Tukey's multiple comparison test.

During the 12 weeks of follow–up after implantation in the sciatic nerve there were no significant changes in the electrophysiological results of the three groups of rats (CTL, MET, and DEXA + MET). The amplitude of the CMAPs (Figure 2A) of the implanted animals did not show significant variations in comparison with the contralateral paw and with the untreated CTL group at any time point, thus indicating that there was no functional damage to the nerve. The only significant

change was a reduction in the amplitude of TA CMAP in the CTL group at 2 weeks (Figure 2A), but this reduction was recovered at 8 weeks. This decrease can be attributed to the surgery alone and not to the implant as was seen in other studies using similar longitudinal implants of ParC (de la Oliva *et al.*, 2018a) or PI (Lago *et al.*, 2007) devices, where mild variations were observed in the latency and amplitude of the CMAP early after implantation, but were restored a few weeks later. The latency of the CMAPs did not show significant differences between groups during follow–up (Figure 2B) indicating that there were not myelin involvement and focal compression.

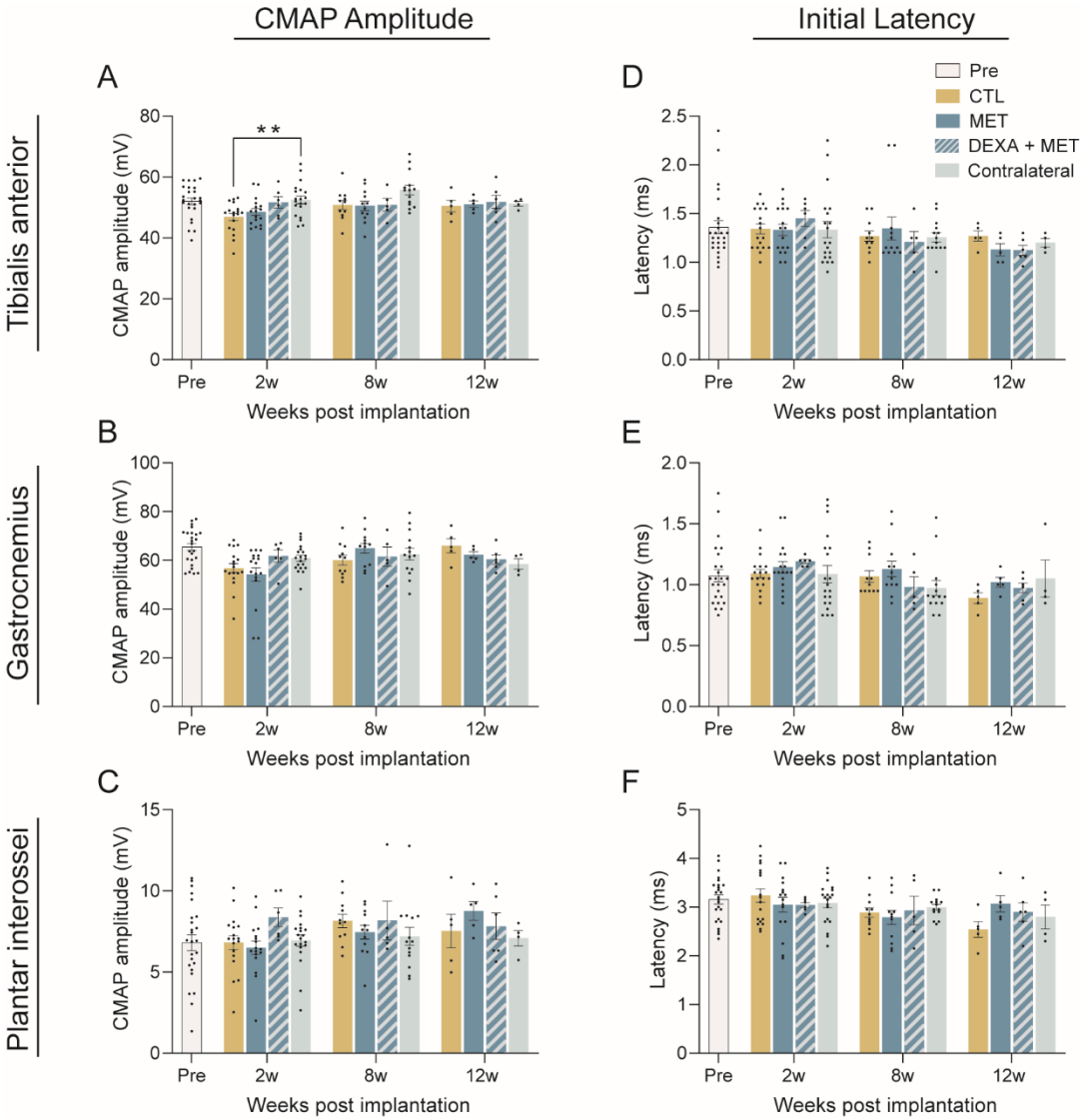

Figure 2. Functional tests. Motor nerve conduction. Motor nerve conduction parameters of animals before implantation (Pre) and after the implantation of PI devices for 12 weeks and drug administration. **A–C)** CMAP amplitude of TA (A), GM (B) and PL (C) muscles. **D–F)** CMAP onset latency of TA (D), GM (E) and PL (F) muscles **p<0.01 vs contralateral, two–way ANOVA followed by Tukey's multiple comparison test.

Inflammatory response

During the initial phase of the FBR, macrophages are the predominant cells. Macrophages are recruited and distributed around the implant, where a high density can be seen (Figure 6), and also within the whole tibial nerve (Figure 4). In the case of intraneural longitudinal implants, de la Oliva et al., (2018b) reported a peak of infiltrating macrophages around 2 weeks after implantation. We also found a high number of macrophages in the tibial nerve fascicle at 2 weeks (Figure 3A). The groups administered with dexamethasone (alone or combined with metformin) exhibited significantly fewer macrophages at 2 weeks but not the group receiving only metformin. As the FBR resolves, the number of macrophages decreased around the implant and in the nerve regardless of treatment. Notably, at 8 weeks, the number of macrophages in the groups administered with dexamethasone for 2 weeks remained lower (not significantly) compared to the groups not administered with dexamethasone. Therefore, while metformin did not affect the number of macrophages present in the tibial nerve, a 2–week daily treatment of dexamethasone significantly reduced the infiltration of hematogenous macrophages, even at late times of 8 and 12 weeks. Figure 4 shows representative immunofluorescence images of labeled macrophages of all treatments and studied times.

The capsule around the implant was measured as the space between the implant and the closest axons and its values are represented in Figure 3B. In the early phases of FBR, the capsule is made up mainly of macrophages that adhere to the implant trying to engulf it (Figure 6 2w). Consequently, the groups administered with dexamethasone had reduced thickness of the capsule at 2 weeks, presumably because there is a decrease in the number of infiltrating macrophages as shown in Figure 3A. On the contrary, the group receiving only metformin did not show such a reduction in capsule thickness at this time point. Then, as the macrophages leave the implant surface, the capsule becomes less cellular (Figure 6 8–12w), more fibrous and compact (Figure 5 8–12w) due to fibroblast presence. At 8 weeks, the capsule thickness of the metformin–administered groups was significantly lower compared to the control group, but not the dexamethasone group. On the other hand, at 12 weeks only the group with both dexamethasone and metformin had a significantly thinner capsule than the control group.

To conclude, dexamethasone decreased macrophage infiltration as it has been described previously (Zhong & Bellamkonda, 2007; de la Oliva *et al.*, 2018c). Therefore, the thickness of the capsule was reduced in the initial phase. The therapeutic effect of metformin targets fibroblast and myofibroblast actions which become noticeable at the last phases of the FBR. Consequently, capsule thickness decreased in metformin–administered groups while dexamethasone alone lost its initial effect. Conversely, the reduction in capsule thickness was not maintained at 12 weeks in the metformin group as it was in the combined treatment (DEXA + MET) suggesting a summative effect of both drugs.

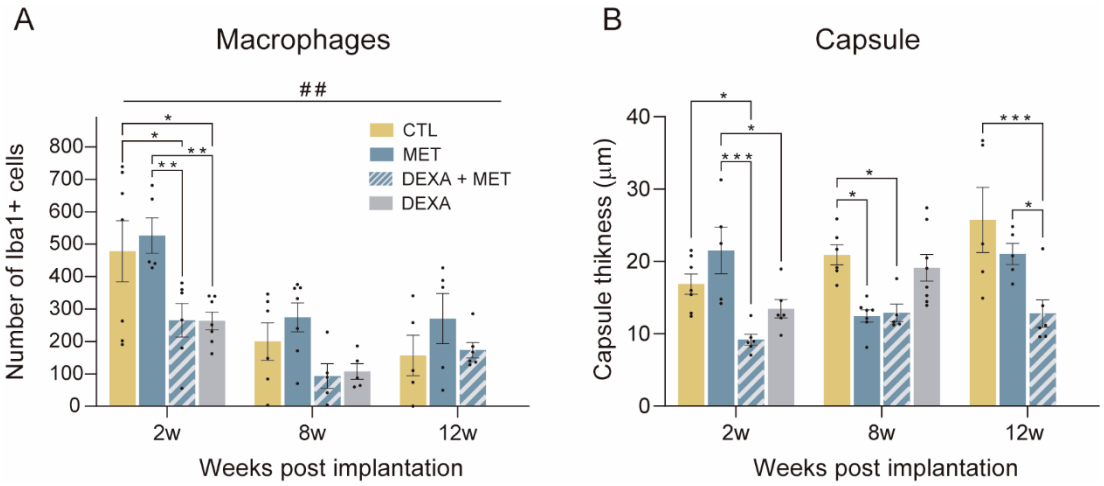

Figure 3. Effect of drug administration on the FBR to intraneural implants. **A)** Number of inflammatory Iba1+ cells in the tibial nerve of animals implanted with PI devices and administered with metformin, dexamethasone, or both. **B)** Tissue capsule thickness around the devices in the tibial nerve of animals implanted with PI and administered with the different treatments. * $p<0.05$, ** $p<0.01$, *** $p<0.001$, ## $p<0.01$ time variable, two–way ANOVA followed by Tukey's multiple comparison test.

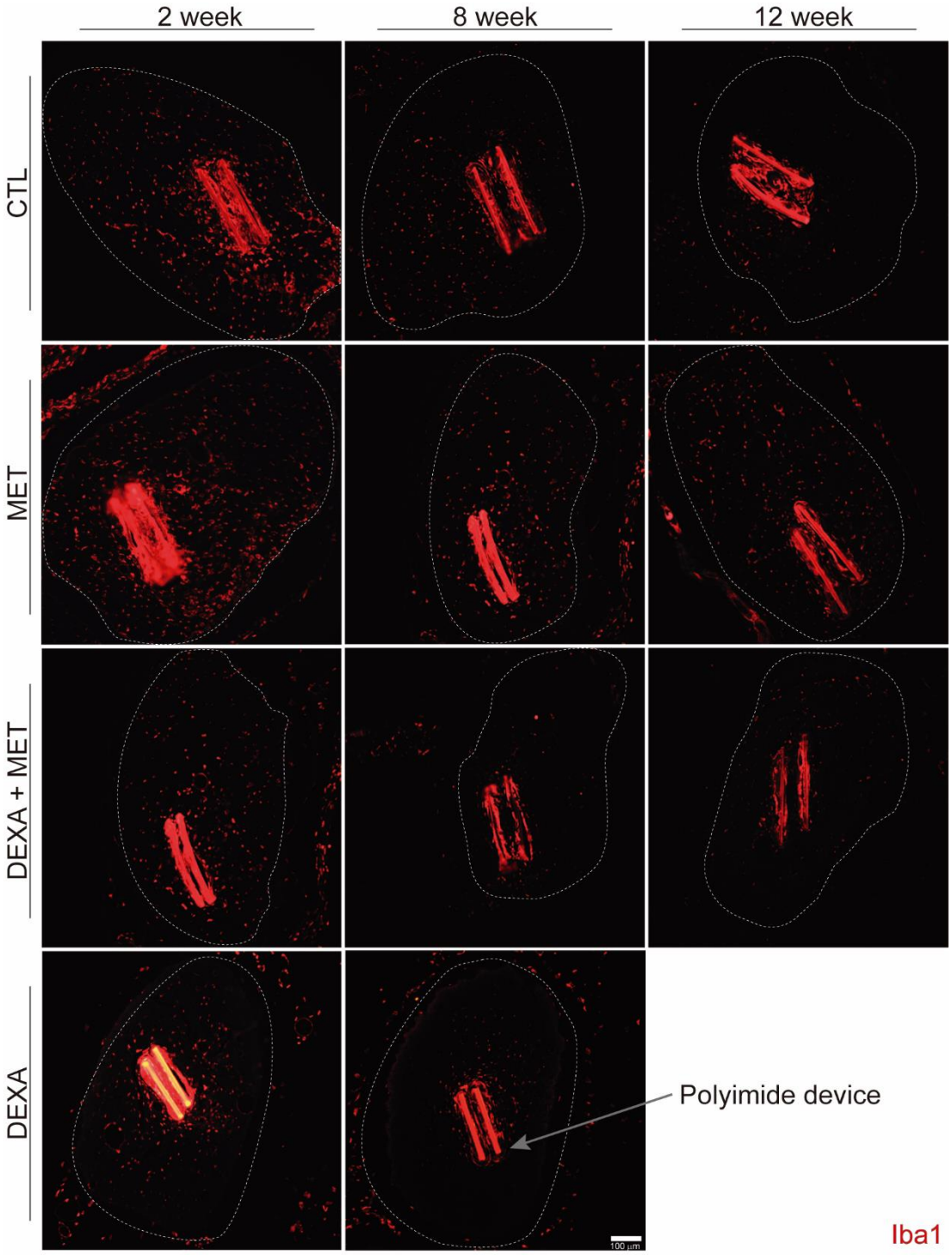

Figure 4. Representative images of Iba1+ cells. Effect of treatments on the number of macrophages (red, Iba 1+ cell) of animals implanted with PI devices after 2, 8 and 12 w. The area limited by the dotted line corresponds to the tibial fascicle of the sciatic nerve that was used to analyze the number of labeled cells. Scale bar: 100 µm.

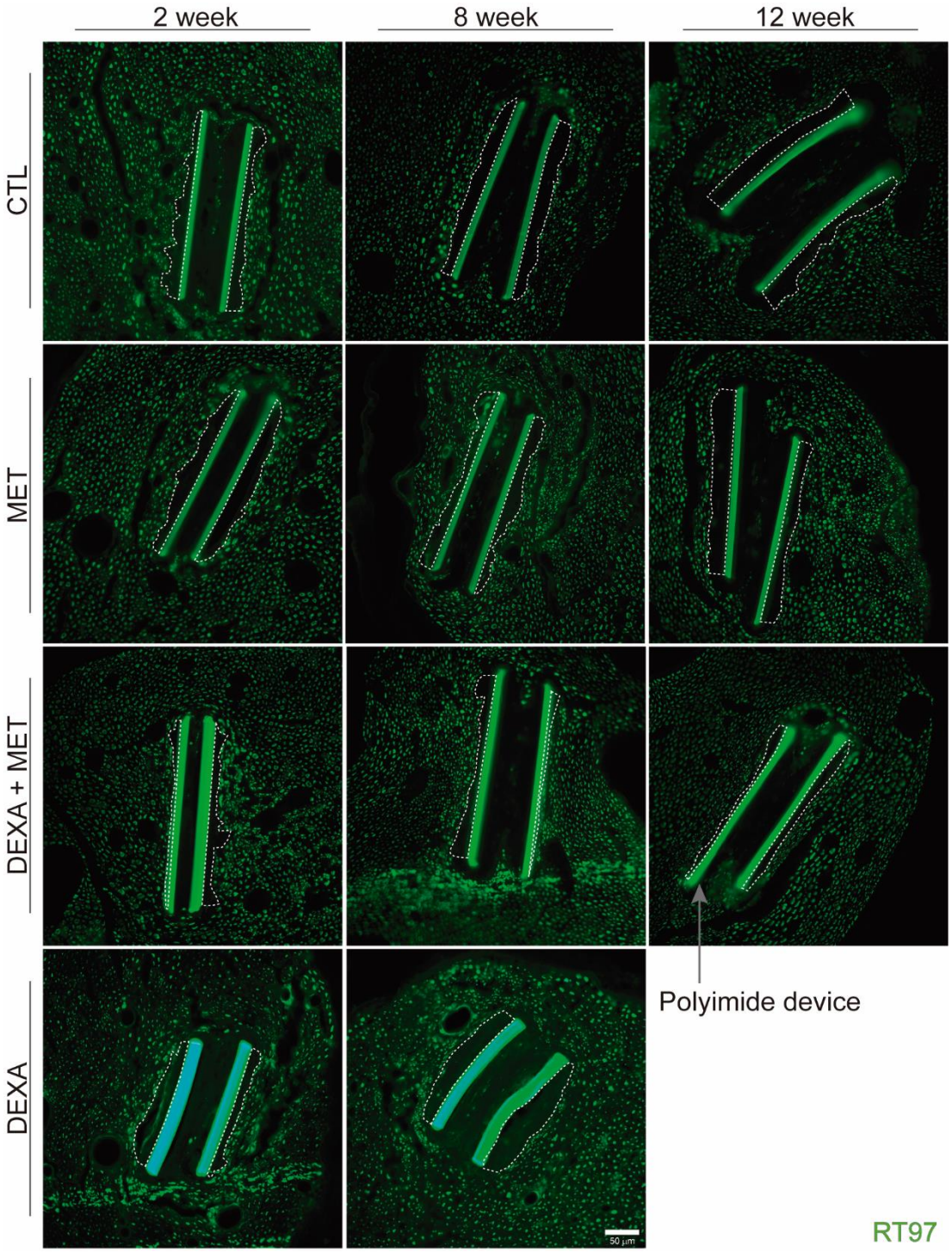

Figure 5. Representative images of the fibrotic capsule. Effect of treatments on the capsule thickness (area limited by the dotted line) of animals implanted with PI devices after 2, 8 and 12 w. Scale bar: 50 µm.

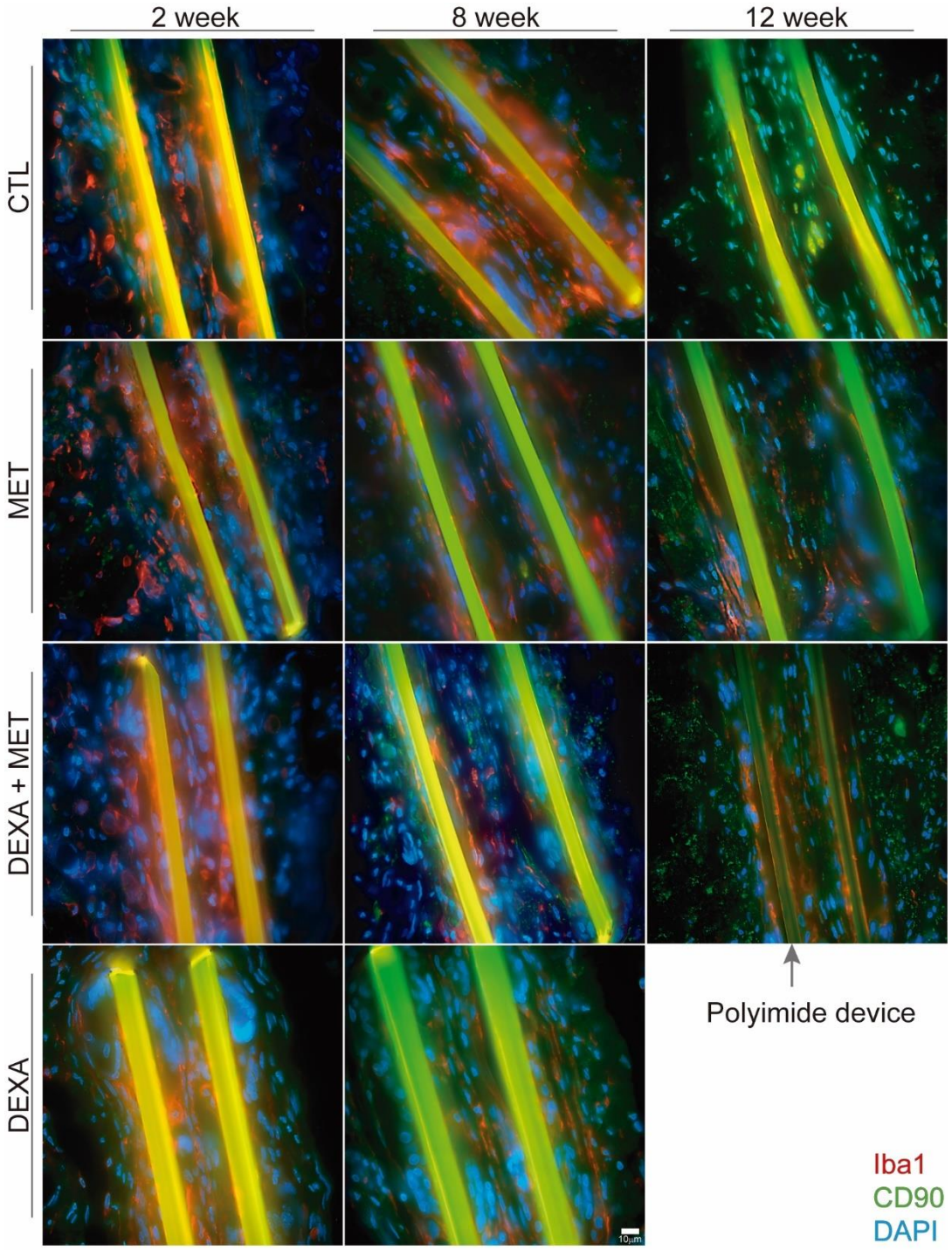

Figure 6. Representative images of capsule composition. Evolution of the capsule composition (red, Iba 1+ macrophages; green CD90 fibroblast; blue, DAPI nuclei) of animals implanted with PI devices after 2, 8 and 12 w. Scale bar: 10 µm.

Conclusions

Metformin is a promising antifibrotic treatment that can be safely administered chronically. The fibrotic capsule around the implant decreased at medium term, although the effect declined at the long term. A combined therapy of dexamethasone and metformin appears to be the most promising strategy to modulate the complex process of the FBR.

VII. Discussion

Electrical stimulation of nerve tissue and recording of neural electrical activity are the bases behind clinical applications of different neuroprostheses (D'Anna *et al.*, 2017), including cochlear and brainstem hearing prostheses (Shepherd & McCreery, 2006), retinal and cortical visual prostheses (Veraart *et al.*, 1998), micturition control (Creasey & Bodner, 1994), pain reduction (Stanton–Hicks & Salamon, 1997) or DBS for essential tremor, Parkinson's disease, epilepsy, dystonia, and depression (Perlmutter & Mink, 2006).

One of the most complex and ambitious neuroprosthetic systems are those designed to replace an amputated hand and its ability to grasp, manipulate and sense the environment. Selective stimulation provides sensory afferent feedback of the movement and the force of the grasp as well as the contact with grasped objects. On the other hand, the recording from specific motor nerve populations (or from proximal residual muscles) facilitates the motion of the bionic prosthesis by attending to the patient's own signals to move the lost limb. Neuroprostheses can also be used to replace a lost function but not the body part, for instance, patients with severe sensorimotor deficits due to stroke or spinal cord injury. In these cases, neuroprostheses artificially replace the central motor control to directly stimulate the intact peripheral motor nerves or muscles (FES systems), enabling the patient to achieve some functional recovery. Besides, the selective recording of sensory axons can be applied in closed–loop systems to modulate such functional stimulation (Micera & Navarro, 2009).

A key component of neuroprostheses is the interface with the nervous system, commonly a multiarray electrode that should be stable over time, biocompatible, adaptable to the tissue and designed to allow highly selective and bidirectional communication. One of the greatest challenges for the use of functional neuroprostheses over extended periods of time lies on the maintenance and performance of the interface. The future of nerve interfaces depends on whether we will be able to handle these main three setbacks: (I) the biological reaction of the body manifested through the FBR to the exogenous device that causes deterioration and encapsulation of the electrodes, decreasing its capacity to interact bidirectionally with the neural tissue; (II) the biocompatibility of the material in the implanted tissue that is directly linked with the severity of FBR and that is related to the correct integration of the device within the tissue; and (III) the failures ranging from wire

breakage to implant motion caused by tethering forces linking the interface to external connection systems.

In this thesis we have evaluated a novel type of neural interface constituted by an engineered graphene, named EGNITE, as conductive element deposited on PI as substrate in the design of intraneural electrode. In the first section, we studied *in vitro* and *in vivo* the biocompatibility of PI and EGNITE devices implanted in the peripheral nerve. Given the excellent results obtained, active functional devices have been assessed in the second chapter as a bidirectional interface for providing stimulation and allowing recording of nerve activity with high effectiveness and selectivity. In the last chapter, we summarized further efforts to find a feasible strategy to modulate the FBR induced by an intraneural device, that may improve the chronic performance of the interface array.

Biocompatibility of the EGNITE electrodes

We found that both PI alone and PI+EGNITE had no adverse effects on neuronal cell viability. Devices implanted in the sciatic nerve of rats did not produce significant functional decrease as evaluated by electrophysiological and functional motor and sensory tests, proving that the implants do not have harmful effects *in vivo*. Moreover, histological analyses revealed that the implant–induced FBR was similar regarding macrophages infiltration and capsule thickness between devices made of PI alone and PI+EGNITE. Comparatively, the FBR of the PI+EGNITE implanted devices showed a similar evolution to that of PI alone devices, as well as to that described previously in similar PI devices (de la Oliva et al 2018a; 2018b), both in terms of inflammatory infiltration and connective capsule around the device.

The biocompatibility of GBM used for neural interfaces has previously been tested *in vitro* (Park *et al.*, 2011; Bendali *et al.*, 2013; Kim *et al.*, 2013; Sahni *et al.*, 2013; Fabbro *et al.*, 2015; Convertino *et al.*, 2018), but only in a few *in vivo* experiments of macroscopic devices (Sydlik *et al.*, 2015) and even fewer evaluated biocompatibility in nervous tissue (Garcia–Cortadella *et al.*, 2021; Nguyen *et al.*, 2021). Moreover, significant changes are made in the structure of graphene to further increase its performance, that may also alter its biocompatibility and stability (Bullock & Bussy, 2019) and even induce toxicity. The GBM used in this work was newly developed

from reduced oxide graphene to create EGNITE graphene (Viana *et al.*, 2022) thus, a thorough biocompatibility assay was needed before it could be exploited for functional electrodes. To further demonstrate the *in vivo* biocompatibility, the devices used contained much larger amount of EGNITE than necessary for functional electrodes; in the case of a LIFE, about 16–20 AS of 25 µm diameter, whereas the devices used contained about 20 times more dots. Besides, the biocompatibility was tested with mock non–functional devices without connecting wires, that may induce some tethering forces in the nerve (Navarro *et al.*, 2005), avoiding external artifacts in the progression of the FBR, whereas focusing only in the reaction to the implanted material.

Cytotoxicity evaluations made with primary DRG cells and primary cortical cells seeded on the PI substrate alone and containing EGNITE showed that both components were inert, and indeed, neuronal cells grew and readily extended neurites on top of the EGNITE coated areas. In the *in vivo* evaluation, devices containing a large amount of EGNITE did not induce neural damage, and the results were indistinguishable from those of the PI alone and similar to those of sham operated animals. Compared with previous data, the present results with PI+EGNITE are in agreement with data reported in similar studies of intraneural electrodes made of PI plus Pt or IrOx (de la Oliva et al 2018b; Lago et al. 2007; del Valle et al. 2015), in which slight functional decline was observed at early days but recovered over a few weeks. This evolution suggests that the surgical implantation procedure is the main reason for these variations and causes only a mild and temporary functional deficit without evidence of axonal damage.

The histological analysis of the FBR was aimed to characterize two specific time points of the process, the inflammation peak occurring at 2 weeks and the late stabilization at 8 weeks after the implantation, as characterized in similar implants performed in our laboratory (de la Oliva et al 2018a). During the early phase of FBR, resident macrophages are stimulated by the damage induced by device implantation and protein adsorption to the biomaterial. Systemic macrophages are also recruited by chemoattractant factors to the damaged area. This early inflammatory phase occurs during the first two weeks. From this time on, the number of macrophages decreases, and a stabilization phase occurs in which invasion of fibroblasts predominates. Since medical implants are generally too large to be fully degraded, fibroblasts around the

implant generate a connective capsule that isolates it from the body. The thicker the capsule, the more difficult the interaction of the neural electrode with the tissue is. The FBR of the PI+EGNITE implanted devices showed a similar evolution to that of PI alone devices, as well as to that previously described in PI devices (de la Oliva et al 2018; 2018b), both in terms of inflammatory infiltration and connective capsule around the electrode device.

Functionality of the EGNITE electrodes

Neural stimulation was proven to activate specific subsets of axons within the fascicles of the sciatic nerve with low current thresholds in acute and sub–chronic conditions. Neural recording of CNAP and ENG elicited by mechanical stimuli were feasible but were more dependent of the decreased functionality over time.

Metal electrodes including stain–less steel, tungsten, platinum, platinum–iridium alloys, IrOx, titanium nitride have been used due to its electrical capabilities. When used on macro or milli scale, these materials allow for an effective stimulation and recording of the nervous system (Cogan, 2008). To provide complex exchange of signals, as needed for natural–like sensations and accurate control of the movement of a prosthesis, it is mandatory to reliably and selectively stimulate and record small populations of afferent and efferent axons in a peripheral nerve (Saal & Bensmaia, 2015). Thus, to enhance selectivity and spatial resolution, the size of the ASs must be reduced while increasing the number of ASs interfacing the nerve. When the size of metallic electrodes is reduced to a micrometer scale, the threshold current to produce the stimulation of the nervous tissue is generally above the CIL. Exceeding CIL of the material leads to faradic reactions in electrode–tissue interface that compromise biocompatibility and integrity of the conductive material, reducing long–term stability. Likewise, the reduction of electrode surface area increases interfacial impedance of the electrode, which translates into recording with lower SNR (Cogan, 2008). Besides, a critical challenge lies in maintaining functional neuroprostheses over extended periods of time that requires stability and robustness of the interface device.

Thus, an ideal microelectrode for neuroprosthetic applications must be able to:

(1) safely stimulate the tissue without compromise biocompatibility and electrode integrity, i.e., increasing CIL.
(2) record neural signals with low SNR, i.e., reducing impedance.
(3) selectively stimulate and record the nervous tissue, i.e., reducing AS size and increasing its number.
(4) maintain its function on the long term, i.e., increased biocompatibility and integration within the tissue.

Driven by these specifications, new materials have been explored to improve classic metallic electrodes, for example, conductive polymers such as PEDOT (Ferrari *et al.*, 2021) or materials derived from carbon (Devi *et al.*, 2021). Among carbon materials, graphene and graphene–derived materials have stood out for their electrical and electrochemical performance and their suitability for integration into flexible devices (Kostarelos et al., 2017).

Nerve stimulation

In this work, EGNITE graphene, designed from modified reduced graphene oxide (Viana et al., 2022), has been used as a conductive material in flexible TIME interfaces of PI as substrate. Given the improvement in the electrical performance of EGNITE compared to other materials (Viana *et al.*, 2022), it has been possible to reduce the size and therefore increase the number of ASs that fit into a TIME. In previous studies with similar transversal intraneural electrodes made on PI, Badia *et al.*, (2011a) used TIMEs with five ASs of 60 µm in diameter made out of platinum (Pt; 300 nm in thickness). Badia *et al.*, (2011b) and de la Oliva *et al.* (2019) used TIME devices implanted in the sciatic nerve of rats whose IrOx contacts had a diameter of 80 µm. In one of the arms of the devices there were 7 AS but 3–4 could be placed simultaneously inside the sciatic nerve of a rat. Cutrone and colleagues, implanted the intraneural electrode SELINE, with 5 gold ASs per arm whose area was 3700 μm^2 each (Cutrone *et al.*, 2015). In comparison, our device has 9 AS of 25 µm in diameter and an area of 490.87 μm^2 per arm, of which 7–8 are inside the nerve. Moreover, the nerve activation threshold current was 2 to 3 times less compared to those found in these previous studies, which may lower power consumption in future long–lasting implantable neuroprostheses (Garcia–Cortadella *et al.*, 2021), representing an important advantage of EGNITE as active element.

Regarding selectivity for stimulation of small nerve fascicles, in the model we used the SI for activation of the three tested muscles ranged between 0.6 and 0.9, similar to values found in previous studies using TIME design of electrodes (Badia *et al.*, 2011a; de la Oliva *et al.*, 2019) Interfascicular selectivity was easy to achieve because of the separation by the perineurium of the tibial and peroneal fascicles, as it was shown by the high SI of the TA muscle, innervated by axons in the peroneal fascicle. On the contrary, intrafascicular selectivity was more difficult for muscles innervated by axons in the same tibial fascicle, thus closer and without a perineurial barrier, as indicated by the lower SI of the GM muscle. It was expected that smaller ASs would improve the focalization of stimuli to the target fibers. However, we did not find higher selectivity than with larger metal ASs used in the cited previous studies. There are two plausible explanations. First, the TIME design by itself allows a high selectivity of stimulation in the peripheral nerve (Badia *et al.*, 2011a). Second, the small size of the rat sciatic nerve used in the study, in which the localization of small subfascicles innervating different muscles in the limb is quite close (Badia *et al.*, 2010), limit the possibilities to selectively activate them when the injected current spills over small distance from the AS.

Nerve recording

Recording nerve signals is a complicated task, compared to recording muscle signals. This difficulty mainly arises because, due to the small size of nerve fibers, extracellularly recorded signals are in the microvolt range, as opposed to muscle signals in the millivolt range. The noise present to a greater or lesser extent in all recording systems can hinder low–amplitude signal acquisition. Recording CNAPs facilitates the study of the recording capabilities of the device because the CNAP is the temporal summation of many nerve fibers activated simultaneously by an electrical stimulus.

The EGNITE based electrodes were able to record CNAPs of a similar amplitude to those recorded with cuff electrodes or with other electrodes implanted within the rat sciatic nerve (Lee *et al.*, 2016; de la Oliva *et al.*, 2019). Additionally, the capacity to selectively record CNAPs from two tributaries of the sciatic nerve, the MPN and the LPN, which innervate the lateral and medial parts of the rat paw, was investigated. Most devices (8 out of 11) were selective for only one nerve. This fact can

be explained by the wide area occupied by the axons coming from each plantar nerve (Badia *et al.*, 2010), so that it may be possible that the TIME crosses the tibial nerve though one or the other. The remaining devices tested were able to record the CNAP of the MPN and LPN with moderate selectivity. These results agree with those found by Badia *et al.* (2016). As in the case of stimulation, selectively recording nerve signals in the same fascicle is complicated because there is no epineurium that isolates nerve signals from different axonal populations.

Electrodes can also be used in FES systems, for instance, to restore basic hand function in tetraplegic patients to grasp and manipulate objects (Popovic *et al.*, 2001). However, their use can extend beyond stimulating target organs to restore the lost function. Due to the lack of sensitive feedback in the hand, the patient must rely on vision and accumulate experience to adjust the grasp force. Moreover, the grasp force may vary over time during functional tasks. To emulate the sensory feedback prior to injury, an electrode can record the sensory information generated while manipulating an object. At the same time this information can be used to regulate the stimulation protocols of another electrode used in FES configuration (Inmann *et al.*, 2001). Additionally recorded neural activity can serve as an event onset detection to trigger a functional stimulation protocol (Haugland & Sinkjær, 1995). These systems, where stimulation is modulated by a sensory signal obtained from the patient, are FES closed–loop system. Moreover, the sensory signals from intact nerves can also be used to stimulate the sensory cortex in order to provide conscious sensory feedback to the patient (Tabot *et al.*, 2015).

The EGNITE device was able to record the neural activity of two types of mechanical stimuli: scratch and light touch. Painful stimuli were also applied to the animal's paw; however, these stimuli easily elicited a withdrawal response, which contaminated the recordings with much larger motor unit potentials. Additionally, despite the small size of the AS (Ø 25 µm), signal recording was possible with a SNR similar to other devices with larger AS (Badia *et al.*, 2016). The electrode size affects its ability to record signals primarily due to increased electrode impedance and thermal noise, which impact the bandwidth of the electrical recordings (Scholvin *et al.*, 2016). Perhaps for this same reason, by connecting all the AS to a single output, the SNR increases, as does the recording area.

In real–life closed–loop neural prosthetic systems, it is not only about detecting sensory signals but also to understand the type of information encoded in the signal. Sensory modalities of proprioceptive, mechanoreceptive, nociceptive and thermal information are transduced by different types of fibers whose functions may be overlapped. For example, Aβ (II) fibers convey proprioception and mechanoreception. Previous studies have demonstrated the ability to discern different stimulus modalities from ENG recordings analyzed with feature–detection algorithms (Citi *et al.*, 2008; Raspopovic *et al.*, 2010; Badia *et al.*, 2016). Interestingly, Badia *et al.*, (2016) demonstrated the superior ability of TIME electrodes to distinguish sensory modalities compared to other electrodes, such as cuffs or LIFE. In this study, we did not verify whether the recordings obtained with the EGNITE TIME devices would allow differentiation between different types of sensory information, that would be an interesting additional study.

One aspect of stimulation and recording that has not been addressed in this study is the electrical configuration of the electrode and the parameters of the stimulation protocol. The monopolar configuration, either using a common reference electrode within the device or an external needle, has been used in this work. However, it has been extensively demonstrated that bipolar, tripolar, or multipolar configurations have a positive impact on the functionality of electrodes in both stimulation (Veraart *et al.*, 1993b; Badia *et al.*, 2011a; Shepherd *et al.*, 2017) and recording (Gouyet *et al.*, 2007; Soulier *et al.*, 2008; Avdeew *et al.*, 2022) modes. For stimulation, the multipolar configuration aims to actively restrict the field of excitation, consequently increasing selectivity. Neural implants such as cuffs benefit the most from multipolar configurations, perhaps because they have lower selectivity compared to intraneural implants. Therefore, multipolar stimulation may have less advantage for intraneural electrodes (Capogrosso *et al.*, 2011). The selectivity of stimulation is also affected by the stimulation protocol. Specifically, it has been shown that short pulses (20 µs) and the introduction of a hyperpolarizing pre–pulse improve stimulation selectivity (Guiho *et al.*, 2021). However, it is important to note that to produce complex stimulation patterns involving multipolar configurations and specific modifications of electrical pulse parameters, stimulators designed for such purposes are necessary, which are not common. Regarding neural activity recordings, the multipolar configuration in cuff devices increases the spatial selectivity of the

recorded tissue due to the higher number of AS. Moreover, the noise decreases, which enhance SNR allowing high–quality neural signal recordings (Soulier *et al.*, 2008; Ortiz–Catalan *et al.*, 2013; Avdeew *et al.*, 2022). Therefore, future studies using the newly developed graphene–based electrodes may assess refinements in the electrode configurations to improve selectivity and efficiency of the bidirectional communication.

Chronic stability of the intraneural electrodes

As broadly reported in the literature, after the implantation of any medical device, the immune system triggers a FBR, a set of processes within the wound healing to isolate the implant with a fibrotic capsule (Anderson & Jiang, 2016). The insulation of the electrode increases the impedance in the electrode–tissue interface. On one hand, the tissue that surrounds implanted electrodes acts as an extra resistive barrier to current altering the spatial distribution of the electrical field (Grill & Thomas Mortimer, 1994). On the other hand, the distance between axons and the electrode increases by the interposed encapsulation, which hinders both stimulation and recording functions. Implanted electrodes may also suffer from corrosion of the conductive material or degradation or delamination of the insulating material. The inflammatory process that is triggered around the implant may accelerate degradation, for example, by acidification of pH favored by the molecules secreted by macrophages (Patrick et al., 2011). Exceeding the CIL may also accelerate the corrosion of conductive materials, producing faradic reactions at the electrode–tissue interface. (Doering et al., 2022). Faradic reactions, as opposed to capacitive, are irreversible mechanisms in which oxidation–reduction reactions occur, causing damage to both the electrode and the tissue (Cogan, 2008).

Biocompatible materials generate a lower immune system response, resulting in a smaller capsule around the implant (del Valle et al 2018). The safety of GBM will depend upon several factors including the physicochemical characteristics of the biomaterial and the intended biological system where it is used. GBM have been used successfully in the nervous tissue resulting in no gross FBR compare with other standard materials (Garcia–Cortadella et al., 2021; Nguyen et al., 2021; Sydlik et al., 2015). However, major changes in the structure of graphene to further increase its performance, may alter its biocompatibility and stability (Bullock & Bussy, 2019).

Thus, a detailed *in vitro* and *in vivo* biocompatibility evaluation of the new EGNITE was addressed, demonstrating that it is biocompatible and does not degrade or delaminate.

Consequently, the loss of functionality with time of implantation due to FBR in EGNITE devices is not expected to be greater than with previous PI based intraneural electrodes. The loss of functionality in the stimulation can be compensated to a limited extent by increasing the injected current, however, as mentioned before, increasing the current can produce hazardous electrochemical processes or deteriorate the conductive material. Signal recording is already difficult compared to stimulation, given the low amplitude of nerve signals, especially non–synchronous nerve signals produced by sensory stimuli rather than those produced by electrical stimuli. When the amplitude of the noise produced by an increase in impedance exceeds or equals the amplitude of the recorded nerve signals, these signals will no longer be distinguishable from the noise. The reduced size of the ASs may also have influenced the difficulty in recording nerve signals.

In this work, jeopardized functionality of EGNITE electrodes translates into an increase in the threshold to produce muscle activation and a decreased in the quality of recorded nerve signals. The specific mechanisms that have produced this loss of functionality have not been studied here. Although the impedance of the ASs was not measured during the follow–up, it could be a useful indicator of decreased functionality due to fibrotic capsule deposition around the implant but also to assess the integrity of the electrode leads within the body (Murphy *et al.*, 2004).

The loss of functionality of the intraneural electrodes has been progressive, as already reported in other studies (Rossini *et al.*, 2010; Wurth *et al.*, 2017; de la Oliva *et al.*, 2019). Although we have shown that some devices can work up to sub–chronic periods of time, the characteristics of the implant have not allowed us to evaluate the implanted animals every week. A higher temporal resolution could be useful to address how fast the functionality decreases and stabilizes. Ideally, neural interfaces should have connectors that allow their evaluation in the least invasive and simple way possible, for example with connectors located on the animal's back (Wurth et al., 2017; De la Oliva et al., 2019) or fixed to the skull (Jiang *et al.*, 2017). In this study, to simplify the implantation procedure, the electrode connection area was maintained subcutaneously; therefore, the electrophysiological evaluation required to open the

skin each time, which could compromise the stability of the device and the well–being of the animal. Furthermore, due to mechanical stress and tethering forces, wire connections and connector systems are one of the least reliable parts of neural interfaces, being a bottleneck for chronic applications (Hoch *et al.*, 2018).

Modulation of the FBR to improve chronic use of intraneural electrodes

The reduction in functionality associated with the FBR is a consistent issue in neural implants (Grill & Thomas Mortimer, 1994; de la Oliva, del Valle *et al.*, 2019; Carnicer–Lombarte *et al.*, 2021). Strategies aimed at mitigating FBR focus on two main approaches: the first involves the use of biocompatible materials or the tunning of the physicochemical properties of materials to enhance their biocompatibility. This can include altering the shape, size, rigidity, and wettability of the materials. The second approach involves the administration of drugs, either systemically or locally, to modulate the FBR. In some cases, these two approaches can overlap, e.g., functionalizing the surface of materials with drugs that are gradually released (Barone *et al.*, 2022).

Systemic administration was selected since it allows the combination of various FBR–modulating drugs at different stages following implantation, according to the expected time window of effectiveness. However, local administration systems have significantly advanced in recent years, allowing drug release after certain stimuli (electrical, pH, light irradiation, etc.) (Sun *et al.*, 2016; Ahmadi *et al.*, 2020), or the sequential delivery of multiple drugs (Yin *et al.*, 2022). Local delivery systems have been used in implants in the CNS (Rennaker *et al.*, 2007; Mercanzini *et al.*, 2010), but less in the PNS and focused on cuff or regenerative electrodes (Park *et al.*, 2015; Fitzgerald, 2016; Heo *et al.*, 2016; Barone *et al.*, 2022). Conversely, drug coatings for intraneural PNS electrodes have not been explored *in vivo* (Gori *et al.*, 2021, 2022). The increase in size and thickness resulting from the addition of coatings or microfluidic systems should be considered, taking into account the volume constraints of peripheral nerves.

Considering the decline in functionality observed in EGNITE–based TIMEs, similar to previous studies with TIMEs (Wurth *et al.*, 2017; de la Oliva *et al.*, 2019), we investigated feasible treatments that might modulate the FBR and reduce the surrounding fibrotic capsule. We found that metformin reduces the thickness of the capsule deposited around the implant in the midterm. Furthermore, a combination treatment with dexamethasone reduces the inflammatory infiltration during the first phase and maintains the thinner capsule in the long term.

Dexamethasone has demonstrated to reduce the FBR to different neural implants. (Spataro *et al.*, 2005; Zhong & Bellamkonda, 2007; de la Oliva *et al.*, 2018c; 2019; Barone *et al.*, 2022). It acts through the glucocorticoid receptor, decreasing the expression of inflammatory mediators and reducing the recruitment and activation of macrophages (Coutinho & Chapman, 2011; Ehrchen *et al.*, 2019). Therefore, its maximum effect is expected to occur during the initial phase of the FBR when macrophages are the predominant cells, and the environment is pro–inflammatory. However, long administration of dexamethasone causes several metabolic disturbances (Desgeorges *et al.*, 2019). Therefore, the selected doses for our study are within the low range administered to humans (Normansell *et al.*, 2016), which are associated with fewer side effects. Additionally, efforts are made to limit the duration of administration. In this regard, an administration period of 2–4 weeks is sufficient to address a reduction in the inflammatory reaction and the capsule around the implant; however, a loss of therapeutic effect compared to longer administrations can be expected (de la Oliva *et al.*, 2018c). Hence, it is necessary to explore drugs that produce fewer adverse effects in chronic administrations.

Metformin, commonly prescribed for lowering blood glucose in patients with type II diabetes, has gained attention in recent years for its potential as an antifibrotic agent in several *in vitro* and *in vivo* models (Biondo *et al.*, 2018; Lee *et al.*, 2018; Rangarajan *et al.*, 2018). The antifibrotic effects of metformin is attributed to its impact on the TGF–β signaling pathway, and oxidative stress (Wu *et al.*, 2021). Of particular importance is the disruption of the TGF–β1 pathway resulting from activation of AMPK leading to the downregulation of fibrosis–associated genes which reduce the production of collagen and fibronectin (Lu *et al.*, 2015; Yi *et al.*, 2021). Additionally, AMPK activation and the decrease in ROS production by metformin, lower migration

and activation of fibroblasts and enhance deactivation of activated myofibroblast (Thakur *et al.*, 2015; Sato *et al.*, 2016).

This is the first work to investigate the effect of metformin on the FBR elicited by an intraneural device. Daily administration of metformin for 12 weeks did not show any noticeable effects on health status of the rats (weight and behavior), indicating that metformin can be given in chronic systemic treatments. The antifibrotic effect exerted by metformin was noticeable at 8 weeks. However, at 12 weeks the capsule thickness enlarged and was not different to that of the control group. Most studies with metformin showing an antifibrotic effect *in vivo* involved sub–chronic administrations lasting 1 week (Xavier *et al.*, 2010; Shen *et al.*, 2016), 2–3 weeks (Sato *et al.*, 2016; Ursini *et al.*, 2016; Zheng *et al.*, 2017; Biondo *et al.*, 2018; Rangarajan *et al.*, 2018; Sisson *et al.*, 2018; Kheirollahi *et al.*, 2019), 4 weeks (Zhang, *et al.*, 2013; Luo *et al.*, 2016; Li *et al.*, 2021; Karatas *et al.*, 2022) and 8 weeks (Tikoo *et al.*, 2016; Shin *et al.*, 2017). It is important to mention that in our model, we did not observe a reduction in fibrosis at 2 weeks because collagen does not start to become appreciable surrounding the implant until 8 weeks (de la Oliva *et al.*, 2018a). Moreover, the role of myofibroblasts in the fibrosis associated with peripheral nerve injuries appears to be focused on collagen contraction rather than production. Myofibroblasts are the main producers of collagen in other tissues, but their presence in the nerve is very scarce (Fertala *et al.*, 2020). Therefore, metformin may not be exerting its full antifibrotic potential in the peripheral nerve. Regarding the anti–inflammatory action of metformin, we did not find a reduction in the number of infiltrated macrophages in the nerve. However, other studies have demonstrated anti–inflammatory effects of metformin, including the reduction in macrophage activation and recruitment, promotion of their differentiation into M2 macrophages, or the reduction in cytokine production (Xavier *et al.*, 2010; Shin *et al.*, 2017; Zhang *et al.*, 2017; Jing *et al.*, 2018; Nassif *et al.*, 2022).

We have also explored the possibility of a combined treatment to mitigate two different stages of the FBR. During the early phases of the FBR, the pro–inflammatory environment primarily generated by macrophages initiates a feedback process in which pro–inflammatory mediators recruit more macrophages that surround the implant site. Since the implant material cannot be eliminated, macrophages transition from a pro–inflammatory phenotype to an anti–inflammatory one and lay the groundwork for the action of fibroblasts and myofibroblasts during the late phase of

the FBR. These cells secrete ECM components such as fibrin or collagen, leading to the formation of a capsule that isolates the implant (Carnicer–Lombarte *et al.*, 2021). Dexamethasone reduces the number and activation of macrophages, promoting an anti–inflammatory environment. Simultaneously, metformin inhibits the action of fibroblasts and myofibroblasts, resulting in a smaller capsule around the implant. As we had hypothesized, this combined treatment was the most effective when compared to separate metformin and dexamethasone.

We have not investigated the molecular mechanism by which metformin exerts its beneficial function, that is difficult due to the small size of the fibrotic capsule produced in our model of FBR compared to pathological fibrotic diseases. Since implanted devices are inside the nerve and must be relatively small, isolating the cells contributing to the capsule may not be feasible. Additionally, lysates of the entire nerve for protein expression analysis may yield unreliable results considering the small size of the capsule compared to the whole nerve and the limited number of fibroblasts compared to other cell types. Indeed, in a previous study, a wide cytokine expression analysis was made on samples of the whole implanted rat sciatic nerve from 6 hours to 8 weeks after implantation of a similar device as used in this study. Only the initial burst of cytokine production resulting from the injury was detected within the first days after implantation. From 2 weeks onward, no significant changes in expression were observed, except for CCL2 and CCL3, that were overexpressed (de la Oliva *et al.*, 2018a) Similarly, other techniques that allow the analysis of specific cell types, such as cell sorting, may face the same problem of not having sufficient cells.

Furthermore, fibroblasts are also present in the three layers in which the nerve is structured, epineurium, perineurium and endoneurium. Therefore, specific markers for activated fibroblast populations in the capsule would need to be identified, or the capsule isolated from the surrounding tissue, as mentioned above. In this regard, many FBR studies use larger subcutaneous implants that generate a thicker capsule and are more easily isolatable from the surrounding tissue (Dondossola *et al.*, 2016; Hernandez *et al.*, 2021; Jeon *et al.*, 2022; Liu *et al.*, 2022). However, as previously pointed out (de la Oliva *et al.*, 2018a), the evolution of FBR cellular events in time differs between intraneural implant and subcutaneous implant.

Another aspect to consider is that neural electrodes are made of conductive material embedded in a substrate material. The implants tested in this study only

consist of substrate material (PI). Even though the conductive material is typically a small part of the entire implanted device, so we expect a similar outcome in terms of the FBR. However, depending on the stimulation protocol applied, there may be an increase in the FBR due to irreversible chemical reactions at the electrode–electrolyte interface that degrade the material or reduce the pH (Cogan *et al.*, 2016; Günter *et al.*, 2020). The wiring of functional devices can also induce tethering forces in the nerve (Navarro *et al.*, 2005).

General remarks

This thesis has addressed two of the main challenges in neural interfaces: the use of novel materials to enhance functionality and the functional loss caused by FBR over time. On one hand, we have evaluated the potential of a GBM to be part of peripheral nerve electrodes. Biocompatibility and functional analyses revealed that the EGNITE integrated properly into nervous tissue and its stimulation and recording capabilities surpassed other materials used in neural electrodes. On the other hand, metformin was used to mitigate the FBR, addressing a reduction in capsule deposition around neural probes, particularly when combined with short duration dexamethasone administration. These findings provide valuable insight to further improve functionality and stability to bidirectionally interact with the PNS.

VIII. Conclusions

The main conclusions of this thesis are summarized for the corresponding chapters as:

Chapter 1. Biocompatibility evaluation of novel graphene–based intraneural electrodes.

- The novel graphene–derived conductive material, termed EGNITE, has good biocompatibility, as assessed both *in vitro* and *in vivo*.
- DRG and cortical neuronal cells seeded on top of EGNITE–based devices have excellent viability.
- Polyimide intraneural devices containing EGNITE can be considered as biocompatible, as they do not cause any alteration in the nerve function and in the nerve structure, after 8 weeks of implantation in the sciatic nerve.
- The number of infiltrating macrophages and the capsule thickness around the EGNITE containing devices are similar to implanted neural devices without EGNITE.

Chapter 2. Novel graphene–based electrode for interfacing the peripheral nervous system.

- Transversally implanted polyimide electrodes (TIME) containing EGNITE as conductive material are adequate to stimulate and to record specific subsets of axons within the fascicles of the rat sciatic nerve.
- The current threshold needed to stimulate axons in the sciatic nerve eliciting a muscle response is significantly lower compared to other metal–based materials, such as IrOx or platinum.
- The implanted electrodes containing EGNITE allow for good stimulation selectivity, inter– and intra–fascicular, with similar values of selectivity index compared with previous TIME designs.
- The intensity of stimulation required to evoke muscle responses increases with time in subchronic implants from one month after the implant.
- Electrophysiology recordings of CNAPs and ENG elicited by mechanical stimuli are adequate in acute implants, but do not have enough signal–to–noise ratio (SNR) in subchronic conditions.

- The high SNR of the EGNITE contacts allows the discrimination of asynchronous action potentials evoked by different modalities of mechanical stimuli.

Chapter 3. Enhancing chronic stability of intraneural implants. Modulation of the foreign body reaction to intraneural implants in the peripheral nerve.

- Long–term metformin treatment does not induce any secondary effects and do not affect neuromuscular function of animals implanted with longitudinal intraneural polyimide mock devices.
- Metformin treatment does not affect the recruitment of macrophages during the first phase of the foreign body reaction (FBR).
- Metformin treatment decreases the capsule thickness of intraneural implants at 8 weeks.
- Dexamethasone administration decreases the number of recruited macrophages and the capsule thickness of intraneural implants at 2 weeks.
- The combined treatment of dexamethasone and metformin is the most effective in reducing both the number of recruited macrophages and the capsule thickness around the intraneural implant.

IX. References

Adusei, K.M., Ngo, T.B., & Sadtler, K. (2021) T lymphocytes as critical mediators in tissue regeneration, fibrosis, and the foreign body response. *Acta Biomater.*, 133, 17–33.

Ahmadi, S., Rabiee, N., Bagherzadeh, M., Elmi, F., Fatahi, Y., Farjadian, F., Baheiraei, N., Nasseri, B., Rabiee, M., Dastjerd, N.T., Valibeik, A., Karimi, M., & Hamblin, M.R. (2020) Stimulus-Responsive Sequential Release Systems for Drug and Gene Delivery. *Nano Today*, 34, 100914.

Ajiboye, A.B., Willett, F.R., Young, D.R., Memberg, W., Walters, B.C., Sweet, J.A., Hoyen, H.A., Keith, M.W., Peckham, P.H., Simeral, J.D., Donoghue, J.P., Miller, J.P., Hochberg, L.R., & Kirsch, R.F. (2017) Restoration of reaching and grasping in a person with tetraplegia through brain-controlled muscle stimulation: a proof-of-concept demonstratio. *Lancet*, 389, 1821–1830.

Amann, L. & Prinz, M. (2020) The origin, fate and function of macrophages in the peripheral nervous system-an update. *Int. Immunol.*, 32, 709–717.

Anderson, J.M. (2008) Foreign body reaction to biometarials. *Semin Immunol.*, 20, 86–100.

Anderson, J.M. & Jiang, S. (2016) Implications of the acute and chronic inflammatory response and the foreign body reaction to the immune response of implanted biomaterials. In *The Immune Response to Implanted Materials and Devices: The Impact of the Immune System on the Success of an Implant*. Springer International Publishing, pp. 15–36.

Antoniu, S.A. (2006) Pirfenidone for the treatment of idiopathic pulmonary fibrosis. *Expert Opin. Investig. Drugs*, 15, 823–828.

Apollo, N. V., Maturana, M.I., Tong, W., Nayagam, D.A.X., Shivdasani, M.N., Foroughi, J., Wallace, G.G., Prawer, S., Ibbotson, M.R., & Garrett, D.J. (2015) Soft, Flexible Freestanding Neural Stimulation and Recording Electrodes Fabricated from Reduced Graphene Oxide. *Adv. Funct. Mater.*, 25, 3551–3559.

Artaud-Macari, E., Goven, D., Brayer, S., Hamimi, A., Besnard, V., Marchal-Somme, J., Ali, Z. El, Crestani, B., Kerdine-Römer, S., Boutten, A., & Bonay, M. (2013) Nuclear factor erythroid 2-related factor 2 nuclear translocation induces myofibroblastic dedifferentiation in idiopathic pulmonary fibrosis. *Antioxidants Redox Signal.*, 18, 66–79.

Avdeew, Y., Le Rolle, V., Laval, V.B., Gestreau, C., & Hernandez, A. (2022) Optimal selection of multipolar electrode configurations for nerve burst detection. *Annu. Int. Conf. IEEE Eng. Med. Biol. Soc. IEEE Eng. Med. Biol. Soc. Annu. Int. Conf.*, 2022, 4123–4126.

Badia, J., Boretius, T., Andreu, D., Azevedo-Coste, C., Stieglitz, T., & Navarro, X. (2011a) Comparative analysis of transverse intrafascicular multichannel, longitudinal intrafascicular and multipolar cuff electrodes for the selective stimulation of nerve fascicles. *J. Neural Eng.*, 8, 036023.

Badia, J., Boretius, T., Pascual-Font, A., Udina, E., Stieglitz, T., & Navarro, X. (2011b) Biocompatibility of chronically implanted transverse intrafascicular multichannel electrode (TIME) in the rat sciatic nerve. *IEEE Trans. Biomed. Eng.*, 58, 2324–2332.

Badia, J., Pascual-Font, A., Vivó, M., Udina, E., & Navarro, X. (2010) Topographical distribution of motor fascicles in the sciatic-tibial nerve of the rat. *Muscle and Nerve*, 42, 192–201.

Badia, J., Raspopovic, S., Carpaneto, J., Micera, S., & Navarro, X. (2016) Spatial and functional selectivity of peripheral nerve signal recording with the transversal intrafascicular multichannel electrode (TIME). *IEEE Trans. Neural Syst. Rehabil. Eng.*, 24, 20–27.

Badylak, S.F., Freytes, D.O., & Gilbert, T.W. (2009) Extracellular matrix as a biological scaffold material: Structure and function. *Acta Biomater.*, *5*, *1–13.*

Barone, D.G., Carnicer-Lombarte, A., Tourlomousis, P., Hamilton, R.S., Prater, M., Rutz, A.L.,

Dimov, I.B., Malliaras, G.G., Lacour, S.P., Robertson, A.A.B., Franze, K., Fawcett, J.W., & Bryant, C.E. (2022) Prevention of the foreign body response to implantable medical devices by inflammasome inhibition. *Proc. Natl. Acad. Sci. U. S. A.*, 119, 1–10.

Barry-Hamilton, V., Spangler, R., Marshall, D., McCauley, S., Rodriguez, H.M., Oyasu, M., Mikels, A., Vaysberg, M., Ghermazien, H., Wai, C., Garcia, C.A., Velayo, A.C., Jorgensen, B., Biermann, D., Tsai, D., Green, J., Zaffryar-Eilot, S., Holzer, A., Ogg, S., Thai, D., Neufeld, G., Van Vlasselaer, P., & Smith, V. (2010) Allosteric inhibition of lysyl oxidase-like-2 impedes the development of a pathologic microenvironment. *Nat. Med.*, 16, 1009–1017.

Barz, M., Luxenhofer, R., Zentel, R., & Vicent, M.J. (2011) Overcoming the PEG-addiction: Well-defined alternatives to PEG, from structure-property relationships to better defined therapeutics. *Polym. Chem.*, 2, 1900-1918.

Bellamri, N., Morzadec, C., Joannes, A., Lecureur, V., Wollin, L., Jouneau, S., & Vernhet, L. (2019) Alteration of human macrophage phenotypes by the anti-fibrotic drug nintedanib. *Int. Immunopharmacol.*, 72, 112–123.

Bellaye, P.S., Shimbori, C., Upagupta, C., Sato, S., Shi, W., Gauldie, J., Ask, K., & Kolb, M. (2018) Lysyl oxidase-like 1 protein deficiency protects mice from adenoviral transforming growth factor-b1-induced pulmonary fibrosis. *Am. J. Respir. Cell Mol. Biol.*, 58, 461–470.

Bendali, A., Hess, L.H., Seifert, M., Forster, V., Stephan, A.F., Garrido, J.A., & Picaud, S. (2013) Purified Neurons can Survive on Peptide-Free Graphene Layers. *Adv. Healthc. Mater.*, 2, 929–933.

Biondo, L.A., Batatinha, H.A., Souza, C.O., Teixeira, A.A.S., Silveira, L.S., Alonso-Vale, M.I., Oyama, L.M., Alves, M.J., Seelaender, M., & Neto, J.C.R. (2018) Metformin Mitigates Fibrosis and Glucose Intolerance Induced by Doxorubicin in Subcutaneous Adipose Tissue. *Front. Pharmacol.*, 9, 452.

Bitar, K.N. & Zakhem, E. (2014) Design Strategies of Biodegradable Scaffolds for Tissue Regeneration. *Biomed. Eng. Comput. Biol.*, 6, 13.

Blair, E.A. & Erlanger, J. (1933) A comparison of the characteristics of axons through their individual electrical responses. *Am. J. Physiol. Content*, 106, 524–564.

Blakney, A.K., Swartzlander, M.D., & Bryant, S.J. (2012) The effects of substrate stiffness on the in vitro activation of macrophages and in vivo host response to poly(ethylene glycol)-based hydrogels. *J. Biomed. Mater. Res. A*, 100, 1375–1386.

Blaschke, B.M., Lottner, M., Drieschner, S., Calia, A.B., Stoiber, K., Rousseau, L., Lissourges, G., & Garrido, J.A. (2016) Flexible graphene transistors for recording cell action potentials. *2D Mater.*, 3, 025007.

Boddupalli, A., Zhu, L., & Bratlie, K.M. (2016) Methods for Implant Acceptance and Wound Healing: Material Selection and Implant Location Modulate Macrophage and Fibroblast Phenotypes. *Adv. Healthc. Mater.*, 5, 2575–2594.

Bond, J.E., Kokosis, G., Ren, L., Selim, M.A., Bergeron, A., & Levinson, H. (2011) Wound contraction is attenuated by fasudil inhibition of Rho-associated kinase. *Plast. Reconstr. Surg.*, 128, 438e.

Boretius, T., Badia, J., Pascual-Font, A., Schuettler, M., Navarro, X., Yoshida, K., & Stieglitz, T. (2010) A transverse intrafascicular multichannel electrode (TIME) to interface with the peripheral nerve. *Biosens. Bioelectron.*, 26, 62–69.

Bostock, H. (1983) The strength-duration relationship for excitation of myelinated nerve: computed dependence on membrane parameters. *J. Physiol.*, 341, 59–74.

Bouton, C.E., Shaikhouni, A., Annetta, N. V., Bockbrader, M.A., Friedenberg, D.A., Nielson, D.M., Sharma, G., Sederberg, P.B., Glenn, B.C., Mysiw, W.J., Morgan, A.G., Deogaonkar, M., & Rezai, A.R. (2016) Restoring cortical control of functional movement in a human with quadriplegia. *Nature*, 533, 247–250.

Branner, A., Stein, R.B., & Normann, R.A. (2001) Selective stimulation of cat sciatic nerve using an array of varying-length microelectrodes. *J. Neurophysiol.*, 85, 1585–1594.

Brodbeck, W.G., MacEwan, M., Colton, E., Meyerson, H., & Anderson, J.M. (2005) Lymphocytes and the foreign body response: lymphocyte enhancement of macrophage adhesion and fusion. *J. Biomed. Mater. Res. A*, 74, 222–229.

Brovold, M., Almeida, J.I., Pla-Palacín, I., Sainz-Arnal, P., Sánchez-Romero, N., Rivas, J.J., Almeida, H., Dachary, P.R., Serrano-Aulló, T., Soker, S., & Baptista, P.M. (2018) Naturally-Derived Biomaterials for Tissue Engineering Applications. *Adv. Exp. Med. Biol.*, 1077, 421.

Brown, B.N., Londono, R., Tottey, S., Zhang, L., Kukla, K.A., Wolf, M.T., Daly, K.A., Reing, J.E., & Badylak, S.F. (2012) Macrophage Phenotype as a Predictor of Constructive Remodeling following the Implantation of Biologically Derived Surgical Mesh Materials. *Acta Biomater.*, 8, 978.

Brunton, E.K., Winther-Jensen, B., Wang, C., Yan, E.B., Gooie, S.H., Lowery, A.J., & Rajan, R. (2015) In vivo comparison of the charge densities required to evoke motor responses using novel annular penetrating microelectrodes. *Front. Neurosci.*, 8, 5.

Brushart, T.M.E. (1991) Central course of digital axons within the median nerve of macaca mulatta. *J. Comp. Neurol.*, 311, 197–209.

Bühling, F., Röcken, C., Brasch, F., Hartig, R., Yasuda, Y., Saftig, P., Brömme, D., & Welte, T. (2004) Pivotal role of cathepsin K in lung fibrosis. *Am. J. Pathol.*, 164, 2203–2216.

Bullock, C.J. & Bussy, C. (2019) Biocompatibility Considerations in the Design of Graphene Biomedical Materials. *Adv. Mater. Interfaces*, 6, 1900229.

Byun, D., Cho, S.J., Lee, B.H., Min, J., Lee, J.H., & Kim, S. (2017) Recording nerve signals in canine sciatic nerves with a flexible penetrating microelectrode array. *J. Neural Eng.*, 14, 046023.

Capogrosso, M., Raspopovic, S., & Micera, S. (2011) Does multipolar stimulation enhance selectivity of the TIME electrode? A simulation study using a genetic algorithm. *2011 5th Int. IEEE/EMBS Conf. Neural Eng. NER 2011*, 124–127.

Carnicer-Lombarte, A., Chen, S.T., Malliaras, G.G., & Barone, D.G. (2021) Foreign Body Reaction to Implanted Biomaterials and Its Impact in Nerve Neuroprosthetics. *Front. Bioeng. Biotechnol.*, 9, 1–22.

Christensen, M.B., Pearce, S.M., Ledbetter, N.M., Warren, D.J., Clark, G.A., & Tresco, P.A. (2014) The foreign body response to the Utah Slant Electrode Array in the cat sciatic nerve. *Acta Biomater.*, 10, 4650–4660.

Christensen, M.B. & Tresco, P.A. (2018) The foreign body response and morphometric changes associated with mesh-style peripheral nerve cuffs. *Acta Biomater.*, 67, 79–86.

Christensen, M.B., Wark, H.A.C., & Hutchinson, D.T. (2016) A histological analysis of human median and ulnar nerves following implantation of Utah slanted electrode arrays. *Biomaterials*, 77, 235–242.

Christie, B.P., Freeberg, M., Memberg, W.D., Pinault, G.J.C., Hoyen, H.A., Tyler, D.J., & Triolo, R.J. (2017) "Long-term stability of stimulating spiral nerve cuff electrodes on human peripheral nerves." *J. Neuroeng. Rehabil.*, 14, 1–12.

Chung, L., Maestas, D.R., Lebid, A., Mageau, A., Rosson, G.D., Wu, X., Wolf, M.T., Tam, A.J., Vanderzee, I., Wang, X., Andorko, J.I., Zhang, H., Narain, R., Sadtler, K., Fan, H., Čiháková, D., Le Saux, C.J., Housseau, F., Pardoll, D.M., & Elisseeff, J.H. (2020) Interleukin 17 and senescent cells regulate the foreign body response to synthetic material implants in mice and humans. *Sci. Transl. Med.*, 12, eaax3799.

Chung, T., Wang, J.Q., Wang, J., Cao, B., Li, Y., & Pang, S.W. (2015) Electrode modifications to lower electrode impedance and improve neural signal recording sensitivity. *J. Neural Eng.*, 12, 056018.

Cipriani, C., Controzzi, M., & Carrozza, M.C. (2011) The SmartHand transradial prosthesis. *J. Neuroeng. Rehabil.*, 8, 29.

Citi, L., Carpaneto, J., Yoshida, K., Hoffmann, K.P., Koch, K.P., Dario, P., & Micera, S. (2008) On the use of wavelet denoising and spike sorting techniques to process electroneurographic signals recorded using intraneural electrodes. *J. Neurosci. Methods*, 172, 294–302.

Clements, I.P., Kim, Y.T., Andreasen, D., & Bellamkonda, R. V. (2007) A regenerative electrode scaffold for peripheral nerve interfacing. *Proc. 3rd Int. IEEE EMBS Conf. Neural Eng.*, 390–393.

Cogan, S.F. (2008) Neural Stimulation and Recording Electrodes. *Annu. Rev. Biomed. Eng.*, 10, 275–309.

Cogan, S.F., Ludwig, K.A., Welle, C.G., & Takmakov, P. (2016) Tissue damage thresholds during therapeutic electrical stimulation. *J. Neural Eng.*, 13, 021001.

Constantin, C.P., Aflori, M., Damian, R.F., & Rusu, R.D. (2019) Biocompatibility of polyimides: A mini-review. *Materials (Basel).*, 12, 3166.

Contreras, E., Traserra, S., Bolívar, S., Forés, J., Jose-Cunilleras, E., García, F., Delgado-Martínez, I., Holmgren, S., Strehl, R., Udina, E., & Navarro, X. (2022) Repair of Long Nerve Defects with a New Decellularized Nerve Graft in Rats and in Sheep. *Cells*, 11, 4074.

Convertino, D., Luin, S., Marchetti, L., & Coletti, C. (2018) Peripheral Neuron Survival and Outgrowth on Graphene 12, 1–8.

Coutinho, A.E. & Chapman, K.E. (2011) The anti-inflammatory and immunosuppressive effects of glucocorticoids, recent developments and mechanistic insights. *Mol. Cell. Endocrinol.*, 335, 2–13.

Creasey, G.H. & Bodner, D.R. (1994) Electrical stimulation of sacral roots for micturition after spinal cord injury. *NeuroRehabilitation*, 4, 266–274.

Cutrone, A., Del Valle, J., Santos, D., Badia, J., Filippeschi, C., Micera, S., Navarro, X., & Bossi, S. (2015) A three-dimensional self-opening intraneural peripheral interface (SELINE). *J. Neural Eng.*, 12, 16016.

Cutrone, A. & Micera, S. (2019) Implantable Neural Interfaces and Wearable Tactile Systems for Bidirectional Neuroprosthetics Systems. *Adv. Healthc. Mater.*, 8, e1801345.

D'Anna, E., Petrini, F.M., Artoni, F., Popovic, I., Simanić, I., Raspopovic, S., & Micera, S. (2017) A somatotopic bidirectional hand prosthesis with transcutaneous electrical nerve stimulation based sensory feedback. *Sci. Rep.*, 7, 1–15.

D'Anna, E., Valle, G., Mazzoni, A., Strauss, I., Iberite, F., Patton, J., Petrini, F.M., Raspopovic, S., Granata, G., Iorio, R. Di, Controzzi, M., Cipriani, C., Stieglitz, T., Rossini, P.M., & Micera, S. (2019) A closed-loop hand prosthesis with simultaneous intraneural tactile and position feedback. *Sci. Robot.*, 4, 262741.

Daniels, C.E., Wilkes, M.C., Edens, M., Kottom, T.J., Murphy, S.J., Limper, A.H., & Leof, E.B. (2004) Imatinib mesylate inhibits the profibrogenic activity of TGF-β and prevents bleomycin-mediated lung fibrosis. *J. Clin. Invest.*, 114, 1308–1316.

Dankerl, M., Hauf, M. V., Lippert, A., Hess, L.H., Birner, S., Sharp, I.D., Mahmood, A., Mallet, P., Veuillen, J.-Y., Stutzmann, M., & Garrido, J.A. (2010) Graphene Solution-Gated Field-Effect Transistor Array for Sensing Applications. *Adv. Funct. Mater.*, 20, 3117–3124.

de la Oliva, N., del Valle, J., Delgado-Martínez, I., Mueller, M., Stieglitz, T., Navarro, X., Delgado-Martinez, I., Mueller, M., Stieglitz, T., Navarro, X., & Delgado-Martínez, I. (2019) Long-Term Functionality of Transversal Intraneural Electrodes Is Improved By Dexamethasone Treatment. *IEEE Trans. Neural Syst. Rehabil. Eng.*, 27, 457–464.

de la Oliva, N., Mueller, M., Stieglitz, T., Navarro, X., & Del Valle, J. (2018a) On the use of Parylene C polymer as substrate for peripheral nerve electrodes. *Sci. Rep.*, 8, 1–12.

de la Oliva, N., Navarro, X., & Del Valle, J. (2018b) Time course study of long-term biocompatibility and foreign body reaction to intraneural polyimide-based implants. *J. Biomed. Mater. Res. - Part A*, 106, 746–757.

de la Oliva, N., Navarro, X., & del Valle, J. (2018c) Dexamethasone Reduces the Foreign Body Reaction to Intraneural Electrode Implants in the Peripheral Nerve of the Rat. *Anat. Rec.*, 301, 1722–1733.

de la Oliva, N., Navarro, X., & del Valle i Macià, J. (2018d), Universitat Autònoma de Barcelona. Departament de Biologia Cel·lular, de F. i d'Immunologia. (2018) Biological response to implanted intraneural electrodes.

de Medinaceli, L., Freed, W.J., & Wyatt, R.J. (1982) An index of the functional condition of rat sciatic nerve based on measurements made from walking tracks. *Exp. Neurol.*, 77, 634–643.

del Valle, J., De la Oliva, N., Müller, M., Stieglitz, T., & Navarro, X. (2015) Biocompatibility evaluation of parylene C and polyimide as substrates for peripheral nerve interfaces. *Int. IEEE/EMBS Conf. Neural Eng. NER*, 2015-July, 442–445.

del Valle, J. & Navarro, X. (2013) *Interfaces with the Peripheral Nerve for the Control of Neuroprostheses*, 1st edn, International Review of Neurobiology. Elsevier Inc.

del Valle, J., Santos, D., Delgado-Martínez, I., de la Oliva, N., Giudetti, G., Micera, S., & Navarro, X. (2018) Segregation of motor and sensory axons regenerating through bicompartmental tubes by combining extracellular matrix components with neurotrophic factors. *J. Tissue Eng. Regen. Med.*, 12, e1991–e2000.

Delgado-Martínez, I., Righi, M., Santos, D., Cutrone, A., Bossi, S., D?Amico, S., Del Valle, J., Micera, S., Navarro, X., & D'Amico, S. (2017) Fascicular nerve stimulation and recording using a novel double-aisle regenerative electrode. *J. Neural Eng.*, 14, 046003.

Desgeorges, T., Caratti, G., Mounier, R., Tuckermann, J., & Chazaud, B. (2019) Glucocorticoids shape macrophage phenotype for tissue repair. *Front. Immunol.*, 10, 1591.

Devi, M., Vomero, M., Fuhrer, E., Castagnola, E., Gueli, C., Nimbalkar, S., Hirabayashi, M., Kassegne, S., Stieglitz, T., & Sharma, S. (2021) Carbon-based neural electrodes: promises and challenges. *J. Neural Eng.*, 18, 041007.

DiEgidio, P., Friedman, H.I., Gourdie, R.G., Riley, A.E., Yost, M.J., & Goodwin, R.L. (2014) Biomedical implant capsule formation lessons learned and the road ahead. *Ann. Plast. Surg.*, 73, 451–460.

Distler, J.H.W., Jüngel, A., Huber, L.C., Schulze-Horsel, U., Zwerina, J., Gay, R.E., Michel, B.A., Hauser, T., Schett, G., Gay, S., & Distler, O. (2007) Imatinib mesylate reduces production of extracellular matrix and prevents development of experimental dermal

fibrosis. *Arthritis Rheum.*, 56, 311–322.

Doering, M., Kieninger, J., Urban, G.A., & Weltin, A. (2022) Electrochemical microelectrode degradation monitoring: in situ investigation of platinum corrosion at neutral pH *Journal of neural engineering*, 19, 016005.

Dondossola, E., Holzapfel, B.M., Alexander, S., Filippini, S., Hutmacher, D.W., & Friedl, P. (2016) Examination of the foreign body response to biomaterials by nonlinear intravital microscopy. *Nat. Biomed. Eng.*, 1, 0007.

Dosen, S., Schaeffer, M.C., & Farina, D. (2014) Time-division multiplexing for myoelectric closed-loop control using electrotactile feedback. *J. Neuroeng. Rehabil.*, 11, 138.

Ehrchen, J.M., Roth, J., & Barczyk-Kahlert, K. (2019) More than suppression: Glucocorticoid action on monocytes and macrophages. *Front. Immunol.*, 10, 2028.

Elyahoodayan, S., Larson, C., Cobo, A.M., Meng, E., & Song, D. (2020) Acute In Vivo Testing of a Polymer Cuff Electrode with Integrated Microfluidic Channels for Stimulation, Recording, and Drug Delivery on Rat Sciatic Nerve. *J. Neurosci. Methods*, 336, 108634.

Fabbro, A., Scaini, D., Leon, V., Vázquez, E., Cellot, G., Privitera, G., Lombardi, L., Torrisi, F., Tomarchio, F., Bosi, S., Ferrari, A.C., Ballerini, L., & Prato, M. (2015) Graphene-Based Interfaces do not Alter Target Nerve Cells. *ACS nano*, 10, 615–623.

Farah, S., Doloff, J.C., Müller, P., Sadraei, A., Han, H.J., Olafson, K., Vyas, K., Tam, H.H., Hollister-Lock, J., Kowalski, P.S., Griffin, M., Meng, A., McAvoy, M., Graham, A.C., McGarrigle, J., Oberholzer, J., Weir, G.C., Greiner, D.L., Langer, R., & Anderson, D.G. (2019) Long-term implant fibrosis prevention in rodents and non-human primates using crystallized drug formulations. *Nat. Mater.*, 18, 892–904.

Fattman, C.L. (2008) Apoptosis in pulmonary fibrosis: Too much or not enough? *Antioxidants Redox Signal.*, 10, 379–385.

Ferrari, L.M., Rodríguez-Meana, B., Bonisoli, A., Cutrone, A., Micera, S., Navarro, X., Greco, F., & del Valle, J. (2021) All-Polymer Printed Low-Cost Regenerative Nerve Cuff Electrodes. *Front. Bioeng. Biotechnol.*, 9, 615218.

Fertala, J., Rivlin, M., Wang, M.L., Beredjiklian, P.K., Steplewski, A., & Fertala, A. (2020) Collagen-rich deposit formation in the sciatic nerve after injury and surgical repair: A study of collagen-producing cells in a rabbit model. *Brain Behav.*, 10, e01802..

Fitzgerald, J.J. (2016) Suppression of scarring in peripheral nerve implants by drug elution. *J. Neural Eng.*, 13, 26006.

Gällentoft, L., Pettersson, L.M.E., Danielsen, N., Schouenborg, J., Prinz, C.N., & Linsmeier, C.E. (2016) Impact of degradable nanowires on long-term brain tissue responses. *J. Nanobiotechnology*, 14, 1–11.

Garcia-Cortadella, R., Schwesig, G., Jeschke, C., Illa, X., Gray, A.L., Savage, S., Stamatidou, E., Schiessl, I., Masvidal-Codina, E., Kostarelos, K., Guimerà-Brunet, A., Sirota, A., & Garrido, J.A. (2021) Graphene active sensor arrays for long-term and wireless mapping of wide frequency band epicortical brain activity. *Nat. Commun.*, 12, 1–17.

Garrison, G., Huang, S.K., Okunishi, K., Scott, J.P., Penke, L.R.K., Scruggs, A.M., & Peters-Golden, M. (2013) Reversal of myofibroblast differentiation by prostaglandin E2. *Am. J. Respir. Cell Mol. Biol.*, 48, 550–558.

Ghirnikar, R.S., Lee, Y.L., & Eng, L.F. (1998) Inflammation in traumatic brain injury: Role of cytokines and chemokines. *Neurochem. Res.*, 23, 329–340.

Golabchi, A., Wu, B., Cao, B., Bettinger, C.J., & Cui, X.T. (2019) Zwitterionic polymer/polydopamine coating reduce acute inflammatory tissue responses to neural

implants. *Biomaterials*, 225, 119519.

Gold, C., Henze, D.A., Koch, C., & Buzsáki, G. (2006) On the origin of the extracellular action potential waveform: A modeling study. *J. Neurophysiol.*, 95, 3113–3128.

Gori, M., Giannitelli, S.M., Vadalà, G., Papalia, R., Zollo, L., Sanchez, M., Trombetta, M., Rainer, A., Di Pino, G., & Denaro, V. (2022) A Soft Zwitterionic Hydrogel as Potential Coating on a Polyimide Surface to Reduce Foreign Body Reaction to Intraneural Electrodes. *Molecules*, 27, 3126.

Gori, M., Vadalà, G., Giannitelli, S.M., Denaro, V., & Di Pino, G. (2021) Biomedical and Tissue Engineering Strategies to Control Foreign Body Reaction to Invasive Neural Electrodes. *Front. Bioeng. Biotechnol.*, 9, 659033

Gorman, P.H. & Mortimer, J.T. (1983) The Effect of Stimulus Parameters on the Recruitment Characteristics of Direct Nerve Stimulation. *IEEE Trans. Biomed. Eng.*, BME-30, 407–414.

Gouyet, L., Cathébras, G., Bernard, S., Guiraud, D., & Bertrand, Y. (2007) A new configuration of multipolar cuff electrode and dedicated IC for afferent signal recording. *Proc. 3rd Int. IEEE EMBS Conf. Neural Eng.*, 578–581.

Gower, R.M., Boehler, R.M., Azarin, S.M., Ricci, C.F., Leonard, J.N., & Shea, L.D. (2014) Modulation of leukocyte infiltration and phenotype in microporous tissue engineering scaffolds via vector induced IL-10 expression. *Biomaterials*, 35, 2024–2031.

Grand, L., Wittner, L., Herwik, S., Göthelid, E., Ruther, P., Oscarsson, S., Neves, H., Dombovári, B., Csercsa, R., Karmos, G., & Ulbert, I. (2010) Short and long term biocompatibility of NeuroProbes silicon probes. *J. Neurosci. Methods*, 189, 216–229.

Graupe, D. & Kohn, K. (1997) Transcutaneous functional neuromuscular stimulation of certain traumatic complete thoracic paraplegics for independent short-distance ambulation. *Neurol. Res.*, 19, 323–333.

Green, R. & Abidian, M.R. (2015) Conducting Polymers for Neural Prosthetic and Neural Interface Applications. *Adv. Mater.*, 27, 7620–7637.

Gretzer, C., Emanuelsson, L., Liljensten, E., & Thomsen, P. (2006) The inflammatory cell influx and cytokines changes during transition from acute inflammation to fibrous repair around implanted materials. *J. Biomater. Sci. Polym. Ed.*, 17, 669–687.

Grill, W.M. & Thomas Mortimer, J. (1994) Electrical properties of implant encapsulation tissue. *Ann. Biomed. Eng.*, 22, 23–33.

Guiho, T., López-álvarez, V.M., Čvančara, P., Hiairrassary, A., Andreu, D., Stieglitz, T., Navarro, X., & Guiraud, D. (2021) New stimulation device to drive multiple transverse intrafascicular electrodes and achieve highly selective and rich neural responses. *Sensors*, 21, 7219.

Gulino, M., Kim, D., Pané, S., Santos, S.D., & Pêgo, A.P. (2019) Tissue response to neural implants: The use of model systems toward new design solutions of implantable microelectrodes. *Front. Neurosci.*, 13, 1–24.

Günter, C., Delbeke, J., & Ortiz-Catalan, M. (2020) Safety of long-term electrical peripheral nerve stimulation: review of the state of the art. *J. Neuroeng. Rehabil.*, 16, 13.

Guo, L., Sandsjö, L., Ortiz-Catalan, M., & Skrifvars, M. (2020) Systematic review of textile-based electrodes for long-term and continuous surface electromyography recording. *Text. Res. J.*, 90, 227–244.

Hall & Edward, J. (2011) *Guyton and Hall Textbook of Medical Physiology Thirteenth Edition*, Twelfth edition. edn, Elsevier. Saunders/Elsevier, Philadelphia Pa.

Hallin, R.G. (1990) Microneurography in relation to intraneural topography: somatotopic

organisation of median nerve fascicles in humans. *J. Neurol. Neurosurg. Psychiatry*, 53, 736–744.

Hamilton, T.A., Zhao, C., Pavicic, P.G., & Datta, S. (2014) Myeloid colony-stimulating factors as regulators of macrophage polarization. *Front. Immunol.*, 5, 554.

Harlow, C.R., Wu, X., van Deemter, M., Gardiner, F., Poland, C., Green, R., Sarvi, S., Brown, P., Kadler, K.E., Lu, Y., Mason, J.I., Critchley, H.O.D., & Hillier, S.G. (2017) Targeting lysyl oxidase reduces peritoneal fibrosis. *PLoS One*, 12, e0183013.

Hassler, C., Boretius, T., & Stieglitz, T. (2011) Polymers for neural implants. *J. Polym. Sci. Part B Polym. Phys.*, 49, 18–33.

Haugland, M.K. & Hoffer, J.A. (1994) Artifact-free sensory nerve signals obtained from cuff electrodes during functional electrical stimulation of nearby muscles. *IEEE Trans. Rehabil. Eng.*, 2, 37–40.

Haugland, M.K., Hoffer, J.A., & Sinkjær, T. (1994) Skin Contact Force Information in Sensory Nerve Signals Recorded by Implanted Cuff Electrodes. *IEEE Trans. Rehabil. Eng.*, 2, 18–28.

Haugland, M.K. & Sinkjær, T. (1995) Cutaneous Whole Nerve Recordings Used for Correction of Footdrop in Hemiplegic Man. *IEEE Trans. Rehabil. Eng.*, 3, 307–317.

He, W. & Bellamkonda, R. V. (2007) A molecular perspective on understanding and modulating the performance of chronic central nervous system (CNS) recording electrodes. In *Indwelling Neural Implants: Strategies for Contending with the in Vivo Environment*. CRC Press, pp. 151–175.

He, Z., Yang, X., Wang, N., Mu, L., Pan, J., Lan, X., Li, H., & Deng, F. (2021) Anti-Biofouling Polymers with Special Surface Wettability for Biomedical Applications. *Front. Bioeng. Biotechnol.*, 9, 1260.

Henneman, E., Somjen, G., & Carpenter, D.O. (1965) Functional Significance of Cell Size in Spinal Motoneurons. *J. Neurophysiol.*, 28, 560–580.

Heo, D. N., Song, S. J., Kim, H. J., Lee, Y. J., Ko, W. K., Lee, S. J., Lee, D., Park, S. J., Zhang, L. G., Kang, J. Y., Do, S. H., Lee, S. H., & Kwon, I. K. (2016) Multifunctional hydrogel coatings on the surface of neural cuff electrode for improving electrode-nerve tissue interfaces. *Acta Biomater.*, 39, 25–33.

Hernandez, J.L., Park, J., Yao, S., Blakney, A.K., Nguyen, H. V., Katz, B.H., Jensen, J.T., & Woodrow, K.A. (2021) Effect of tissue microenvironment on fibrous capsule formation to biomaterial-coated implants. *Biomaterials*, 273, 120806.

Herrero-Cervera, A., Soehnlein, O., & Kenne, E. (2022) Neutrophils in chronic inflammatory diseases. *Cell. Mol. Immunol. 2022 192*, 19, 177–191.

Hess, L.H., Jansen, M., Maybeck, V., Hauf, M. V, Seifert, M., Stutzmann, M., Sharp, I.D., Offenhäusser, A., & Garrido, J.A. (2011) Graphene Transistor Arrays for Recording Action Potentials from Electrogenic Cells. *Adv. Mater.*, 5045–5049.

Hinz, B. & Lagares, D. (2020) Evasion of apoptosis by myofibroblasts: a hallmark of fibrotic diseases. *Nat. Rev. Rheumatol.*, 16, 11–31.

Hirsh, S.L., McKenzie, D.R., Nosworthy, N.J., Denman, J.A., Sezerman, O.U., & Bilek, M.M.M. (2013) The Vroman effect: Competitive protein exchange with dynamic multilayer protein aggregates. *Colloids Surfaces B Biointerfaces*, 103, 395–404.

Hoch, K., Pothof, F., Becker, F., Paul, O., & Ruther, P. (2018) Development, Modeling, Fabrication, and Characterization of a Magnetic, Micro-Spring-Suspended System for the Safe Electrical Interconnection of Neural Implants. *Micromachines*, 9, 424.

Hochberg, L.R., Bacher, D., Jarosiewicz, B., Masse, N.Y., Simeral, J.D., Vogel, J., Haddadin, S.,

Liu, J., Cash, S.S., Van Der Smagt, P., & Donoghue, J.P. (2012) Reach and grasp by people with tetraplegia using a neurally controlled robotic arm. *Nature*, 485, 372–375.

Hoffer, J.A., Stein, R.B., Haugland, M.K., Sinkjaer, T., Durfee, W.K., Schwartz, A.B., Loeb, G.E., Kantor, C., & others (1996) Neural signals for command control and feedback in functional neuromuscular stimulation: a review. *J Rehabil Res Dev*, 33, 145–157.

Holmkvist, A.D., Agorelius, J., Forni, M., Nilsson, U.J., Linsmeier, C.E., & Schouenborg, J. (2020) Local delivery of minocycline-loaded PLGA nanoparticles from gelatin-coated neural implants attenuates acute brain tissue responses in mice. *J. Nanobiotechnology*, 18, 27.

Horch, K.W., Tuckett, R.P., & Burgess, P.R. (1977) A key to the classification of cutaneous mechanoreceptors. *J. Invest. Dermatol.*, 69, 75–82.

Horn, A., Kireva, T., Palumbo-Zerr, K., Dees, C., Tomcik, M., Cordazzo, C., Zerr, P., Akhmetshina, A., Ruat, M., Distler, O., Beyer, C., Schett, G., & Distler, J.H.W. (2012) Inhibition of hedgehog signalling prevents experimental fibrosis and induces regression of established fibrosis. *Ann. Rheum. Dis.*, 71, 785–789.

Hutchings, K.M., Lisabeth, E.M., Rajeswaran, W., Wilson, M.W., Sorenson, R.J., Campbell, P.L., Ruth, J.H., Amin, A., Tsou, P.S., Leipprandt, J.R., Olson, S.R., Wen, B., Zhao, T., Sun, D., Khanna, D., Fox, D.A., Neubig, R.R., & Larsen, S.D. (2017) Pharmacokinetic optimitzation of CCG-203971: Novel inhibitors of the Rho/MRTF/SRF transcriptional pathway as potential antifibrotic therapeutics for systemic scleroderma. *Bioorganic Med. Chem. Lett.*, 27, 1744–1749.

Ikenaga, N., Peng, Z.W., Vaid, K.A., Liu, S.B., Yoshida, S., Sverdlov, D.Y., Mikels-Vigdal, A., Smith, V., Schuppan, D., & Popov, Y. V. (2017) Selective targeting of lysyl oxidase-like 2 (LOXL2) suppresses hepatic fibrosis progression and accelerates its reversal. *Gut*, 66, 1697–1708.

Inmann, A., Haugland, M., Haase, J., Biering-Sørensen, F., & Sinkjaer, T. (2001) Signals from skin mechanoreceptors used in control of a hand grasp neuroprosthesis. *Neuroreport*, 12, 2817–2820.

Ishida, W., Mori, Y., Lakos, G., Sun, L., Shan, F., Bowes, S., Josiah, S., Lee, W.C., Singh, J., Ling, L.E., & Varga, J. (2006) Intracellular TGF-β receptor blockade abrogates smad-dependent fibroblast activation in vitro and in vivo. *J. Invest. Dermatol.*, 126, 1733–1744.

Jafarinejad-Farsangi, S., Farazmand, A., Mahmoudi, M., Gharibdoost, F., Karimizadeh, E., Noorbakhsh, F., Faridani, H., & Jamshidi, A.R. (2015) MicroRNA-29a induces apoptosis via increasing the Bax:Bcl-2 ratio in dermal fibroblasts of patients with systemic sclerosis. *Autoimmunity*, 48, 369–378.

Jain, S., Tran, T.H., & Amiji, M. (2015) Macrophage repolarization with targeted alginate nanoparticles containing IL-10 plasmid DNA for the treatment of experimental arthritis. *Biomaterials*, 61, 162–177.

Jeon, H.J., Kang, M.J., Lee, J.S., Kang, J., Kim, E.A., Jin, H.K., Bae, J. sung, & Yang, J.D. (2022) Impact on capsule formation for three different types of implant surface tomography. *Sci. Rep.*, 12, 13535.

Jiang, J. Le, Marathe, A.R., Keene, J.C., & Taylor, D.M. (2017) A testbed for optimizing electrodes embedded in the skull or in artificial skull replacement pieces used after injury. *J. Neurosci. Methods*, 277, 21.

Jing, Y., Wu, F., Li, D., Yang, L., Li, Q., & Li, R. (2018) Metformin improves obesity-associated inflammation by altering macrophages polarization. *Mol. Cell. Endocrinol.*, 461, 256–264.

Jinnin, M., Ihn, H., & Tamaki, K. (2006) Characterization of SIS3, a novel specific inhibitor of

Smad3, and its effect on transforming growth factor-β1-induced extracellular matrix expression. *Mol. Pharmacol.*, 69, 597–607.

John, A.A., Subramanian, A.P., Vellayappan, M.V., Balaji, A., Mohandas, H., & Jaganathan, S.K. (2015) Carbon nanotubes and graphene as emerging candidates in neuroregeneration and neurodrug delivery. *Int. J. Nanomedicine*, 10, 4267–4277.

Jones, J.A., Chang, D.T., Meyerson, H., Colton, E., Il, K.K., Matsuda, T., & Anderson, J.M. (2007) Proteomic analysis and quantification of cytokines and chemokines from biomaterial surface-adherent macrophages and foreign body giant cells. *J. Biomed. Mater. Res. - Part A*, 83, 585–596.

Kaczmarek, K.A., Webster, J.G., Bach-y-Rita, P., & Tompkins, W.J. (1991) Electrotactile and Vibrotactile Displays for Sensory Substitution Systems. *IEEE Trans. Biomed. Eng.*, 38, 1–16.

Kang, Y.N., Chou, N., Jang, J.W., Byun, D., Kang, H., Moon, D.J., Kim, J., & Kim, S. (2019) An Intrafascicular Neural Interface with Enhanced Interconnection for Recording of Peripheral Nerve Signals. *IEEE Trans. Neural Syst. Rehabil. Eng.*, 27, 1312–1319.

Karatas, A., Oz, B., Celik, C., Akar, Z.A., Akkoc, R.F., Etem, E.O., Dagli, A.F., & Koca, S.S. (2022) Tofacitinib and metformin reduce the dermal thickness and fibrosis in mouse model of systemic sclerosis. *Sci. Rep.*, 12, 2553.

Keller, T. & Kuhn, A. (2008) Electrodes for transcutaneous (surface) electrical stimulation. *J. Autom. Control*, 18, 35–45.

Kennedy, W.R., Navarro, X., & Kamal, H. (1988) Reinnervation of sweat glands in the mouse: Axonal regeneration versus collateral sprouting. *Muscle Nerve*, 11, 603–609.

Kheirollahi, V., Wasnick, R.M., Biasin, V., Vazquez-Armendariz, A.I., Chu, X., Moiseenko, A., Weiss, A., Wilhelm, J., Zhang, J.S., Kwapiszewska, G., Herold, S., Schermuly, R.T., Mari, B., Li, X., Seeger, W., Günther, A., Bellusci, S., & El Agha, E. (2019) Metformin induces lipogenic differentiation in myofibroblasts to reverse lung fibrosis. *Nat. Commun.*, 10, 2987.

Khodagholy, D., Gelinas, J.N., Thesen, T., Doyle, W., Devinsky, O., Malliaras, G.G., & Buzsáki, G. (2014) NeuroGrid: recording action potentials from the surface of the brain. *Nat. Neurosci. 2015 182*, 18, 310–315.

Kim, D.H. & Martin, D.C. (2006) Sustained release of dexamethasone from hydrophilic matrices using PLGA nanoparticles for neural drug delivery. *Biomaterials*, 27, 3031–3037.

Kim, S.M., Joo, P., Ahn, G., Cho, I.H., Kim, D.H., Song, W.K., Kim, B.S., & Yoon, M.H. (2013) Transparent conducting films based on reduced graphene oxide multilayers for biocompatible neuronal interfaces. *J. Biomed. Nanotechnol.*, 9, 403–408.

Kinoshita, K., Aono, Y., Azuma, M., Kishi, J., Takezaki, A., Kishi, M., Makino, H., Okazaki, H., Uehara, H., Izumi, K., Sone, S., & Nishioka, Y. (2013) Antifibrotic effects of focal adhesion kinase inhibitor in bleomycin-induced pulmonary fibrosis in mice. *Am. J. Respir. Cell Mol. Biol.*, 49, 536–543.

Kohler, F., Gkogkidis, C.A., Bentler, C., Wang, X., Gierthmuehlen, M., Fischer, J., Stolle, C., Reindl, L.M., Rickert, J., Stieglitz, T., Ball, T., & Schuettler, M. (2017) Closed-loop interaction with the cerebral cortex: a review of wireless implant technology§. *Brain-Computer Interfaces*, 4, 146–154.

Kostarelos, K., Vincent, M., Hebert, C., & Garrido, J.A. (2017) Graphene in the Design and Engineering of Next-Generation Neural Interfaces. *Adv. Mater.*, 29, 1–7.

Kozai, T.D.Y., Vazquez, A.L., Weaver, C.L., Kim, S.-G., & Cui, X.T. (2012) In vivo two-photon microscopy reveals immediate microglial reaction to implantation of microelectrode through extension of processes. *J. Neural Eng.*, 9, 066001.

Krzyszczyk, P., Schloss, R., Palmer, A., Berthiaume, F., Krzyzczyk, P., Schloss, R., Palmer, A., & Berthiaume, F. (2018) The role of macrophages in acute and chronic wound healing and interventions to promote pro-wound healing phenotypes. *Front. Physiol.*, 9, 1–22.

Kuzum, D., Takano, H., Shim, E., Reed, J.C., Juul, H., Richardson, A.G., De Vries, J., Bink, H., Dichter, M.A., Lucas, T.H., Coulter, D.A., Cubukcu, E., & Litt, B. (2014) Transparent and flexible low noise graphene electrodes for simultaneous electrophysiology and neuroimaging. *Nat. Commun.*, 5, 5259.

Kyriakides, T.R., Kim, H.J., Zheng, C., Harkins, L., Tao, W., & Deschenes, E. (2022) Foreign body response to synthetic polymer biomaterials and the role of adaptive immunity. *Biomed. Mater.*, 17.

Labow, R.S., Meek, E., & Santerre, J.P. (2001) Neutrophil-mediated biodegradation of medical implant materials. *J. Cell. Physiol.*, 186, 95–103.

Lacour, S.P., Courtine, G., & Guck, J. (2016) Materials and technologies for soft implantable neuroprostheses. *Nat. Rev. Mater.*, 1.

Lagares, D., Busnadiego, O., García-Fernández, R.A., Kapoor, M., Liu, S., Carter, D.E., Abraham, D., Shi-Wen, X., Carreira, P., Fontaine, B.A., Shea, B.S., Tager, A.M., Leask, A., Lamas, S., & Rodríguez-Pascual, F. (2012) Inhibition of focal adhesion kinase prevents experimental lung fibrosis and myofibroblast formation. *Arthritis Rheum.*, 64, 1653–1664.

Lago, N., Ceballos, D., J Rodríguez, F., Stieglitz, T., & Navarro, X. (2005) Long term assessment of axonal regeneration through polyimide regenerative electrodes to interface the peripheral nerve. *Biomaterials*, 26, 2021–2031.

Lago, N., Udina, E., & Navarro, X. (2006) Regenerative electrodes for interfacing injured periph- eral nerves: neurobiological assessment. *First IEEE/RAS-EMBS Int. Conf. Biomed. Robot. Biomechatronics, 2006. BioRob 2006.*, 35094, 1149–1153.

Lago, N., Yoshida, K., Koch, K.P., & Navarro, X. (2007) Assessment of biocompatibility of chronically implanted polyimide and platinum intrafascicular electrodes. *IEEE Trans. Biomed. Eng.*, 54, 281–290.

Lawrence, S.M., Dhillon, G.S., Jensen, W., Yoshida, K., & Horch, K.W. (2004) Acute peripheral nerve recording ch1 Yoshida Kozai TD et al. Nat. Mater. 11, 1065–1073. 2012aracteristics of polymer-based longitudinal intrafascicular electrodes. *IEEE Trans. Neural Syst. Rehabil. Eng.*, 12, 345–348.

Lee, M., Katerelos, M., Gleich, K., Galic, S., Kemp, B.E., Mount, P.F., & Power, D.A. (2018) Phosphorylation of acetyl-CoA carboxylase by AMPK reduces renal fibrosis and is essential for the anti-fibrotic effect of metformin. *J. Am. Soc. Nephrol.*, 29, 2326–2336.

Lee, S., Sheshadri, S., Xiang, Z., Delgado-Martinez, I., Xue, N., Sun, T., Thakor, N. V., Yen, S.C., & Lee, C. (2017) Selective stimulation and neural recording on peripheral nerves using flexible split ring electrodes. *Sensors Actuators, B Chem.*, 242, 1165–1170.

Lee, S., Yen, S.C., Sheshadri, S., Martinez, I.D., Xue, N., Xiang, Z., Thakor, N. V., & Lee, C. (2016) Flexible Epineural Strip Electrode for Recording in Fine Nerves. *IEEE Trans. Biomed. Eng.*, 63, 581–587.

Leventhal, D.K., Cohen, M., & Durand, D.M. (2006) Chronic histological effects of the flat interface nerve electrode. *J. Neural Eng.*, 3, 102–113.

Leventhal, D.K. & Durand, D. (2003) Subfascicle Stimulation Selectivity with the Flat Interface Nerve Electrode. *Ann. Biomed. Eng.*, 31, 643–652.

Li, S.X., Li, C., Pang, X.R., Zhang, J., Yu, G.C., Yeo, A.J., Lavin, M.F., Shao, H., Jia, Q., & Peng, C. (2021) Metformin Attenuates Silica-Induced Pulmonary Fibrosis by Activating Autophagy via the AMPK-mTOR Signaling Pathway. *Front. Pharmacol.*, 12, 719589.

Li, X., Zhu, L., Wang, B., Yuan, M., & Zhu, R. (2017) Drugs and targets in fibrosis. *Front. Pharmacol.*,. 8, 855.

Liang, M., Lv, J., Chu, H., Wang, J., Chen, X., Zhu, X., Xue, Y., Guan, M., & Zou, H. (2014) Vertical inhibition of PI3K/Akt/mTOR signaling demonstrates in vitro and in vivo anti-fibrotic activity. *J. Dermatol. Sci.*, 76, 104–111.

Lis-López, L., Bauset, C., Seco-Cervera, M., & Cosín-Roger, J. (2021) Is the Macrophage Phenotype Determinant for Fibrosis Development? *Biomedicines*, 9, 1747.

Liu, B., Kim, E., Meggo, A., Gandhi, S., Luo, H., Kallakuri, S., Xu, Y., & Zhang, J. (2017) Enhanced biocompatibility of neural probes by integrating microstructures and delivering anti-inflammatory agents via microfluidic channels. *J. Neural Eng.*, 14, 026008.

Liu, F., Lagares, D., Choi, K.M., Stopfer, L., Marinković, A., Vrbanac, V., Probst, C.K., Hiemer, S.E., Sisson, T.H., Horowitz, J.C., Rosas, I.O., Fredenburgh, L.E., Feghali-Bostwick, C., Varelas, X., Tager, A.M., & Tschumperlin, D.J. (2015) Mechanosignaling through YAP and TAZ drives fibroblast activation and fibrosis. *Am. J. Physiol. - Lung Cell. Mol. Physiol.*, 308, L344–L357.

Liu, P., Huang, T., Liu, P., Shi, S., Chen, Q., Li, L., & Shen, J. (2016) Zwitterionic modification of polyurethane membranes for enhancing the anti-fouling property. *J. Colloid Interface Sci.*, 480, 91–101.

Liu, W., Xiong, S., Du, J., Song, Y., Wang, T., Zhang, Y., Dong, C., Huang, Z.S., He, Q., Yu, Z., & Ma, X. (2022) Deciphering Key Foreign Body Reaction-Related Transcription Factors and Genes Through Transcriptome Analysis. *Front. Mol. Biosci.*, 9, 228.

Lotti, F., Ranieri, F., Vadalà, G., Zollo, L., & Di Pino, G. (2017) Invasive intraneural interfaces: Foreign body reaction issues. *Front. Neurosci.*, 11, 1–14.

Lu, J., Shi, J., Li, M., Gui, B., Fu, R., Yao, G., Duan, Z., Lv, Z., Yang, Y., Chen, Z., Jia, L., & Tian, L. (2015) Activation of AMPK by metformin inhibits TGF-β-induced collagen production in mouse renal fibroblasts. *Life Sci.*, 127, 59–65.

Lu, Y., Lyu, H., Richardson, A.G., Lucas, T.H., & Kuzum, D. (2016) Flexible Neural Electrode Array Based-on Porous Graphene for Cortical Microstimulation and Sensing. *Sci. Reports 2016 61*, 6, 1–9.

Luo, T., Nocon, A., Fry, J., Sherban, A., Rui, X., Jiang, B., Xu, X.J., Han, J., Yan, Y., Yang, Q., Li, Q., & Zang, M. (2016) AMPK activation by metformin suppresses abnormal extracellular matrix remodeling in adipose tissue and ameliorates insulin resistance in obesity. *Diabetes*, 65, 2295–2310.

Malagodi, M.S., Horch, K.W., & Schoenberg, A.A. (1989) An intrafascicular electrode for recording of action potentials in peripheral nerves. *Ann. Biomed. Eng.*, 17, 397–410.

Mannard, A., Stein, R.B., & Charles, D. (1974) Regeneration Electrode Units: Implants for Recording from Single Peripheral Nerve Fibers in Freely Moving Animals Abstract. *Science (80-.).*, 183, 547–549.

Mariani, E., Lisignoli, G., Borzì, R.M., & Pulsatelli, L. (2019) Biomaterials: Foreign bodies or tuners for the immune response? *Int. J. Mol. Sci.*, 20, 636.

Marquez-Chin, C. & Popovic, M.R. (2020) Functional electrical stimulation therapy for restoration of motor function after spinal cord injury and stroke: A review. *Biomed. Eng. Online*, 19, 1–25.

Martínez-Martínez, E., Rodríguez, C., Galán, M., Miana, M., Jurado-López, R., Bartolomé, M.V., Luaces, M., Islas, F., Martínez-González, J., López-Andrés, N., & Cachofeiro, V. (2016) The lysyl oxidase inhibitor (β-aminopropionitrile) reduces leptin profibrotic

effects and ameliorates cardiovascular remodeling in diet-induced obesity in rats. *J. Mol. Cell. Cardiol.*, 92, 96–104.

Matlaga, B.F., Yasenchak, L.P., & Salthouse, T.N. (1976) Tissue response to implanted polymers: the significance of sample shape. *J. Biomed. Mater. Res.*, 10, 391–397.

McCarty, L.P. (1965) A stimulating electrode for nerves. *J. Appl. Physiol.*, 20, 542.

McCreery, D., Cogan, S., Kane, S., & Pikov, V. (2016) Correlations between histology and neuronal activity recorded by microelectrodes implanted chronically in the cerebral cortex. *J. Neural Eng.*, 13, 036012.

Mercanzini, A., Reddy, S.T., Velluto, D., Colin, P., Maillard, A., Bensadoun, J.C., Hubbell, J.A., & Renaud, P. (2010) Controlled release nanoparticle-embedded coatings reduce the tissue reaction to neuroprostheses 145, 196–202.

Meziani, L., Mondini, M., Petit, B., Boissonnas, A., De Montpreville, V.T., Mercier, O., Vozenin, M.C., & Deutsch, E. (2018) CSF1R inhibition prevents radiation pulmonary fibrosis by depletion of interstitial macrophages. *Eur. Respir. J.*, 51, 1702120.

Micera, S., Carpaneto, J., Raspopovic, S., S., M., J., C., & S., R. (2010) Control of hand prostheses using peripheral information. *IEEE Rev. Biomed. Eng.*, 3, 48–68.

Micera, S. & Navarro, X. (2009) Bidirectional Interfaces with the Peripheral Nervous System. *Int. Rev. Neurobiol.*, 86, 23–38.

Micera, S., Navarro, X., Carpaneto, J., Citi, L., Tonet, O., Rossini, P.M., Carrozza, M.C., Hoffmann, K.P., Vivo, M., Yoshida, K., & Dario, P. (2008) On the Use of Longitudinal Intrafascicular Peripheral Interfaces for the Control of Cybernetic Hand Prostheses in Amputees. *IEEE Trans. Neural Syst. Rehabil. Eng.*, 16, 453–472.

Micera, S., Navarro, X., Carpaneto, J., Citi, L., Tonet, O., Rossini, P.M., Carrozza, M.C., Hoffmann, K.P., Vivó, M., Yoshida, K., & Dario, P. (2008) On the use of longitudinal intrafascicular peripheral interfaces for the control of cybernetic hand prostheses in amputees. *IEEE Trans. Neural Syst. Rehabil. Eng.*, 16, 453–472.

Micera, S., Rossini, P.M., Rigosa, J., Citi, L., Carpaneto, J., Raspopovic, S., Tombini, M., Cipriani, C., Assenza, G., Carrozza, M.C., Hoffmann, K.-P., Yoshida, K., Navarro, X., & Dario, P. (2011) Decoding of grasping information from neural signals recorded using peripheral intrafascicular interfaces. *J. Neuroeng. Rehabil.*, 8, 53.

Minardi, S., Corradetti, B., Taraballi, F., Byun, J.H., Cabrera, F., Liu, X., Ferrari, M., Weiner, B.K., & Tasciotti, E. (2016) IL-4 Release from a Biomimetic Scaffold for the Temporally Controlled Modulation of Macrophage Response. *Ann. Biomed. Eng.*, 44, 2008–2019.

Moncsek, A., Al-Suraih, M., Trussoni, C., O'Hara, S., Splinter, P., Zuber, C., Patsenker, E., Valli, P., Fingas, C., Weber, A., Zhu, Y., Tchkonia, T., Kirkland, J., Gores, G., Büllhaupt, B., LaRusso, N., & Mertens, J. (2017) Targeting senescent cholangiocytes and activated fibroblasts with Bcl-xL inhibitors ameliorates fibrosis in Mdr2-/- mice. *Hepatology*, , 1–36.

Moore, L.B. & Kyriakides, T.R. (2015) Molecular characterization of macrophage-biomaterial interactions. *Adv. Exp. Med. Biol.*, 865, 109–122.

Moss, J., Ryder, T., Aziz, T.Z., Graeber, M.B., & Bain, P.G. (2004) Electron microscopy of tissue adherent to explanted electrodes in dystonia and Parkinson's disease. *Brain*, 127, 2755–2763.

Moyano, D.F., Goldsmith, M., Solfiell, D.J., Landesman-Milo, D., Miranda, O.R., Peer, D., & Rotello, V.M. (2012) Nanoparticle Hydrophobicity Dictates Immune Response. *J. Am. Chem. Soc.*, 134, 3965.

Murphy, B., Krieger, C., & Hoffer, J.A. (2004) Chronically implanted epineural electrodes for repeated assessment of nerve conduction velocity and compound action potential amplitude in rodents. *J. Neurosci. Methods*, 132, 25–33.

Murphy, K. & Weaver, C. (2017) *Janeway's Immunobiology*, Murphy, Kenneth (Kenneth M.) Weaver, Casey Janeway, Charles.

Nagaraju, C.K., Robinson, E.L., Abdesselem, M., Trenson, S., Dries, E., Gilbert, G., Janssens, S., Van Cleemput, J., Rega, F., Meyns, B., Roderick, H.L., Driesen, R.B., & Sipido, K.R. (2019) Myofibroblast Phenotype and Reversibility of Fibrosis in Patients With End-Stage Heart Failure. *J. Am. Coll. Cardiol.*, 73, 2267–2282.

Nassif, R.M., Chalhoub, E., Chedid, P., Hurtado-Nedelec, M., Raya, E., Dang, P.M.C., Marie, J.C., & El-Benna, J. (2022) Metformin Inhibits ROS Production by Human M2 Macrophages via the Activation of AMPK. *Biomedicines*, 10.

Navarro, X., Calvet, S., Butí, M., Gómez, N., Cabruja, E., Garrido, P., Villa, R., & Valderrama, E. (1996) Peripheral nerve regeneration through microelectrode arrays based on silicon technology. *Restor. Neurol. Neurosci.*, 9, 151–160.

Navarro, X., Krueger, T.B., Lago, N., Micera, S., Stieglitz, T., & Dario, P. (2005) A critical review of interfaces with the peripheral nervous system for the control of neuroprostheses and hybrid bionic systems. *J. Peripher. Nerv. Syst.*, 10, 229–258.

Navarro, X., Lago, N., Vivó, M., Yoshida, K., Koch, K.P., Poppendieck, W., & Micera, S. (2007) Neurobiological evaluation of thin-film longitudinal intrafascicular electrodes as a peripheral nerve interface. *2007 IEEE 10th Int. Conf. Rehabil. Robot. ICORR'07*, 00, 643–649.

Navarro, X. & Verdú, E. (2004) Cell Transplants and Artificial Guides for Nerve Repair. *Brain Damage and Repair*, 451–471.

Negi, S., Bhandari, R., & Solzbacher, F. (2012) A novel technique for increasing charge injection capacity of neural electrodes for efficacious and safe neural stimulation. *Proc. Annu. Int. Conf. IEEE Eng. Med. Biol. Soc. EMBS*, 5142–5145.

Nguyen, D., Valet, M., Dégardin, J., Boucherit, L., Illa, X., de la Cruz, J., del Corro, E., Bousquet, J., Garrido, J.A., Hébert, C., & Picaud, S. (2021) Novel Graphene Electrode for Retinal Implants: An in vivo Biocompatibility Study. *Front. Neurosci.*, 15, 1–10.

Normansell, R., Kew, K.M., & Mansour, G. (2016) Different oral corticosteroid regimens for acute asthma. *Cochrane database Syst. Rev.*, 2016(5), CD011801.

Novoselov, K.S., Fal'Ko, V.I., Colombo, L., Gellert, P.R., Schwab, M.G., & Kim, K. (2012) A roadmap for graphene. *Nature*, 490, 192–200.

Oakes, R.S., Polei, M.D., Skousen, J.L., & Tresco, P.A. (2018) An astrocyte derived extracellular matrix coating reduces astrogliosis surrounding chronically implanted microelectrode arrays in rat cortex. *Biomaterials*, 154, 1–11.

Ode Boni, B.O., Lamboni, L., Souho, T., Gauthier, M., & Yang, G. (2019) Immunomodulation and cellular response to biomaterials: The overriding role of neutrophils in healing. *Mater. Horizons*, 6, 1122–1137.

Olsen, K.C., Epa, A.P., Kulkarni, A.A., Kottmann, R.M., McCarthy, C.E., Johnson, G. V., Thatcher, T.H., Phipps, R.P., & Sime, P.J. (2014) Inhibition of transglutaminase 2, a novel target for pulmonary fibrosis, by two small electrophilic molecules. *Am. J. Respir. Cell Mol. Biol.*, 50, 737–747.

Ortiz-Catalan, M., Marin-Millan, J., Delbeke, J., Håkansson, B., & Brånemark, R. (2013) Effect on signal-to-noise ratio of splitting the continuous contacts of cuff electrodes into smaller recording areas. *J. Neuroeng. Rehabil.*, 10, 22.

Pan, J., Li, D., Xu, Y., Zhang, J., Wang, Y., Chen, M., Lin, S., Huang, L., Chung, E.J., Citrin, D.E., Wang, Y., Hauer-Jensen, M., Zhou, D., & Meng, A. (2017) Inhibition of Bcl-2/xl With ABT-263 Selectively Kills Senescent Type II Pneumocytes and Reverses Persistent Pulmonary Fibrosis Induced by Ionizing Radiation in Mice. *Int. J. Radiat. Oncol. Biol. Phys.*, 99, 353–361.

Panetsos, F., Avendano, C., Negredo, P., Castro, J., & Bonacasa, V. (2008) Neural prostheses: Electrophysiological and histological evaluation of central nervous system alterations due to long-term implants of sieve electrodes to peripheral nerves in cats. *IEEE Trans. Neural Syst. Rehabil. Eng.*, 16, 223–232.

Park, D.W., Schendel, A.A., Mikael, S., Brodnick, S.K., Richner, T.J., Ness, J.P., Hayat, M.R., Atry, F., Frye, S.T., Pashaie, R., Thongpang, S., Ma, Z., & Williams, J.C. (2014) Graphene-based carbon-layered electrode array technology for neural imaging and optogenetic applications. *Nat. Commun.*, 5, 5258.

Park, S.J., Lee, Y.J., Heo, D.N., Kwon, I.K., Yun, K.-S.S., Kang, J.Y., & Lee, S.H. (2015) Functional nerve cuff electrode with controllable anti-inflammatory drug loading and release by biodegradable nanofibers and hydrogel deposition. *Sensors Actuators B Chem.*, 215, 133–141.

Park, S.Y., Park, J., Sim, S.H., Sung, M.G., Kim, K.S., Hong, B.H., & Hong, S. (2011) Enhanced differentiation of human neural stem cells into neurons on graphene. *Adv. Mater.*, 23, 263–267.

Patrick, E., Orazem, M.E., Sanchez, J.C., & Nishida, T. (2011) Corrosion of tungsten microelectrodes used in neural recording applications 198, 158–171.

Penke, L.R. & Peters-Golden, M. (2019) Molecular determinants of mesenchymal cell activation in fibroproliferative diseases. *Cell. Mol. Life Sci.*, 76, 4179–4201.

Perlmutter, J.S. & Mink, J.W. (2006) Deep brain stimulation. *Annu. Rev. Neurosci.*, 29, 229–257.

Philp, C.J., Siebeke, I., Clements, D., Miller, S., Habgood, A., John, A.E., Navaratnam, V., Hubbard, R.B., Jenkins, G., & Johnson, S.R. (2018) Extracellular matrix cross-linking enhances fibroblast growth and protects against matrix proteolysis in lung fibrosis. *Am. J. Respir. Cell Mol. Biol.*, 58, 594–603.

Pierucci, A., De Duek, E.A.R., & De Oliveira, A.L.R. (2008) Peripheral nerve regeneration through biodegradable conduits prepared using solvent evaporation. *Tissue Eng. Part A*, 14, 595–606.

Pigeon, S., Meunier, M., Sawan, M., & Martel, S. (2003) Design and Fabrication of a Microelectrode Array Dedicated for Cortical Electrical Stimulation. In *Canadian Conference on Electrical and Computer Engineering*. pp. 813–816.

Polikov, V.S., Tresco, P.A., & Reichert, W.M. (2005) Response of brain tissue to chronically implanted neural electrodes. *J. Neurosci. Methods*, 148, 1–18. .

Popović, D.B. (2014) Advances in functional electrical stimulation (FES). *J. Electromyogr. Kinesiol.*, 24, 795–802.

Popovic, M.R., Curt, A., Keller, T., & Dietz, V. (2001) Functional electrical stimulation for grasping and walking: indications and limitations. *Spinal Cord*, 39, 403–412.

Raghu, G., Brown, K.K., Collard, H.R., Cottin, V., Gibson, K.F., Kaner, R.J., Lederer, D.J., Martinez, F.J., Noble, P.W., Song, J.W., Wells, A.U., Whelan, T.P.M., Wuyts, W., Moreau, E., Patterson, S.D., Smith, V., Bayly, S., Chien, J.W., Gong, Q., Zhang, J.J., & O'Riordan, T.G. (2017) Efficacy of simtuzumab versus placebo in patients with idiopathic pulmonary fibrosis: a randomised, double-blind, controlled, phase 2 trial. *Lancet Respir. Med.*, 5, 22–32.

Ranck, J.B. (1975) Which elements are excited in electrical stimulation of mammalian central nervous system: a review. *Brain Res.*, 98, 417–440.

Rangarajan, S., Bone, N.B., Zmijewska, A.A., Jiang, S., Park, D.W., Bernard, K., Locy, M.L., Ravi, S., Deshane, J., Mannon, R.B., Abraham, E., Darley-Usmar, V., Thannickal, V.J., & Zmijewski, J.W. (2018) Metformin reverses established lung fibrosis in a bleomycin model. *Nat. Med.*, 24, 1121–1131.

Rao, S.S., Han, N., & Winter, J.O. (2011) Polylysine-modified PEG-based hydrogels to enhance the neuro-electrode interface. *J. Biomater. Sci. Polym. Ed.*, 22, 611–625.

Raspopovic, S., Capogrosso, M., Petrini, F.M., Bonizzato, M., Rigosa, J., Pino, G. Di, Carpaneto, J., Controzzi, M., Boretius, T., Fernandez, E., Granata, G., Oddo, C.M., Citi, L., Ciancio, A.L., Cipriani, C., Carrozza, M.C., Jensen, W., Guglielmelli, E., Stieglitz, T., Rossini, P.M., & Micera, S. (2014) Restoring natural sensory feedback in real-time bidirectional hand prostheses. *Sci. Transl. Med.*, 6, 1–10.

Raspopovic, S., Carpaneto, J., Udina, E., Navarro, X., & Micera, S. (2010) On the identification of sensory information from mixed nerves by using single-channel cuff electrodes. *J. Neuroeng. Rehabil.*, 7, 17.

Raspopovic, S., Cimolato, A., Panarese, A., Vallone, F., del Valle, J., Micera, S., & Navarro, X. (2020) Neural signal recording and processing in somatic neuroprosthetic applications. A review. *J. Neurosci. Methods*, 337, 108653.

Raspopovic, S., Petrini, F.M., Zelechowski, M., & Valle, G. (2017) Framework for the Development of Neuroprostheses: From Basic Understanding by Sciatic and Median Nerves Models to Bionic Legs and Hands. *Proc. IEEE*, 105, 34–49.

Ravikumar, M., Sunil, S., Black, J., Barkauskas, D.S., Haung, A.Y., Miller, R.H., Selkirk, S.M., & Capadona, J.R. (2014) The roles of blood-derived macrophages and resident microglia in the neuroinflammatory response to implanted Intracortical microelectrodes. *Biomaterials*, 35, 8049.

Redente, E.F., Keith, R.C., Janssen, W., Henson, P.M., Ortiz, L.A., Downey, G.P., Bratton, D.L., & Riches, D.W.H. (2014) Tumor necrosis factor-α accelerates the resolution of established pulmonary fibrosis in mice by targeting profibrotic lung macrophages. *Am. J. Respir. Cell Mol. Biol.*, 50, 825–837.

Reed, N.I., Jo, H., Chen, C., Tsujino, K., Arnold, T.D., DeGrado, W.F., & Sheppard, D. (2015) The αvβ1 integrin plays a critical in vivo role in tissue fibrosis. *Sci. Transl. Med.*, 7, 288ra79.

Rennaker, R.L., Miller, J., Tang, H., & Wilson, D.A. (2007) Minocycline increases quality and longevity of chronic neural recordings. *J. Neural Eng.*, 4, L1.

Ricard-Blum, S., Baffet, G., & Théret, N. (2018) Molecular and tissue alterations of collagens in fibrosis. *Matrix Biol.*, 68-69, 122–149.

Richardson, R.R., Miller, J.A., & Reichert, W.M. (1993) Polyimides as biomaterials: preliminary biocompatibility testing. *Biomaterials*, 14, 627–635.

Righi, M., Puleo, G.L., Tonazzini, I., Giudetti, G., Cecchini, M., & Micera, S. (2018) Peptide-based coatings for flexible implantable neural interfaces. *Sci. Rep.*, 8(1), 502.

Rodriguez, A., Voskerician, G., Meyerson, H., Macewan, S.R., & Anderson, J.M. (2007) T cell subset distributions following primary and secondary implantation at subcutaneous biomaterial implant sites. *J. Biomed. Mater. Res. A*, 85, 556–565.

Rodríguez, F.J., Ceballos, D., Schüttler, M., Valero, A., Valderrama, E., Stieglitz, T., Navarro, X., Rodriguez, F.J., & Schuttler, M. (2000) Polyimide cuff electrodes for peripheral nerve stimulation. *J. Neurosci. Methods*, 98, 105–118.

Rosenbloom, J., Mendoza, F.A., & Jimenez, S.A. (2013) Strategies for anti-fibrotic therapies. *Biochim. Biophys. Acta - Mol. Basis Dis.*, 1832, 1088–1103..

Rossini, P.M., Micera, S., Benvenuto, A., Carpaneto, J., Cavallo, G., Citi, L., Cipriani, C., Denaro, L., Denaro, V., Di Pino, G., Ferreri, F., Guglielmelli, E., Hoffmann, K.P., Raspopovic, S., Rigosa, J., Rossini, L., Tombini, M., & Dario, P. (2010) Double nerve intraneural interface implant on a human amputee for robotic hand control. *Clin. Neurophysiol.*, 121, 777–783.

Rousche, P.J., Pellinen, D.S., Pivin, D.P., Williams, J.C., Vetter, R.J., & Kipke, D.R. (2001) Flexible polyimide-based intracortical electrode arrays with bioactive capability. *IEEE Trans. Biomed. Eng.*, 48, 361–370.

Rubehn, B. & Stieglitz, T. (2010) In vitro evaluation of the long-term stability of polyimide as a material for neural implants. *Biomaterials*, 31, 3449–3458.

Rutten, W.L.C., Smit, J.P.A., Frieswijk, T.A., Bielen, J.A., Brouwer, A.L.H., Buitenweg, J.R., & Heida, C. (1999) Neuro-electronic interfacing with multielectrode arrays: Selectivity and efficiency of motor-fiber stimulation, toward a cultured probe. *IEEE Eng. Med. Biol. Mag.*, 18, 47–55.

Saal, H.P. & Bensmaia, S.J. (2015) Biomimetic approaches to bionic touch through a peripheral nerve interface. *Neuropsychologia*, 79, 344–353.

Sahni, D., Jea, A., Mata, J.A., Marcano, D.C., Sivaganesan, A., Berlin, J.M., Tatsui, C.E., Sun, Z., Luerssen, T.G., Meng, S., Kent, T.A., & Tour, J.M. (2013) Biocompatibility of pristine graphene for neuronal interface: Laboratory investigation. *J. Neurosurg. Pediatr.*, 11, 575–583.

Saito, S., Zhuang, Y., Shan, B., Danchuk, S., Luo, F., Korfei, M., Guenther, A., & Lasky, J.A. (2017) Tubastatin ameliorates pulmonary fibrosis by targeting the TGFβ-PI3K-Akt pathway. *PLoS One*, 12(10), e0186615.

Sato, N., Takasaka, N., Yoshida, M., Tsubouchi, K., Minagawa, S., Araya, J., Saito, N., Fujita, Y., Kurita, Y., Kobayashi, K., Ito, S., Hara, H., Kadota, T., Yanagisawa, H., Hashimoto, M., Utsumi, H., Wakui, H., Kojima, J., Numata, T., Kaneko, Y., Odaka, M., Morikawa, T., Nakayama, K., Kohrogi, H., & Kuwano, K. (2016) Metformin attenuates lung fibrosis development via NOX4 suppression. *Respir. Res.*, 17, 1–12.

Sawada, S.I., Sakaki, S., Iwasaki, Y., Nakabayashi, N., & Ishihara, K. (2003) Suppression of the inflammatory response from adherent cells on phospholipid polymers. *J. Biomed. Mater. Res. - Part A*, 64, 411–416.

Scatena, M., Eaton, K. V., Jackson, M.F., Lund, S.A., & Giachelli, C.M. (2016) Macrophages: The bad, the ugly, and the good in the inflammatory response to biomaterials. In *The Immune Response to Implanted Materials and Devices: The Impact of the Immune System on the Success of an Implant*. Springer International Publishing, pp. 37–62.

Scholvin, J., Kinney, J.P., Bernstein, J.G., Moore-Kochlacs, C., Kopell, N., Fonstad, C.G., & Boyden, E.S. (2016) Close-Packed Silicon Microelectrodes for Scalable Spatially Oversampled Neural Recording. *IEEE Trans. Biomed. Eng.*, 63, 120.

Schulz, J.N., Plomann, M., Sengle, G., Gullberg, D., Krieg, T., & Eckes, B. (2018) New developments on skin fibrosis - Essential signals emanating from the extracellular matrix for the control of myofibroblasts. *Matrix Biol.*, 68-69, 522–532.

Shen, Y., Miao, N., Xu, J., Gan, X., Xu, D., Zhou, L., Xue, H., Zhang, W., & Lu, L. (2016) Metformin Prevents Renal Fibrosis in Mice with Unilateral Ureteral Obstruction and Inhibits Ang II-Induced ECM Production in Renal Fibroblasts. *Int. J. Mol. Sci.*, 17 , 146.

Shepherd, R.K. & McCreery, D.B. (2006) Basis of electrical stimulation of the cochlea and the

cochlear nucleus. *Adv. Otorhinolaryngol.*, 64, 186–205.

Shepherd, R.K., Wise, A.K., Enke, Y.L., Carter, P.M., & Fallon, J.B. (2017) Evaluation of focused multipolar stimulation for cochlear implants: a preclinical safety study. *J. Neural Eng.*, 14, 046020.

Shin, H.S., Ko, J., Kim, D.A., Ryu, E.S., Ryu, H.M., Park, S.H., Kim, Y.L., Oh, E.S., & Kang, D.H. (2017) Metformin ameliorates the Phenotype Transition of Peritoneal Mesothelial Cells and Peritoneal Fibrosis via a modulation of Oxidative Stress. *Sci. Rep.*, 7, 5690.

Shiraishi, K. & Yokoyama, M. (2019) Toxicity and immunogenicity concerns related to PEGylated-micelle carrier systems: a review. *Sci. Technol. Adv. Mater.*, 20(1), 324–336.

Sieber, P., Schäfer, A., Lieberherr, R., Le Goff, F., Stritt, M., Welford, R.W.D., Gatfield, J., Peter, O., Nayler, O., & Lüthi, U. (2018) Novel high–throughput myofibroblast assays identify agonists with therapeutic potential in pulmonary fibrosis that act via EP 2 and EP 4 receptors. *PLoS One*, 13 (11), e0207872.

Sisson, T.H., Christensen, P.J., Muraki, Y., Dils, A.J., Chibucos, L., Subbotina, N., Tohyama, K., Horowitz, J.C., Matsuo, T., Bailie, M., Nikam, S., & Hazama, M. (2018) Phosphodiesterase 4 inhibition reduces lung fibrosis following targeted type II alveolar epithelial cell injury. *Physiol. Rep.*, 6, e13753.

Soulier, F., Gouyet, L., Cathébras, G., Bernard, S., Guiraud, D., & Bertrand, Y. (2008) Multipolar electrode and preamplifier design for ENG-signal acquisition. *Commun. Comput. Inf. Sci.*, 25 CCIS, 148–159.

Spataro, L., Dilgen, J., Retterer, S., Spence, A.J., Isaacson, M., Turner, J.N., & Shain, W. (2005) Dexamethasone treatment reduces astroglia responses to inserted neuroprosthetic devices in rat neocortex. *Exp. Neurol.*, 194, 289–300.

Sperling, C., Fischer, M., Maitz, M.F., & Werner, C. (2017) Neutrophil extracellular trap formation upon exposure of hydrophobic materials to human whole blood causes thrombogenic reactions. *Biomater. Sci.*, 5, 1998–2008.

Srinivasan, A., Tipton, J., Tahilramani, M., Kharbouch, A., Gaupp, E., Song, C., Venkataraman, P., Falcone, J., Lacour, S.P., Stanley, G.B., English, A.W., & Bellamkonda, R. (2015) A Regenerative Microchannel Device for Recording Multiple Single Unit Action Potentials in Awake, Ambulatory Animals. *Eur. J. Neurosci.*, 43, 474–485.

Stanton-Hicks, M. & Salamon, J. (1997) Stimulation of the central and peripheral nervous system for the control of pain. *J. Clin. Neurophysiol.*, 14, 46–62.

Stieglitz, T. (2001) Flexible biomedical microdevices with double-sided electrode arrangements for neural applications. *Sensors Actuators, A Phys.*, 90, 203–211.

Stieglitz, T., Beutel, H., Keller, R., Blau, C., & Meyer, J.U. (1997) Development of flexible stimulation devices for a retina implant system. *Annu. Int. Conf. IEEE Eng. Med. Biol. - Proc.*, 5, 2307–2310.

Stieglitz, T., Beutel, H., Schuettler, M., & Meyer, J.U. (2000) Micromachined, polyimide-based devices for flexible neural interfaces. *Biomed. Microdevices*, 2, 283–294.

Sugimoto, H., LeBleu, V.S., Bosukonda, D., Keck, P., Taduri, G., Bechtel, W., Okada, H., Carlson, W., Bey, P., Rusckowski, M., Tampe, B., Tampe, D., Kanasaki, K., Zeisberg, M., & Kalluri, R. (2012) Activin-like kinase 3 is important for kidney regeneration and reversal of fibrosis. *Nat. Med.*, 18, 396–404.

Sulaiman, W. & Gordon, T. (2013) Neurobiology of Peripheral Nerve Injury, Regeneration, and Functional Recovery: From Bench Top Research to Bedside Application. *Ochsner J.*, 13, 100.

Sun, H., Zhang, L., Xia, W., Chen, L., Xu, Z., & Zhang, W. (2016) Fabrication of graphene oxide-modified chitosan for controlled release of dexamethasone phosphate. *Appl. Phys. A Mater. Sci. Process.*, 122, 1–8.

Sydlik, S.A., Jhunjhunwala, S., Webber, M.J., Anderson, D.G., & Langer, R. (2015) In vivo compatibility of graphene oxide with differing Oxidation states. *ACS Nano*, 9, 3866–3874.

Szarowski, D.H., Andersen, M.D., Retterer, S., Spence, A.J., Isaacson, M., Craighead, H.G., Turner, J.N., & Shain, W. (2003) Brain responses to micro-machined silicon devices. *Brain Res.*, 983, 23–35.

Szostak, K.M., Grand, L., & Constandinou, T.G. (2017) Neural interfaces for intracortical recording: Requirements, fabrication methods, and characteristics. *Front. Neurosci.*, 11, 665.

Tabot, G.A., Kim, S.S., Winberry, J.E., & Bensmaia, S.J. (2015) Restoring tactile and proprioceptive sensation through a brain interface. *Neurobiol. Dis.*, 83, 191.

Tan, D.W., Schiefer, M.A., Keith, M.W., Anderson, R., & Tyler, D.J. (2015) Stability and selectivity of a chronic, multi-contact cuff electrode for sensory stimulation in a human amputee. *J. Neural Eng.*, 12, 026002.

Thakur, S., Viswanadhapalli, S., Kopp, J.B., Shi, Q., Barnes, J.L., Block, K., Gorin, Y., & Abboud, H.E. (2015) Activation of AMP-Activated Protein Kinase Prevents TGF-β1-Induced Epithelial-Mesenchymal Transition and Myofibroblast Activation. *Am. J. Pathol.*, 185, 2168–2180.

Thannickal, V.J. & Horowitz, J.C. (2006) Evolving concepts of apoptosis in idiopathic pulmonary fibrosis. *Proc. Am. Thorac. Soc.*, 3, 350–356.

Tikoo, K., Sharma, E., Amara, V.R., Pamulapati, H., & Dhawale, V.S. (2016) Metformin improves metabolic memory in high fat diet (HFD)- Induced renal dysfunction. *J. Biol. Chem.*, 291, 21848–21856.

Trel, ana, Rita Salgarella, A., Ricotti, L., Giudetti, G., Cutrone, A., Zahoranova, A., Chorva, an, Has, D., Canale, C., Micera, S., Kronek, J., Menciassi, A., & Lacík, I. (2018) Soft Hydrogel Zwitterionic Coatings Minimize Fibroblast and Macrophage Adhesion on Polyimide Substrates 35, 1085–1099.

Tyler, D.J. & Durand, D.M. (2002) Functionally selective peripheral nerve stimulation with a flat interface nerve electrode. *IEEE Trans. Neural Syst. Rehabil. Eng.*, 10, 294–303.

Tyler, D.J. & Durand, D.M. (2003) Chronic response of the rat sciatic nerve to the flat interface nerve electrode. *Ann. Biomed. Eng.*, 31, 633–642.

Tyler, D.J., Polasek, K.H., & Schiefer, M.A. (2015) *Peripheral Nerve Interfaces*, Nerves and Nerve Injuries. Elsevier Ltd.

Ursini, F., Grembiale, R.D., D'Antona, L., Gallo, E., D'Angelo, S., Citraro, R., Visca, P., Olivieri, I., De Sarro, G., Perrotti, N., & Russo, E. (2016) Oral Metformin Ameliorates Bleomycin-Induced Skin Fibrosis. *J. Invest. Dermatol.*, 136, 1892–1894.

Valle, G., D'Anna, E., Strauss, I., Clemente, F., Granata, G., Di Iorio, R., Controzzi, M., Stieglitz, T., Rossini, P.M., Petrini, F.M., & Micera, S. (2020) Hand Control With Invasive Feedback Is Not Impaired by Increased Cognitive Load. *Front. Bioeng. Biotechnol.*, 8, 1–7.

Valle, G., Mazzoni, A., Iberite, F., D'Anna, E., Strauss, I., Granata, G., Controzzi, M., Clemente, F., Rognini, G., Cipriani, C., Stieglitz, T., Petrini, F.M., Rossini, P.M., & Micera, S. (2018) Biomimetic Intraneural Sensory Feedback Enhances Sensation Naturalness, Tactile Sensitivity, and Manual Dexterity in a Bidirectional Prosthesis. *Neuron*, 100, 37-45.e7.

Veiseh, O., Doloff, J.C., Ma, M., Vegas, A.J., Tam, H.H., Bader, A.R., Li, J., Langan, E., Wyckoff, J., Loo, W.S., Jhunjhunwala, S., Chiu, A., Siebert, S., Tang, K., Hollister-Lock, J., Aresta-Dasilva, S., Bochenek, M., Mendoza-Elias, J., Wang, Y., Qi, M., Lavin, D.M., Chen, M., Dholakia, N., Thakrar, R., Lacík, I., Weir, G.C., Oberholzer, J., Greiner, D.L., Langer, R., & Anderson, D.G. (2015) Size- and shape-dependent foreign body immune response to materials implanted in rodents and non-human primates. *Nat. Mater.*, 14, 643.

Veraart, C., Grill, W.M., & Mortimer, J.T. (1993a) Selective control of muscle activation with a multipolar nerve cuff electrode. *IEEE Trans. Biomed. Eng.*, 40, 640–653.

Veraart, C., Raftopoulos, C., Mortimer, J.T., Delbeke, J., Pins, D., Michaux, G., Vanlierde, A., Parrini, S., & Wanet-Defalque, M.C. (1998) Visual sensations produced by optic nerve stimulation using an implanted self-sizing spiral cuff electrode. *Brain Res.*, 813, 181–186.

Viana, D., Walston, S.T., Illa, X., Valle, J. del, Hayward, A., Dodd, A., Loret, T., Prats-Alfonso, E., de la Oliva, N., Palma, M., Corro, E. del, Rodríguez-Meana, B., Bernicola, M. del P., Rodríguez-Lucas, E., Gener, T.A., Cruz, J.M. de la, Torres-Miranda, M., Duvan, F.T., Ria, N., Sperling, J., Martí-Sánchez, S., Spadaro, M.C., Hébert, C., Masvidal-Codina, E., Savage, S., Arbiol, J., Guimerà-Brunet, A., Puig, M.V., Navarro, X., Yvert, B., Kostarelos, K., & Garrido, J.A. (2022) Graphene-based thin film microelectrode technology for in vivo high resolution neural recording and stimulation. *bioRxiv*, 2022.11.16.515761.

Viswam, V., Obien, M.E.J., Franke, F., Frey, U., & Hierlemann, A. (2019) Optimal electrode size for multi-scale extracellular-potential recording from neuronal assemblies. *Front. Neurosci.*, 13, 385.

Vroman, L. (1988) The life of an artificial device in contact with blood: initial events and their effect on its final state. *Bull. N. Y. Acad. Med.*, 64, 352–357.

Wallman, L., Zhang, Y., Laurell, T., & Danielsen, N. (2001) The geometric design of micromachined silicon sieve electrodes influences functional nerve regeneration. *Biomaterials*, 22, 1187–1193.

Walton, K.L., Johnson, K.E., & Harrison, C.A. (2017) Targeting TGF-β mediated SMAD signaling for the prevention of fibrosis. *Front. Pharmacol.*, 8, 461.

Wang, S., Chen, Y., Ling, Z., Li, J., Hu, J., He, F., & Chen, Q. (2022) The role of dendritic cells in the immunomodulation to implanted biomaterials. *Int. J. Oral Sci.*, 14, 52.

Wark, H.A., Sharma, R., Mathews, K.S., Fernandez, E., Yoo, J., Christensen, M.B., Tresco, P., Rieth, L., Solzbacher, F., Normann, R. a, & Tathireddy, P. (2013) A new high-density (25 electrodes/mm^2) penetrating microelectrode array for recording and stimulating sub-millimeter neuroanatomical structures. *J. Neural Eng.*, 10, 045003.

Wark, H.A.C., Mathews, K.S., Normann, R.A., & Fernandez, E. (2014) Behavioral and cellular consequences of high-electrode count Utah Arrays chronically implanted in rat sciatic nerve. *J. Neural Eng.*, 11, 046027.

Waters, R.L., McNeal, D., & Perry, J. (1975) Experimental correction of footdrop by electrical stimulation of the peroneal nerve. *J. Bone Jt. Surg. - Ser. A*, 57, 1047–1054.

Wei, W. & Wang, X. (2021) Graphene-Based Electrode Materials for Neural Activity Detection. *Materials (Basel).*, 14, 6170.

Wellman, S.M., Eles, J.R., Ludwig, K.A., Seymour, J.P., Michelson, N.J., McFadden, W.E., Vazquez, A.L., & Kozai, T.D.Y. (2018) A Materials Roadmap to Functional Neural Interface Design. *Adv. Funct. Mater.*, 28, 1701269.

Wendelken, S., Page, D.M., Davis, T., Wark, H.A.C.C., Kluger, D.T., Duncan, C., Warren, D.J., Hutchinson, D.T., & Clark, G.A. (2017) Restoration of motor control and proprioceptive and cutaneous sensation in humans with prior upper-limb amputation via multiple

Utah Slanted Electrode Arrays (USEAs) implanted in residual peripheral arm nerves. *J. Neuroeng. Rehabil.*, 14, 121.

Wendelken, S., Page, D.M., Davis, T., Wark, H.A.C.C., Kluger, D.T., Duncan, C., Warren, D.J., Hutchinson, D.T., Clark, G.A., Warren, D.J., O'Neill, K., Scheinblum, T., Clark, G.A., Normann, R.A., Greger, B., Wendelken, S., Page, D.M., Davis, T., Wark, H.A.C.C., Kluger, D.T., Duncan, C., Warren, D.J., Hutchinson, D.T., & Clark, G.A. (2016) Restoring motor control and sensory feedback in people with upper extremity amputations using arrays of 96 microelectrodes implanted in the median and ulnar nerves. *J. Neural Eng.*, 13, 36001.

Westra, I.M., Oosterhuis, D., Groothuis, G.M.M., & Olinga, P. (2014) The effect of antifibrotic drugs in rat precision-cut fibrotic liver slices. *PLoS One*, 9, e95462.

Wieler, M., Stein, R.B., Ladouceur, M., Whittaker, M., Smith, A.W., Naaman, S., Barbeau, H., Bugaresti, J., & Aimone, E. (1999) Multicenter evaluation of electrical stimulation systems for walking. *Arch. Phys. Med. Rehabil.*, 80, 495–500.

Wipff, P.J., Rifkin, D.B., Meister, J.J., & Hinz, B. (2007) Myofibroblast contraction activates latent TGF-β1 from the extracellular matrix. *J. Cell Biol.*, 179, 1311.

Witherel, C.E., Abebayehu, D., Barker, T.H., & Spiller, K.L. (2019) Macrophage and Fibroblast Interactions in Biomaterial-Mediated Fibrosis. *Adv. Healthc. Mater.*, 8, 1–35.

Wohlfahrt, T., Rauber, S., Uebe, S., Luber, M., Soare, A., Ekici, A., Weber, S., Matei, A.E., Chen, C.W., Maier, C., Karouzakis, E., Kiener, H.P., Pachera, E., Dees, C., Beyer, C., Daniel, C., Gelse, K., Kremer, A.E., Naschberger, E., Stürzl, M., Butter, F., Sticherling, M., Finotto, S., Kreuter, A., Kaplan, M.H., Jüngel, A., Gay, S., Nutt, S.L., Boykin, D.W., Poon, G.M.K., Distler, O., Schett, G., Distler, J.H.W., & Ramming, A. (2019) PU.1 controls fibroblast polarization and tissue fibrosis. *Nature*, 566, 344–349.

Won, S.M., Song, E., Zhao, J., Li, J., Rivnay, J., & Rogers, J.A. (2018) Recent Advances in Materials, Devices, and Systems for Neural Interfaces. *Adv. Mater.*, 30, 1–19.

Wu, J., Lin, W., Wang, Z., Chen, S., & Chang, Y. (2012) Investigation of the hydration of nonfouling material poly(sulfobetaine methacrylate) by low-field nuclear magnetic resonance. *Langmuir*, 28, 7436–7441.

Wu, M., Xu, H., Liu, J., Tan, X., Wan, S., Guo, M., Long, Y., & Xu, Y. (2021) Metformin and Fibrosis: A Review of Existing Evidence and Mechanisms. *J. Diabetes Res.*, 2021, 6673525.

Wurth, S., Capogrosso, M., Raspopovic, S., Gandar, J., Federici, G., Kinany, N., Cutrone, A., Piersigilli, A., Pavlova, N., Guiet, R., Taverni, G., Rigosa, J., Shkorbatova, P., Navarro, X., Barraud, Q., Courtine, G., & Micera, S. (2017) Long-term usability and bio-integration of polyimide-based intra-neural stimulating electrodes. *Biomaterials*, 122, 114–129.

Xavier, D.O., Amaral, L.S., Gomes, M.A., Rocha, M.A., Campos, P.R., Cota, B.D.C.V., Tafuri, L.S.A., Paiva, A.M.R., Silva, J.H., Andrade, S.P., & Belo, A. V. (2010) Metformin inhibits inflammatory angiogenesis in a murine sponge model. *Biomed. Pharmacother.*, 64, 220–225.

Xiang, Z., Sheshadri, S., Lee, S., Wang, J., Xue, N., Thakor, N. V, Yen, S., & Lee, C. (2016) Mapping of Small Nerve Trunks and Branches Using Adaptive Flexible Electrodes 3, 1500386.

Xue, N., Sun, T., Tsang, W.M., Delgado-Martinez, I., Lee, S.H., Sheshadri, S., Xiang, Z., Merugu, S., Gu, Y., Yen, S.C., & Thakor, N. V. (2015) Polymeric C-shaped cuff electrode for recording of peripheral nerve signal. *Sensors Actuators, B Chem.*, 210, 640–648.

Yang, X., Chen, B., Liu, T., & Chen, X. (2014) Reversal of myofibroblast differentiation: A review. *Eur. J. Pharmacol.*, 734, 83–90.

Yao, Q., Li, S., Li, X., Wang, F., & Tu, C. (2020) Myricetin Modulates Macrophage

Polarization and Mitigates Liver Inflammation and Fibrosis in a Murine Model of Nonalcoholic Steatohepatitis. *Front. Med.*, 7, 71.

Ydens, E., Amann, L., Asselbergh, B., Scott, C.L., Martens, L., Sichien, D., Mossad, O., Blank, T., De Prijck, S., Low, D., Masuda, T., Saeys, Y., Timmerman, V., Stumm, R., Ginhoux, F., Prinz, M., Janssens, S., & Guilliams, M. (2020) Profiling peripheral nerve macrophages reveals two macrophage subsets with distinct localization, transcriptome and response to injury. *Nat. Neurosci.*, 23, 676.

Yi, H., Huang, C., Shi, Y., Cao, Q., Chen, J., Chen, X.M., & Pollock, C.A. (2021) Metformin Attenuates Renal Fibrosis in a Mouse Model of Adenine-Induced Renal Injury Through Inhibiting TGF-β1 Signaling Pathways. *Front. Cell Dev. Biol.*, 9, 603802.

Yin, W.H., Zhou, C.H., Ju, X.J., Deng, Y., Zhang, L., Xie, R., Wang, W., Liu, Z., & Chu, L.Y. (2022) Dual-functional polyetheretherketone surface with programmed sequential drug release coating. *Colloids Surfaces B Biointerfaces*, 219, 112806.

Yoshida, K., Farina, D., Akay, M., & Jensen, W. (2010) Multichannel intraneural and intramuscular techniques for multiunit recording and use in active prostheses. *Proc. IEEE*, 98, 432–449.

Yoshida, K. & Horch, K.W. (1993) Selective Stimulation of Peripheral Nerve Fibers using Dual Intrafascicular Electrodes. *IEEE Trans. Biomed. Eng.*, 40, 492–494.

Yoshida, K., Jovanović, K., & Stein, R.B. (2000) Intrafascicular electrodes for stimulation and recording from mudpuppy spinal roots. *J. Neurosci. Methods*, 96, 47–55.

Yoshida Kozai, T.D., Langhals, N.B., Patel, P.R., Deng, X., Zhang, H., Smith, K.L., Lahann, J., Kotov, N.A., & Kipke, D.R. (2012) Ultrasmall implantable composite microelectrodes with bioactive surfaces for chronic neural interfaces. *Nat. Mater.*, 11, 1065–1073.

Yrjänheikki, J., Tikka, T., Keinänen, R., Goldsteins, G., Chan, P.H., & Koistinaho, J. (1999) A tetracycline derivative, minocycline, reduces inflammation and protects against focal cerebral ischemia with a wide therapeutic window. *Proc. Natl. Acad. Sci. U. S. A.*, 96, 13496–13500.

Zhang, L., Cao, Z., Bai, T., Carr, L., Ella-Menye, J.R., Irvin, C., Ratner, B.D., & Jiang, S. (2013) Zwitterionic hydrogels implanted in mice resist the foreign-body reaction. *Nat. Biotechnol.*, 31, 553–556.

Zhang, X., Shang, F., Hui, L., Zang, K., & Sun, G. (2017) The alleviative effects of metformin for lipopolysaccharide-induced acute lung injury rat model and its underlying mechanism. *Saudi Pharm. J. SPJ*, 25, 666.

Zhang, X., Zhang, C., Shen, S., Xia, Y.J., Yi, L., Gao, Q., & Wang, Y. (2013) Dehydroepiandrosterone induces ovarian and uterine hyperfibrosis in female rats. *Hum. Reprod.*, 28, 3074–3085.

Zheng, W., Song, J., Zhang, Y., Chen, S., Ruan, H., & Fan, C. (2017) Metformin prevents peritendinous fibrosis by inhibiting transforming growth factor-β signaling. *Oncotarget*, 8, 101784–101794.

Zhong, Y. & Bellamkonda, R. V. (2007) Dexamethasone-coated neural probes elicit attenuated inflammatory response and neuronal loss compared to uncoated neural probes. *Brain Res.*, 1148, 15–27.

Zhou, Y., Huang, X., Hecker, L., Kurundkar, D., Kurundkar, A., Liu, H., Jin, T.H., Desai, L., Bernard, K., & Thannickal, V.J. (2013) Inhibition of mechanosensitive signaling in myofibroblasts ameliorates experimental pulmonary fibrosis. *J. Clin. Invest.*, 123, 1096–1108.

Zigrino, P., Brinckmann, J., Niehoff, A., Lu, Y., Giebeler, N., Eckes, B., Kadler, K.E., & Mauch,

C. (2016) Fibroblast-Derived MMP-14 Regulates Collagen Homeostasis in Adult Skin. *J. Invest. Dermatol.*, 136, 1575–1583.